The Development of an African Horse Sickness Virus VP7 Quasi-Crystal Vaccine Candidate in *N. benthamiana*

Shelley Helen Fearon

Dissertation presented for the degree of Master of Science
University of Cape Town
July 2019

Supervisor: Dr Ann Meyers
Co-supervisor: A/Prof Inga Hitzeroth
Co-supervisor: Prof Ed Rybicki

University of Cape Town
Department of Molecular and Cell Biology
Private Bag Rondebosch 7701 Cape Town - South Africa
Telephone: 27 21 650 5071 - Facsimile: 27 21 689 7573

ACKNOWLEDGEMENTS

I would like to thank every single member of the BRU team. You have all played an important part in assembling this dissertation, whether it be advice, kind words or sharing your buffers. In particular, sincerest thanks to my supervisor, Dr Ann Meyers, thank you for your sage advice, guidance, support and incredible patience and calm demeanour throughout this pursuit and including the writing of this dissertation. Sincerest thanks to my co-supervisors, Prof Ed Rybicki and A/Prof Inga Hitzeroth, for your invaluable guidance and support, and Inga for kindly reviewing this dissertation. And thank you Ed for kindly allowing me the privilege to be a part of such a fantastic team. A huge thanks too to Dr Susan Dennis, for your welcoming smile from day one, your advice, encouragement and all the great conversations. I admire you greatly. Thank you to Dr Megan Hendrickse, for your constructive advice, support and all the friendly chats along the way. A special thanks to Dr Alta van Zyl for letting me pick your brain on way more than just one occasion, Dr Rosemary Meggersee for making RNA extraction less tedious than expected and Matt Verbeek, my lab bench buddy, for helping me troubleshoot and all the friendly conversations.

I am very grateful to the Poliomyelitis Research Foundation (PRF) and the National Research Foundation (NRF) for their financial support.

I am also very thankful to the following individuals: Mohammed Jaffer at the Electron Microscopy Unit for his advice, encouragement and patience during many hours of tirelessly searching for protein crystals. Keren Cooper (MCB Department, UCT) for her meticulous assistance in leaf sectioning. Rodney Lucas from the Research Animal Facility at UCT for kindly handling and caring for the ten guinea-pigs acquired for this study. Guy Regnard (BRU, MCB Department, UCT) for providing the pRIC3.0 expression vector and George Lomonossoff from the John Innes Centre, UK, for providing the pEAQ-*HT* expression vector.

Last, but definitely not least, I feel extremely blessed to have an incredibly supportive and loving family. I am so thankful to all of you: My late father, George Smith, I still hear your wise words every day, and they continuously give me strength. My mother, Helen Smith, you have been there through every moment, whenever I need you, you are absolutely selfless. My endlessly supportive husband, Giles Fearon, without you

this would truly not have been possible. Thanks for your constant love, encouragement and wisdom. We have been on so many magnificent adventures together, thank you for sharing this one with me. My incredible daughter, Isabella Georgia Fearon, thank you for being the extraordinary little girl that you are. You are truly all the motivation that I need. *"Open hands love"*

University of Cape Town

Faculty of Science

Master of Science Dissertation

Full name: Shelley Helen Fearon

Student number: SMTSHE005

Course code: MCB5005W

Department: Molecular and Cell Biology

Degree: Master of Science

Plagiarism Declaration

1. I know that plagiarism is wrong. Plagiarism is to use another's work and to pretend that it is one's own.
2. This report is my own work.
3. I have not allowed, and will not allow, anyone to copy my work with the intention of passing it off as his or her own work.

Signed by candidate

.....

Shelley Helen Fearon Date: 14/07/2019

ABSTRACT

African horse sickness (AHS) is a debilitating viral disease affecting equines and has resulted in many disastrous epizootics. To date, no successful therapeutic treatment exists for AHS and the commercially used live-attenuated vaccines (LAVs) have various side effects. Insoluble particulates have been shown to increase immunogenicity when compared to soluble subunit vaccines and previous studies demonstrated protection of BALB/c mice immunised with African horse sickness virus (AHSV) VP7 against a lethal challenge of AHSV-7 (Bailey 2016; Rutkowska et al. 2011; St Clair et al. 1999; Storni et al. 2005; Wade-Evans et al. 1997). This study investigates a safer monovalent vaccine alternative based on plant-produced quasi-crystals of the serogroup-specific AHSV structural protein, VP7.

AHSV serotype 5 (AHSV-5) VP7 was expressed in *Nicotiana benthamiana* by means of *Agrobacterium*-mediated infiltration of plant expression vector pRIC3.0 encoding VP7 and quasi-crystals purified by means of density gradient ultracentrifugation. The presence of AHSV VP7 quasi-crystals was confirmed by western immunoblotting with anti-AHSV VLP guinea-pig serum and characterized using transmission electron microscopy. After optimizing the purification protocol and achieving satisfactory concentrations, AHSV-5 VP7 quasi-crystals were used in guinea-pig immunogenicity studies where the experimental group (n=5) was inoculated with prime- and boost-inoculations of between 10 and 50 µg of purified AHSV VP7 quasi-crystals, and the control group (n=5) inoculated with a control inoculum prepared in the identical manner as the vaccine but using a pRIC3.0 expression vector lacking VP7. Western immunoblot analysis of the humoral response showed stimulation of very high titres of anti-VP7 antibodies 28 days after the boost-inoculation. In addition, RNA-seq transcriptome profiling of guinea-pig spleen derived RNA was used to investigate the global immune response to AHSV-5 VP7 quasi-crystals. Thirty genes involved in innate and adaptive immunity were found to be significantly differentially expressed ($q \leq 0.05$) in experimental transcriptome data when compared to the control. Differential expression of genes involved in T-helper (Th)1, Th2 and Th17 cell differentiation and the T-cell receptor signalling pathway suggest a possible cell-mediated immune response to AHSV-5 VP7 quasi-crystals. Upregulation of several important cytokines and cytokine receptors were noted in response to VP7 quasi-crystals e.g. TNFSF14,

CX3CR1, IFNLR1 and IL17RA. TNFSF14 and CX3CR1 play a role in T-cell proliferation and cytotoxic T-cell responses respectively. And IFNLR1 and IL17RA are key cytokines in antiviral defences. Upregulation of IL17RA suggests a Th17 response which has been reported as a key component in AHSV immunity.

To the best of our knowledge, this study is the first to report the expression of plant-produced AHSV VP7 quasi-crystals and the first time that the cell-mediated immune response to these particles has been assessed. While further investigation is needed, these results suggest that AHSV-5 VP7 quasi-crystals produced in *N. benthamiana* are immunogenic, inducing both humoral and cell-mediated responses.

ABBREVIATIONS

aa	amino acid
AEC	Animal Ethics Committee
AHS	African horse sickness
AHSV	African horse sickness virus
APC	antigen presenting cell
BCIP	5-bromo-4-chloro-3-indoxyl-phosphate
BeYDV	Bean yellow dwarf virus
bp	base pair(s)
BSA	bovine serum albumin
BTV	Bluetongue virus
CaMV	Cauliflower mosaic virus
CD	cluster of differentiation
CLP(s)	core-like particle(s)
CLR(s)	C-type lectin receptor(s)
CPMV	Cowpea mosaic virus
CTL(s)	cytotoxic T-lymphocyte(s)
DE	differentially expressed
DISA	Disabled Infectious Single Animal
DIVA	differentiate infected from vaccinated animals
DNA	deoxyribonucleic acid
dpi	days post-infiltration
ds	double-stranded
ECRA	Entry-component Replication-Abortive
EDTA	ethylenediamine tetra-acetic acid
EHDV	Epizootic haemorrhagic disease of deer virus
ELISA	enzyme-linked immunosorbent assay
EU	endotoxin unit
FDR	false discovery rate
FHS	Faculty of Health Sciences
FMDV	Foot-and-mouth disease virus
g	gram(s)
GO	gene ontology
hr(s)	hour(s)
IFN	interferon
IL	interleukin
kb	kilobase(s)
kDa	kilodalton(s)
KEGG	Kyoto Encyclopedia of Genes and Genomes
LAV	live-attenuated vaccine
LB	lysogeny broth

LBB	Luria-Bertani broth
LIR	long intergenic region
LSD	lysosomal storage disorder
M	molar
MES	2-morpholinoethanesulfonic acid
mg	milligram(s)
MHC-I	major histocompatibility complex class I
MHC-II	major histocompatibility complex class II
min	minute(s)
ml	millilitre(s)
mM	millimolar
MVA	modified vaccinia Ankara
NBT	nitroblue tetrazolium
NFDM	non-fat dairy milk
ng	nanogram(s)
NK	natural killer
NKT	natural killer T-cells
nm	nanometre(s)
NS	non-structural
OBP	Onderstepoort Biological Product
OD	optical density
OIE	Office International des Epizooties (World Organisation for Animal Health)
O/N	overnight
p	plasmid
PAGE	polyacrylamide gel electrophoresis
PAMP	pathogen-associated molecular pattern
PBMC	peripheral blood mononuclear cells
PBS	phosphate-buffered saline
PBS-T	PBS-Tween
PCR	polymerase chain reaction
pp	post-purification
PRR	pattern recognition receptor
RAF	Research Animal Facility
RCF	relative centrifugal field
RIN	RNA integrity number
RNA	ribonucleic acid
RT-qPCR	reverse-transcription polymerase chain reaction
rpm	revolutions per minute
s	second(s)
SDS	sodium dodecyl sulphate
SHUV	Shuni virus
SIR	short intergenic region
SNT	Serum neutralisation tests
ss	single-stranded
SUV	subunit vaccine
SWV	swine fever virus
TBSV	Tomato bushy stunt virus
T-DNA	transfer DNA

TEM	transmission electron microscopy
Tfh	T follicular helper
Th	T-helper
Ti	tumour-inducing
Tris	Tris(hydroxymethyl)aminomethane
TSP	total soluble protein
V	Volts
v	volume
VIB	virus inclusion bodies
VLP	virus-like particle(s)
VP	viral protein(s)
w	weight
WT	wild type

Symbols

α	alpha
β	beta
µg	microgram(s)
µl	microlitre(s)
µm	micrometre(s)
%	percentage
°C	degrees Celsius

TABLE OF CONTENTS

ABSTRACT **4**
ABBREVIATIONS **6**
TABLE OF CONTENTS **9**
CHAPTER 1: LITERATURE REVIEW **11**

1.1 Introduction **11**
1.2 AHSV Geographical Distribution **12**
1.3 African Horse Sickness Virus **15**

1.3.1 *Orbiviruses*: AHSV and Blue Tongue Virus (BTV) 15
1.3.2 AHSV Capsid Structure 16
1.3.3 AHSV Genome 17
1.3.4 AHSV Protein Function 19
1.3.5 AHSV VP7 Trimer Structure and Quasi-Crystal Formations 21
1.3.6 *Orbivirus* Transcription and Replication Cycle 24

1.4 AHSV Vaccines **26**

1.4.1 Challenges Surrounding Current AHSV Vaccines 26
1.4.2 Current AHSV Prophylactic Vaccine Research 27
1.4.3 Host Immune Responses and Vaccine Design 31
1.4.4 Particulates and Quasi-Crystals as Vaccines 32
1.4.5 AHSV VP7 Quasi-Crystals as a Potential Candidate Vaccine 32

1.5 Plant Expression Systems **34**
1.6 Conclusions **35**
1.7 Project Aims and Objectives **36**

CHAPTER 2: EXPRESSION & PURIFICATION OPTIMISATION OF AHSV-5 VP7 QUASI-CRYSTALS **38**

2.1 Introduction **38**
2.2 Materials & Methods **42**

2.2.1 Constructs 42
2.2.2 *Agrobacterium* Inoculum Preparation for Infiltration of recombinant AHSV-5 VP7 in *N. benthamiana* leaves 44
2.2.3 Agroinfiltration and Optimisation of AHSV-5 VP7 Transient Expression in *N. benthamiana* 45
2.2.4 Agroinfiltration and Optimisation of AHSV-5 VP7 Quasi-Crystal Purification by Density Gradient Ultracentrifugation 46
2.2.5 SDS-PAGE, Coomassie Staining and Western Immunoblot Analysis 53
2.2.6 Transmission Electron Microscopy 54
2.2.7 Fixing, Dehydration and Embedding of Agroinfiltrated Leaf Sections for *In Situ* TEM 55

2.3 Results **56**

2.3.1 Transient Expression of AHSV-5 VP7 in *N. benthamiana* 56
2.3.2 Purification of AHSV-5 VP7 Quasi-Crystals by Density Gradient Ultracentrifugation 61
2.3.3 *In Situ* TEM of Recombinant pRIC-AHSV5-VP7 Agroinfiltrated *N. benthamiana* Leaves 83

2.4 Discussion **83**

CHAPTER 3: TESTING THE IMMUNOGENICITY OF AHSV-5 VP7 QUASI-CRYSTALS AS A CANDIDATE VACCINE **90**

3.1 Introduction 90
3.2 Materials & Methods 94
3.2.1 Assessing AHSV-5 VP7 Quasi-Crystal Stability 94
3.2.2 AHSV-5 VP7 Quasi-Crystal Vaccine Preparation for Immunogenicity Studies 95
3.2.3 Guinea-Pig Immunogenicity Study 96
3.2.4 Testing Neutralisation Capability of AHSV-5 VP7 Quasi-Crystals 98
3.2.5 Analysis of Humoral Immune Response to AHSV-5 VP7 Quasi-Crystals 98
3.2.6 Transcriptome Profiling: Analysing the Cell-mediated Immune Response to AHSV-5 VP7 Quasi-crystals 100
3.3 Results 105
3.3.1 Assessing Stability of AHSV-5 VP7 Quasi-Crystals 105
3.3.2 Guinea-Pig Immunogenicity Study 109
3.3.3 Analysis of Humoral Immune Response to AHSV-5 VP7 Quasi-Crystal 110
3.3.4 RNA-seq Transcriptome Profiling 115
3.4 Discussion 140
CHAPTER 4: CONCLUSIONS 146
APPENDIX A: GenBank Accession Numbers 151
REFERENCES 152

CHAPTER 1: LITERATURE REVIEW

1.1 Introduction

African horse sickness (AHS) is a noncontagious but highly infectious arthropod-borne disease affecting equines, and due to many disastrous epizootics it is considered a notifiable viral disease by the World Organisation for Animal Health (OIE) (Bekker et al. 2014). During infection, AHSV successfully replicates in endothelial cells and macrophages, and endothelial cell damage results in the deterioration of the vascular system. Circulatory and respiratory impairments manifest in four pathological forms of the disease: horse sickness fever, a cardiac form (dikkop), a mixed form and a pulmonary form (dunkop) (Bailey 2016; Clift and Penrith 2010). The pulmonary and mixed forms are most common amongst horses, ponies and European donkeys, with a mortality rate of approximately 95% in susceptible horses (Wade-Evans et al. 1997; Zientara et al. 2015; Mellor et al. 1990; Bekker et al. 2014; Maree et al. 2016). Mules and African donkeys are commonly affected by milder forms of the disease, horse sickness fever and the cardiac form, with a mortality rate of less than 50% (Wade-Evans et al. 1997; Zientara et al. 2015). Zebras on the other hand are generally asymptomatic and are likely to be a natural reservoir for AHSV (Maree and Paweska 2005).

The causative agent of AHS is the African horse sickness virus (AHSV), a non-enveloped *Orbivirus* from the *Reoviridae* family, which is predominantly transmitted by the biting midge, *Culicoides imicola* (Bekker et al. 2014; Maree et al. 2016; Wade-Evans et al. 1997; Zientara et al. 2015). AHSV spreads rapidly and replicates efficiently in both mammalian and insect hosts and is therefore a major threat to equids (Venter et al. 2009). All nine AHSV serotypes are endemic to sub-Saharan Africa, particularly eastern and southern Africa, with many reoccurring outbreaks extending to northern parts of Africa and the Mediterranean region (Maree et al. 2016; Wade-Evans et al. 1997; Zientara et al. 2015). AHS has placed a severe burden on the South African equine industry. Horses, donkeys and mules support many people's livelihoods in South Africa and millions of people globally, particularly in poor and marginalised communities. These working animals are used in numerous sectors including agriculture, construction, tourism, mining, public transport and sport (Bekker

et al. 2014; Zientara et al. 2015). The horse racing industry is reported to contribute 2.71 billion ZAR annually to South Africa's GDP and, according to a recent audit, supports approximately 100 000 employees (Ngalonkulu 2018). South Africa's horse export industry also attracts substantial financial investment, and stringent quarantine restrictions and trade embargoes pose a great threat to this industry (Bekker et al. 2014).

The only effective way to control AHS is by widespread vaccination programmes as no successful therapeutic treatment exists. However, commercially used live-attenuated multivalent vaccines cause viraemia in the host and pose the threat of generating novel viruses through re-assortment between field and vaccine strains. These biosafety concerns have motivated the search for safer and more affordable vaccines that are also effective against multiple AHSV serotypes (Mellor et al. 1990; Wade-Evans et al. 1997).

This study aims to produce AHSV-5 VP7 quasi-crystals in *Nicotiana benthamiana* with the intention of producing a safer and potentially more economical prophylactic vaccine.

1.2 AHSV Geographical Distribution

AHS was first recognised during the 1719 epizootics in South Africa where 1700 animal fatalities were documented (Zientara et al. 2015). The causative agent of AHS, AHSV, is endemic to sub-Saharan Africa. However, repeated wide-scale epizootics have extended to North Africa, the Arabian Peninsula and many Mediterranean countries as a result of international horse trade (Maree et al. 2016; Wade-Evans et al. 1997; Zientara et al. 2015; Bailey 2016; Martinez-Torrecuadrada et al. 1996). Five years of AHS outbreaks occurred from 1987 to 1992 in Spain, Morocco and Portugal (Basak et al. 1996; Bailey 2016). And very recently (March/April 2019) outbreaks in Chad (http://www.oie.int/wahis_2/public/wahid.php/Reviewreport/Review?page_refer=MapFullEventReport&reportid=30236) and Cameroon (http://www.oie.int/wahis_2/public/wahid.php/Reviewreport/Review?page_refer=MapFullEventReport&reportid=30190) were reported. Only 69 countries are listed by the World Organisation for Animal Health (OIE) as AHS-free member countries (**Figure 1.1**).

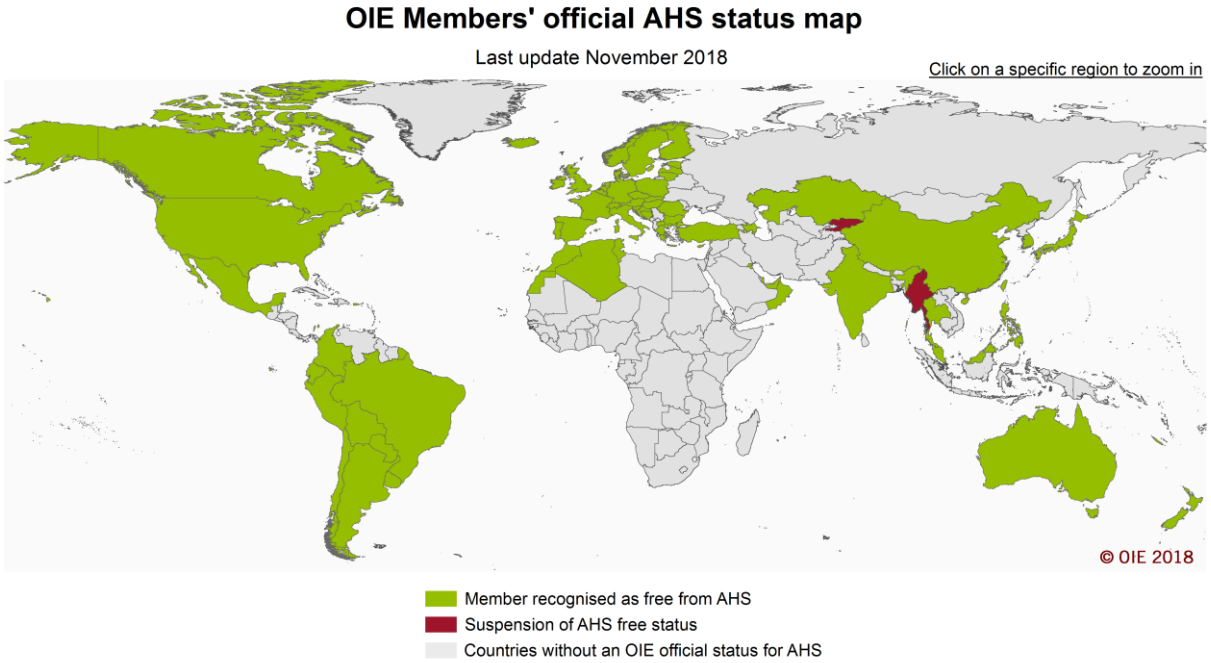

Figure 1.1: OIE representation of AHS status globally as per November 2018. Green indicates AHS free regions, Maroon indicates that the OIE AHS free status has been suspended for these countries, and Grey indicates countries which do not have an OIE official AHS free status. The above image can be found at: http://www.oie.int/en/animal-health-in-the-world/official-disease-status/african-horse-sickness/en-ahs-carte/. (World Organisation for Animal Health 2018)

The distribution of AHS is seasonal as it depends on the abundance and prevalence of its insect vectors. For many years *C. imicola* was considered to be the main field vector for AHS but research by Venter et al. (2000) disputed this and showed that *C. bolitinos,* a common bluetongue virus (BTV) vector, can also efficiently transmit AHSV. *C. imicola* is commonly active during the rainy season in the tropics and during summer and autumn in the temperate regions, while *C. bolitinos* is widely spread across southern Africa and commonly found in cooler regions where *C. imicola* is scarce (Venter et al. 2009; Zientara et al. 2015). Climate change has had an indisputable impact on the distribution of AHSV insect vectors (Zientara et al. 2015). In the last decade, *C. imicola* has expanded northwards to AHS-free regions and devastating outbreaks of the closely related BTV, which is also transmitted by several *Culicoides* species, have been reported in northern Europe. These observations along with the spread of serotype 2 and 7 into western and eastern Africa, where typically

only serotype 9 was present, suggests that AHSV may follow closely behind BTV's expansion (Zientara et al. 2015; Bailey 2016).

The occasional explosive emergence of AHSV over a short period of time indicates that a large number of infected insect vectors are present and that AHSV is presumably circulating continuously in a reservoir herd. These reservoir herds may be the large populations of wild zebra in the Kruger National Park in South Africa, as zebra herds breed throughout the year enabling the continual transmission of AHSV to naive foals (Zientara et al. 2015). It is likely that outbreaks amongst these populations spread southwards and consequently threaten the surrounding horse populations (Thompson et al. 2012). To facilitate the safe exportation of horses to Europe, the South African authorities implemented an AHS-free zone, -surveillance zone and -protection zone in the Western Cape Province which was accepted by the European Union in 1997 (**Figure 1.2**). In recent years, numerous outbreaks have been reported in the surveillance zone, the most notable ones occurring in 1999, 2004, 2011, 2013, 2014 and 2016. These outbreaks have devastating impacts on the equine export industry and concerns have been raised about the spread and elevated frequency of AHSV outbreaks in national and international AHS-free zones (Zientara et al. 2015; Grewar et al. 2019).

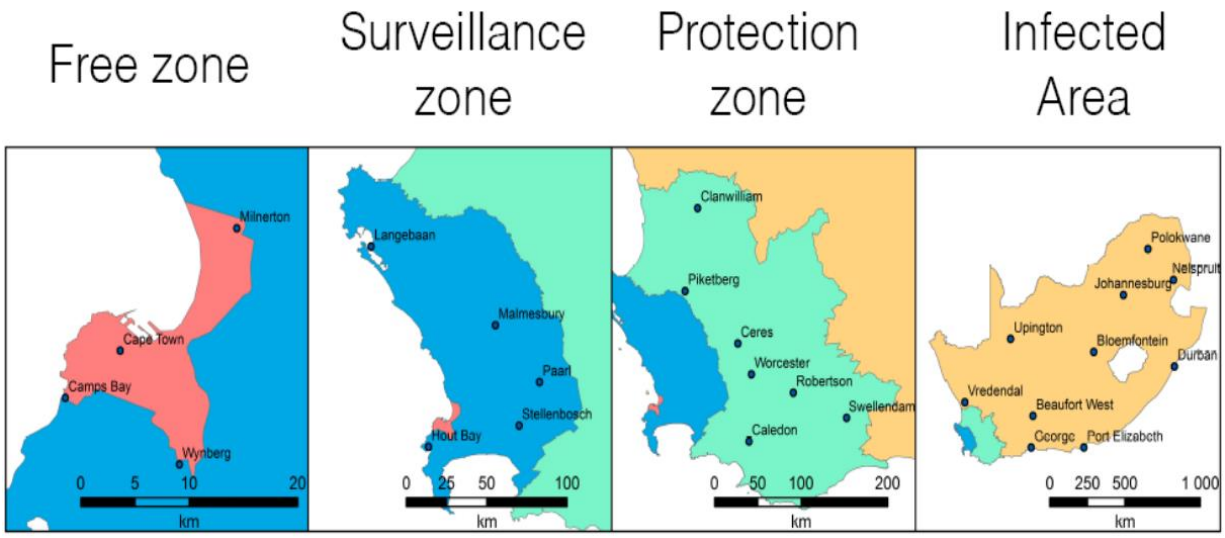

Figure 1.2: Depiction of the AHS-controlled area (free zone, surveillance zone and protection zone) in South Africa. Pink indicates AHS free zones, Blue indicates the AHS surveillance zone, Green indicates the AHS protection zone, and Orange indicates the endemic region for AHS/ AHS infected area. The above image can be found at: https://www.agriorbit.com/registration-of-zebra-in-ahs-controlled-areas-in-sa/. Image courtesy of the State Veterinarian: Boland and Directorate: Animal Health at the Department of Agriculture, Forestry and Fisheries (DAFF). *Image used with permission from the publisher.*

1.3 African Horse Sickness Virus

1.3.1 *Orbiviruses*: AHSV and Bluetongue Virus (BTV)

AHSV is a non-enveloped *Orbivirus* from the *Reoviridae* family, a family which consists of 15 genera. The *Orbivirus* genus is the largest genus comprising 29 species of non-enveloped viruses characterised by a circular capsid composed of 32 capsomeres. These capsomeres enclose the segmented and double-stranded RNA genome (Zientara et al. 2015; Bailey 2016; Roy et al. 1994). The bluetongue virus (BTV) is the prototype of the *Orbivirus* genus, and AHSV and BTV are closely related members as demonstrated by comparisons of the amino acid sequences of AHSV-4 and BTV-10. (Bekker et al. 2014; Wade-Evans et al. 1997). These comparisons suggest a recent common ancestor and that strong selective pressures of their specific host's immune system may have caused their divergence (Zientara et al. 2015). As a closely related virus, the AHSV virion is modelled around the structure of the *Orbivirus* prototype, BTV, which has been studied more extensively.

1.3.2 AHSV Capsid Structure

The non-enveloped icosahedral virions of AHSV are approximately 80 nm in diameter and the genome consists of ten linear double stranded (ds) RNA segments encoding seven structural proteins (VP1 – VP7) and four non-structural proteins (NS1, NS2, NS3, NS3a and NS4) which have been observed in AHSV-infected cells (**Figure 1.3**) (Faber et al. 2016; Maree et al. 2016; Zientara et al. 2015; Bailey 2016; Basak et al. 1996; Dennis 2019; Monastyrskaya et al. 1997). The structural proteins are arranged in three clear concentric layers: VP2 and VP5 form the outer capsid shell of mature virions and the inner capsid consists of two major core proteins, a VP7 surface layer and a VP3 lower layer (**Figure 1.3**) (Mertens et al. 2004). VP7 and VP3, the inner capsid, encloses the core particle which forms the transcriptase complex and consists of the (ds) RNA genome arranged in three layers of RNA and three minor enzymatic proteins (VP1, VP4 and VP6) (Maree et al. 2016; Zientara et al. 2015; Zwart et al. 2015; Mertens et al. 2004).

The VP2 and VP5 outer capsid shell is removed when the virus passes through the cell membrane (Basak et al. 1996). The subcore remains, consisting of 120 copies of VP3 which are arranged as 12 decamers and this is stabilised by 780 molecules of VP7 arranged as 260 trimers forming a highly ordered T=13 lattice (Basak et al. 1996; Bekker et al. 2017; Monastyrskaya et al. 1997; Williams et al. 1998).

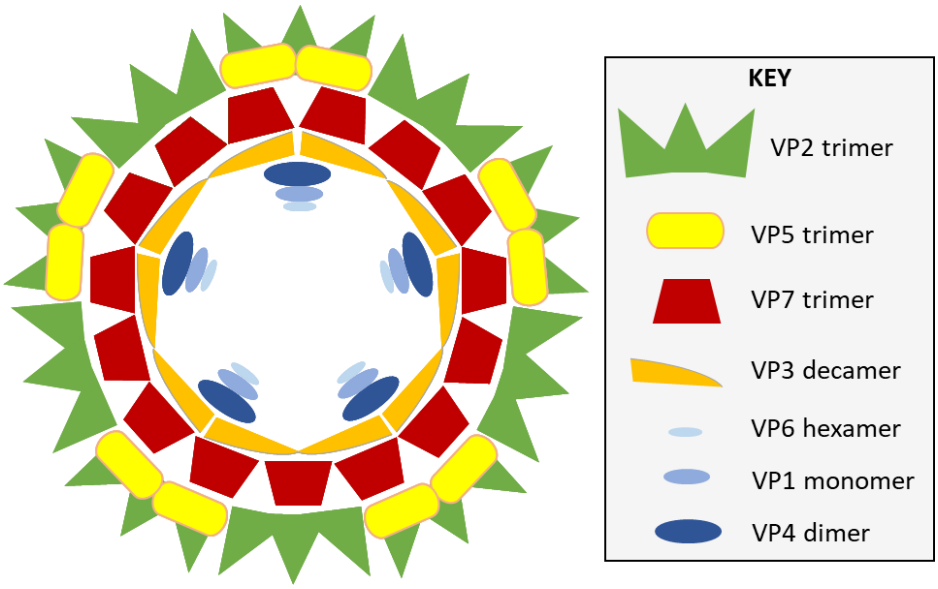

Figure 1.3: A diagrammatic representation of the structure of AHSV, including the outer capsid proteins (VP2 and VP5), the major core proteins (VP3 and VP7) and the minor structural proteins (VP1, VP4 and VP6). Image adapted from Mertens *et al*. (2004)**.**

1.3.3 AHSV Genome

The AHSV genome consists of ten linear (ds)RNA segments which can be differentiated according to their molecular mass using polyacrylamide gel electrophoresis. These (ds)RNA segments have been characterised according to their order of migration, three large (L1-L3), three medium (M4-M6) and four small segments (S7-S10) (**Figure 1.4**). The AHSV genome has been sequenced in its entirety with the sequences mainly based on serotype 4 (AHSV-4) (Zientara et al. 2015).

Each of the (ds)RNA genome segments encode one polypeptide with the exception of the two smallest segments (S9 and S10) (**Figure 1.4**). S9 encodes both the enzymatic minor protein VP6 and the non-structural protein NS4. And the S10 gene contains two in-frame AUG initiation codons for translation initiation and these are responsible for the synthesis of two alternative NS3 gene products, the minor non-structural proteins NS3 and NS3A (van Staden et al. 1995; Zwart et al. 2015). The outer capsid proteins, VP2 and VP5, are encoded by the L2 and M6 (ds)RNA segments respectively (**Figure 1.4**) (Thompson et al. 2012). The L2 gene is 3203 nucleotides in length encoding a 1051 amino acid VP2 protein, and the M6 gene is 1564 nucleotides in length encoding a 504 amino acid VP5 protein product (Williams et al. 1998). The

major core proteins, VP3 and VP7, are encoded by segments L3 and S7 respectively and contain serogroup-specific antigenic determinants (**Figure 1.4**) (Zientara et al. 2015). The L3 RNA segment is 2715 nucleotides in length and encodes a 905 amino acid VP3 protein, while the S7 gene is only 1047 nucleotides and encodes for a 349 amino acid VP7 protein product (Williams et al. 1998). The enzymatic minor proteins, VP1 and VP4 are encoded by L1 and M4 respectively, and the third enzymatic minor protein, VP6, is encoded by the S9 gene, 1169 nucleotides in length and translating into a 369 amino acid protein (**Figure 1.4**). The non-structural proteins NS1 and NS2 are encoded by the RNA segments M5 and S8 respectively and along with NS3 and NS3A are involved in virus replication, morphogenesis and the release of viral particles from the infected cell (**Figure 1.4**). The RNA segments, which encode for NS1 and NS2, are highly conserved amongst all serotypes. Whereas segments encoding NS3/NS3A, VP2 and VP5 are more variable with VP2 holding the dominant serotype-specific antigenic sites (Kanai et al. 2014). Due to the genetic variability amongst VP2 serotypes, nine serotypes of AHSV have been determined. In addition, VP2 holds the virus receptor-binding site and is commonly used in recombinant vaccine development (Bekker et al. 2014; Kanai et al. 2014; Maree et al. 2016; Thompson et al. 2012; Zientara et al. 2015).

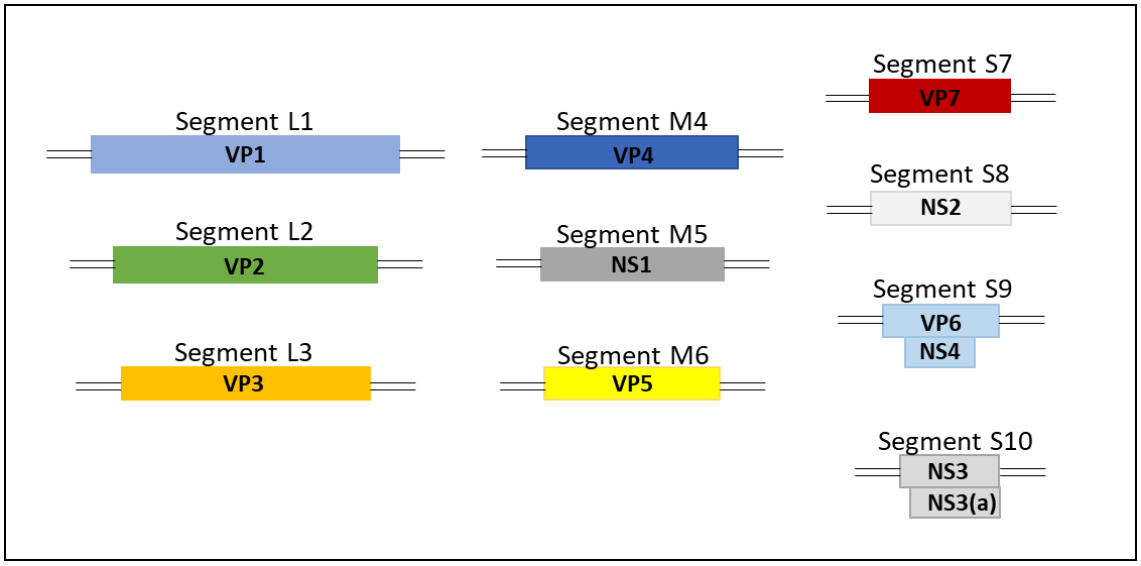

Figure 1.4: A representation of the (ds)RNA *Orbivirus* genome. The genome consists of three large (L1-L3), three medium (M4-M6) and four small (S7-S10) (ds)RNA segments. Image adapted from Viralzone**.**

1.3.4 AHSV Protein Function

The outer capsid proteins, VP2 and VP5 are the most variable structural proteins of AHSV and during infection are responsible for virus attachment and cell entry. After entry the loosely bound outer capsid proteins are shed and the core particle is released into the cytoplasm to become transcriptionally active (Bekker et al. 2014; Hassan et al. 2001; Thompson et al. 2012; Chuma et al. 1992). Both trimeric VP2 and VP5 are capable of interacting with the surface of the core in the absence of their fellow outer capsid protein (Maree et al. 2016). Hassan et al (1999 and 2001) investigated the biological functions of BTV-10 VP2 and VP5. Purified VP2 demonstrated virus hemagglutinin activity and was shown to be solely responsible for virus entry into mammalian cells. In addition, purified VP2 showed a strong affinity for binding to glycophorin A, which is a major intrinsic membrane protein of erythrocytes. This suggests that VP2 may play a role in the transmission of BTV by its hematophagous insect vector to its mammalian host. Furthermore, AHSV VP2 elicits serotype-specific antibodies and contains the main sites for antibody-mediated virus neutralisation as a result of being the most exposed outer capsid protein (Martínez-Torrecuadrada and Casal 1995; Zientara et al. 2015). The outer capsid protein VP5 also contains neutralising epitopes but does not induce antibody-mediated neutralisation to the same degree as VP2, which is likely due to its low surface exposure. Sequence-based structure analysis of BTV-10 VP5 showed that VP5 possesses two amino-terminal amphipathic helices which are characteristic features for virus-cell penetration. Furthermore, purified VP5 was able to modify the permeability of mammalian and *Culicoide* cell membranes and induce cytotoxicity (Hassan et al. 2001; Hassan and Roy 1999b).

VP3 and VP7 are the major core proteins. VP3 dimers form a thin inner scaffolding on which the capsomeres are arranged and VP7 is the principal component of these core capsomeres (Basak et al. 1996; Kar et al. 2004; Williams et al. 1998; Bailey 2016; Mertens 2004). Both VP3 and VP7 are highly conserved amongst the nine AHSV serotypes with VP7 having greater than 98% amino acid identity between serotypes. VP3 is the most conserved protein between the orbiviruses AHSV and BTV. In contrast, AHSV VP7 is serogroup-specific and partially conserved between the serogroups AHSV, BTV and epizootic haemorrhagic disease of deer virus (EHDV) with the AHSV and BTV VP7 amino acid sequence sharing only 43% identity (Bailey

2016; Bekker et al. 2017; Zientara et al. 2015; Basak et al. 1996; Guthrie et al. 2009; Martinez-Torrecuadrada et al. 1996). VP3 controls the size and organisation of the capsid structure, and VP7 is the major immunodominant antigen and plays a role in cell entry (Bailey 2016; Mertens 2004). The AHSV VP7 protein has 349 amino acid residues and consists of 260 trimers forming a T=13 lattice. It is a highly hydrophobic protein and forms insoluble crystals ranging between 3-5 µm during natural AHSV infection (Basak et al. 1996; Bailey 2016). Orbivirus serogroups are distinguishable by serological assays and recognised as distinct species using the serogroup-specific antigen VP7 (Maree and Paweska 2005). AHSV VP7 is also highly immunogenic which has been concluded from various experiments including one by Martinez-Torrecuadrada et al. (1996), where the inclusion of purified AHSV VP7 to an AHSV VP2 and VP5 inoculate increased antibody titres in horses from 1280 to 20 480 (enzyme-linked immunosorbent assay (ELISA) titres were determined by the authors as the reciprocal of the highest dilution giving three times the blank (pre-immunisation sera) A_{405}). Additionally, due to its immunodominance, VP7 is widely utilised in serological assays to identify AHSV infections (Maree and Paweska 2005; Martinez-Torrecuadrada et al. 1996).

AHSV VP1, VP4 and VP6 are the three core enzymatic minor proteins. VP1 is highly conserved and has been identified as the putative viral RNA polymerase, and VP4 the capping enzyme with typical guanylyltransferase features (Martinez-Costas et al. 1998; Vreede and Huismans 1998; Bailey 2016; Mertens 2004). VP6 is suspected to be the helicase of AHSV, binding to both single-stranded (ss)RNA and (ds)RNA and is likely to play a role in the encapsidation of RNA (de Waal and Huismans 2005; Turnbull et al. 1996).

The non-structural proteins (NS1-NS4) are involved in virus replication, virus assembly and the release of viral particles from the infected cell (Kanai et al. 2014; Roy et al. 1994). NS1 self-assembles into tubules within the cytoplasm of infected cells and attaches to intermediate filaments of the cytoskeleton. NS1 may be involved in virus transportation and morphogenesis (Zwart et al. 2015). NS2 is responsible for the formation of virus inclusion bodies (VIBs); these VIBs are involved in the replication and assembly of new viral core particles. NS3 and NS3A are glycosylated membrane proteins which mediate the release of mature virus particles from the cell by membrane association and permeabilisation. The exact function of NS4 in viral morphogenesis is

unclear, however, it seems to play a role in nuclear localisation (Zwart et al. 2015; Bailey 2016; Mertens 2004).

1.3.5 AHSV VP7 Trimer Structure and Quasi-Crystal Formations

As mentioned previously, VP7 is one of the major core AHSV structural proteins consisting of 349 amino acids (aa) and is approximately 37.8 kDa in size (Williams et al. 1998; Zientara et al. 2015; Bailey 2016). AHSV VP7 is highly immunodominant, and is therefore commonly used as an AHSV antigen for serogroup-specific diagnostic assays (Bekker et al. 2017; Zientara et al. 2015). Furthermore, it is largely insoluble and highly hydrophobic, as determined by amino acid sequence analyses and the Kyte and Doolittle (1992) algorithm, and consists of a high amount of hydrophobic amino acids: alanines (12.9%), prolines (6.6%), valines (10.9%), leucines (7.2%) and methionines (3.7%) (aa percentages were calculated using the peptide property online tool ProtParam on the ExPASy bioinformatics resource portal (https://web.expasy.org/protparam/)) (Basak et al. 1996; Kyte and Doolittle 1982; Roy et al. 1991; Gasteiger et al. 2005). During AHSV infection of cells or in isolation in insect cells, VP7 spontaneously aggregates into large flat hexagonal crystal arrays consisting of six-membered rings, a feature which is unique to AHSV (Basak et al. 1996; Bekker et al. 2014; Burroughs et al. 1994). Researchers have observed a wide range of AHSV VP7 quasi-crystal sizes after recombinant baculovirus infections i.e. 100 nm to 25 µm (Burroughs et al. 1994; Chuma et al. 1992; Maree and Paweska 2005; Wall et al. 2017; Bailey 2016). However, during natural AHSV infection of mammalian and insect cells or expression by Modified vaccinia virus Ankara (MVA) the sizes of crystals observed in the cytoplasm generally range between 3-5 µm (Bailey 2016). The role of VP7 quasi-crystals during AHSV infection remains unclear (Basak et al. 1996; Bekker et al. 2014; Burroughs et al. 1994). However, similar insoluble aggregates have been found to be beneficial to viruses as sites where viral replication and assembly is promoted. It has also been hypothesised that these crystalline-particles may contribute to the pathogenesis of the virus as they are likely to be detrimental to normal cellular functions and destroy the cell membrane (Bekker et al. 2014).

The AHSV VP7 crystalline-structure is homotrimeric and the monomers (denoted A, B and C) are likely bound by intermolecular disulphide bridges between Cys_{161} and Cys_{195} residues (Basak et al. 1996; Bekker et al. 2017). Each VP7 monomer has two

well defined domains, an upper domain and a lower domain (**Figure 1.5**) (Roy 2008). Due to AHSV VP7's insolubility, only the more hydrophilic upper domain has been resolved by X-ray crystallography, which consists of the central region of the polypeptide (aa 121-249) and is folded into an anti-parallel β-sandwich (**Figure 1.6**) (Basak et al. 1996). The lower domain is predicted to be similar to the closely related BTV VP7, containing five α-helices from the N-terminal region (aa 1-120) and four α-helices from the C-terminal region (aa 250-349) connected by a series of hydrophobic loops (Basak et al. 1996; Monastyrskaya et al. 1997). The two domains are twisted in an anticlockwise direction around the three-fold axis so that the upper domain of one monomer rests on the C-terminal region of its adjacent monomer's lower domain (**Figure 1.5**) (Basak et al. 1996). The C-terminal helices of the lower domain are generally positioned above the N-terminal helices, with one of the latter helices forming a flat surface which interacts with the VP3 sub core (Basak et al. 1996; Monastyrskaya et al. 1997; Rutkowska et al. 2011).

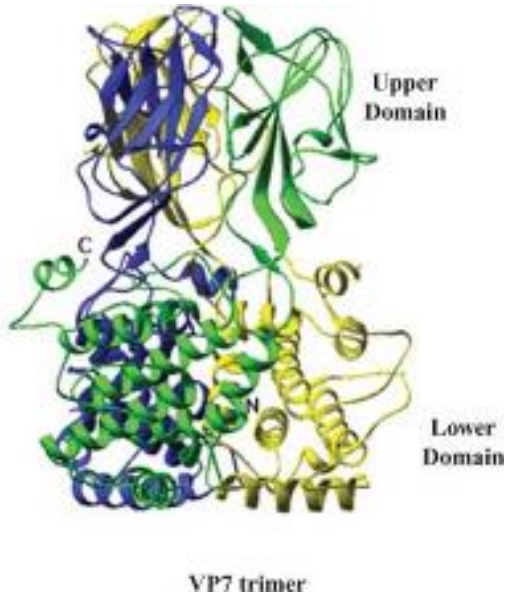

Figure 1.5: An image of the VP7 trimer atomic structure based on the prototypical *Orbivirus* BTV. VP7 monomer interaction and upper and lower domains are displayed (https://link.springer.com/article/10.1007%2Fs12013-008-9009-4). Image courtesy of Springer Nature (Roy 2008). *Image used with permission from the publisher.* (RCSB Protein Data Bank DOI: 10.2210/pdb1BVP/pdb).

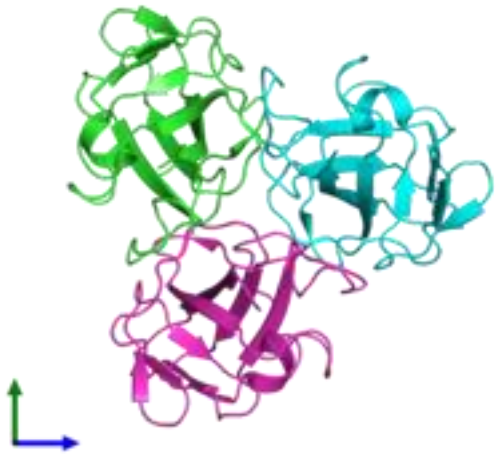

Figure 1.6: An image of the AHSV VP7 upper domain homo-trimer arrangement. The above image can be found at: https://www.ebi.ac.uk/pdbe/entry/pdb/1ahs/analysis. Image courtesy of the Protein Data Bank in Europe (PDBe) (Basak et al. 1996). *Image used with permission from the publisher.*

The trimerisation of VP7 is not sufficient for the stable formation of virus particles. VP7 therefore interacts with both outer capsid proteins, VP2 and VP5 and its fellow core protein VP3. Helix 2 (aa 26-43) forms part of the flat-bottomed base in the lower domain of VP7 and is rich in hydrophobic amino acids. The correct amino acid composition and folding of the hydrophobic flat base is essential for stable interactions between the VP3 scaffold and VP7 trimers (Maree et al. 2016; Monastyrskaya et al. 1997). With regard to AHSV VP7 trimer-trimer interactions and crystal formation, Bekker *et al*. (2017) recently highlighted the hydrophobic amino acids $Ile_{228,}$ Pro_{230} and Ala_{167} as contributors to the inherently strong trimer-trimer interactions and therefore to the assembly of AHSV VP7 crystals.

AHSV VP7 and the closely related BTV VP7 have 29% aa identity and 51% aa homology in the upper domains, whilst the N-terminal region of the lower domain has 65% identity and 82% homology and the C-terminal region has 42% identity and 61% homology (Monastyrskaya et al. 1997). Differences between these closely related *Orbivirus* proteins include an AHSV VP7 RGD motif Ala-167, Gly-168, and Gln-169 located on a flexible loop found deep within the core in comparison to the easily accessible BTV VP7 RGD motif Arg-168–Gly-169–Asp-170 (Basak et al. 1996). In

contrast to AHSV VP7, BTV VP7 is soluble and does not form crystals during natural infection. By inserting BTV derived peptides into specific VP7 hydrophobic regions various researchers have attempted to manipulate the solubility of AHSV VP7 (Bekker et al. 2017; Monastyrskaya et al. 1997; Rutkowska et al. 2011).

1.3.6 *Orbivirus* Transcription and Replication Cycle

The AHSV transcription and replication process has not been as well studied as that of the closely related prototypic *Orbivirus* BTV. However, due to their highly similar biochemical properties and nearly identical morphology, much of the AHSV transcription and replication process has been modelled around that of BTV's (Manole et al. 2012; Roy and Sutton 1998; Dennis et al. 2019). The degree of similarity between AHSV and BTV is further demonstrated by the exchange of genome segments during simultaneous infection. This re-assortment amongst *Orbiviruses* has been hypothesised as a reason for their rapid evolution (Zientara et al. 2015).

The initial contact and binding of the *Orbivirus* to the host cell receptors is mediated by the outer capsid protein VP2 leading to receptor-mediated endocytosis. VP7 is hypothesised to also play a role in cell entry (Basak et al. 1996; Hassan et al. 2001; Hassan and Roy 1999b; Roy et al. 1991; Roy et al. 1994). The clathrin-coated virus then moves into the host's cell and fuses with its endosome (**Figure 1.7**) (Hassan and Roy 1999a; Mertens et al. 2004). The outer capsid proteins VP2 and VP5 separate from the virus core after translocating into the low pH environment within the endosome. VP5 then penetrates the endosomal membrane which causes the release of the virus core into the host cell's cytoplasm. VP2 and VP5 are subsequently degraded and the core-associated transcriptase complex is activated (**Figure 1.7**) (Mertens et al. 2004). The enzymatic minor-proteins, VP1 (RNA polymerase), VP4 (RNA capping enzyme) and VP6 (RNA helicase) are responsible for transcription of the ten dsRNA genome segments. The enzymatic proteins and dsRNA are housed safely within the core to protect the virus from the host's antiviral system. The synthesised mRNA is then released from pores in the VP3 core layer into the host cell's cytoplasm and is subsequently translated into viral proteins. Viral proteins are transported to virus inclusion bodies (VIBs), the sites where virus assembly and replication occurs in the host cell's cytoplasm. NS2 mediates VIB formation and core particle assembly (Bailey 2016; Mertens 2004; Hassan and Roy 1999a; Mertens et al.

2004). Further research has shown that BTV VP3 is essential for the recruitment of VP7 trimers to VIBs during particle assembly and that VP7 does not form any morphological structures unless in the presence of VP3 (Bailey 2016; Bekker et al. 2014; Kar et al. 2007). The addition of VP7 to the sub-core is important for the core's stability and therefore protection of the transcriptase complex. VP7 is therefore added prior to the release of the particles from VIBs (Matsuo and Roy 2013). VP2 and VP5 are however added subsequent to the release of the assembled core particles from VIBs. Fully formed virus particles are then released via budding, a process which is likely to be mediated by NS3 (**Figure 1.7**) (Bailey 2016; van Niekerk et al. 2003; Mertens et al. 2004).

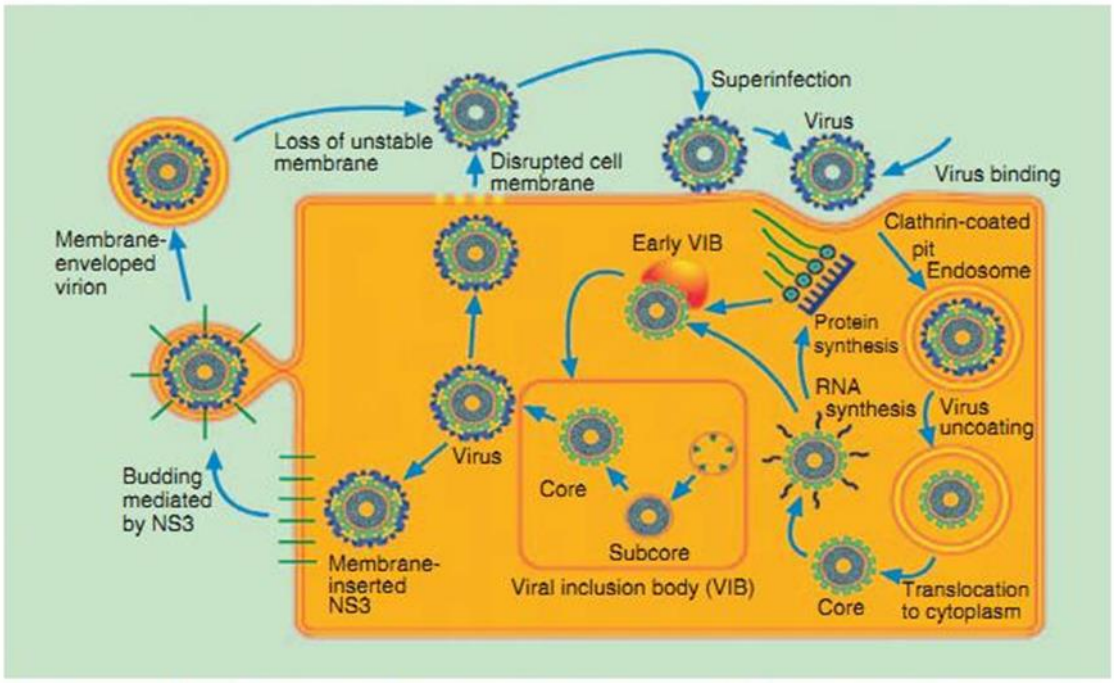

Figure 1.7: *Orbivirus* replication cycle. Transcription and replication cycle based on the prototypic *Orbivirus* BTV. Image courtesy of *Veterinaria Italiana* (Mertens et al. 2004). *Image used with permission from the publisher.*

AHSV replication takes place in regional lymph nodes and subsequently spreads through the host's circulatory system by infecting and replicating in hematocytes such as peripheral blood mononuclear cells (PBMCs). Secondary viraemia occurs once AHSV has further infected and replicated in the lungs, spleen and lymphoid tissues (Bailey 2016).

1.4 AHSV Vaccines

1.4.1 Challenges Surrounding Current AHSV Vaccines

To date, no successful therapeutic treatment exists for AHS and in South Africa the disease is controlled primarily by preventative vaccination programmes, surveillance and zoning regulations (Maree et al. 2016; Maree and Paweska 2005). Unfortunately, the commercially used multivalent inactivated or live-attenuated vaccines (LAV) are associated with several disadvantages: the generation of progeny viruses with novel phenotypes can occur due to gene segment re-assortment between different serotypes; inoculating animals from new geographical regions with vaccines originating from South Africa may introduce foreign topotypes into that region; and lack of DIVA (differentiating infected from vaccinated animals) compliance which complicates import/export processes (Kushnir et al. 2012; Maree et al. 2016; Mellor et al. 1990; Wade-Evans et al. 1997; Dennis et al. 2018; Zientara et al. 2015). A recent AHSV serotype 1 outbreak in the Western Cape Province AHS-surveillance zone, during April and May 2016, was caused by a reversion to virulence of the presently used LAV (Grewar et al. 2019). Due to the above mentioned risks the AHSV live-attenuated vaccines have not been licenced for use within the European Union (Bailey 2016).

The first AHSV vaccines produced in the 1930's were based on attenuated virus strains which had been accomplished by passing the live virus through the brain of a juvenile mouse. This resulted in a high level of protection in equids but often caused side effects such as encephalitis. Further attenuation was then established by means of viral passage in cell culture and surprisingly these attenuated viruses remain as the basis of the present day Onderstepoort Biological Product (OBP) vaccines (Zientara et al. 2015; Mellor and Hamblin 2004; Mertens 2004). During the 1987-1991 AHSV epizootics in Europe an inactive vaccine was administered, however after the epizootic was concluded this vaccine was withdrawn as it was reported to be too expensive to produce and multiple boosters were needed to induce protection (Kushnir et al. 2012; Bailey 2016; Mellor and Hamblin 2004; Mirchamsy and Taslimi 1968).

Developing more effective prophylactic vaccines is a difficult task as these vaccines need to protect susceptible equids against multiple serotypes. In the case of AHSV,

immunisation using a single serotype is highly ineffective as it does not generate a broad immune response, and in endemic regions like South Africa multiple serotypes circulate during outbreaks. Consequently, combinatorial vaccines are currently administered in South Africa in the form of two polyvalent vaccines from OBP which must be administered 28 days apart. The first vaccine includes the AHSV serotypes 1,3 and 4 and the second includes serotypes 2, 6, 7 and 8. These vaccines do not contain serotype 9 as serotype 6 and 9 generally cross-react. In addition, AHSV-9 is considered to have low virulence and its prevalence in South Africa is seldom reported. Furthermore, serotype 5 has been excluded from the OBP vaccine as its inclusion has resulted in severe side effects and fatalities (Maree et al. 2016; Wade-Evans et al. 1997; Zientara et al. 2015; Maree and Paweska 2005).

The Terrestrial Animal Health Code of the OIE recommends that strict regulations are adhered to during equid exportation to prevent movement of infected equines into AHSV-free countries. One of these unfortunate but necessary recommendations is that these horses should not have been vaccinated against AHS within the last 40 days due to the difficulty in distinguishing between vaccinated and infected animals (DIVA compliance) (Zientara et al. 2015).

1.4.2 Current AHSV Prophylactic Vaccine Research

Vaccination is central to the control of AHSV and many potential vaccines have been investigated with little success in producing a more effective, safe and affordable vaccine than the conventional prophylactics (Maree et al. 2016). These have included DNA vaccines (Romito et al. 1999), inactivated vaccines (House et al. 1994; Lelli et al. 2013a; Mellor and Hamblin 2004; Mirchamsy and Taslimi 1968), various recombinant subunit vaccines (SUVs) using baculovirus expression vectors (Martínez-Torrecuadrada and Casal 1995; Scanlen et al. 2002; Roy and Sutton 1998; Kanai et al. 2014; Martinez-Torrecuadrada et al. 1996) and those based on attenuated poxvirus vectors (Castillo-Olivares et al. 2011; Chiam et al. 2009; Guthrie et al. 2009; Calvo-Pinilla et al. 2014; Alberca et al. 2014; Manning et al. 2017; Calvo-Pinilla et al. 2018), core-like particle (CLP) vaccines (Maree et al. 1998), virus-like particle (VLP) vaccines (Dennis 2019; Maree et al. 2016), ‘synthetically derived’ reassortments of AHSV using reverse genetics (Lulla et al. 2017; Lulla et al. 2016; van de Water et al. 2015; van Rijn

et al. 2018) and VP7 trimer based vaccines (Bailey 2016; Rutkowska et al. 2011; Wade-Evans et al. 1997).

During the AHSV outbreaks in Europe from 1987 to 1992 an inactivated monovalent AHSV-4 vaccine called Equipest® was available. The vaccine was based on purified AHSV-4 inactivated using formalin. This vaccine resulted in immunity and protection in horses against AHSV-4 for a period of 6 months post-vaccination. However, this vaccine had various disadvantages in that it was serotype specific, multiple inoculation boosters were needed and the vaccine was reported to be expensive to produce. It was therefore removed off the market after AHSV was eradicated in Europe after 1992 (Bailey 2016; Mellor and Hamblin 2004; Mirchamsy and Taslimi 1968).

Recombinant SUVs are usually based on the surface components of a virus such as the outer capsid or major core proteins and are safer than live attenuated or inactivated vaccines as they do not contain any replicative properties. Unfortunately, SUVs often elicit a low immune response therefore requiring higher doses and boosters and the co-administration of adjuvants. One such recombinant SUV was investigated by Martinez-Torrecuadrada (1996) and colleagues: this study showed that a recombinant baculovirus vector co-expressing VP2, VP5 and VP7 induced neutralising antibodies and protection. A few years later, another study focusing on the baculovirus vector, demonstrated that soluble AHSV-5 VP2, triggers neutralising antibodies in guinea pigs and induces full protection in horses when combined with saponin adjuvants (Scanlen et al. 2002).

Many SUV studies have focused on live attenuated poxvirus vectors such as recombinant modified vaccinia Ankara (MVA) and the recombinant canarypox virus vector (Alberca et al. 2014; Chiam et al. 2009; Guthrie et al. 2009; Calvo-Pinilla et al. 2014; Manning et al. 2017; Calvo-Pinilla et al. 2018; Castillo-Olivares et al. 2011). One such pilot study demonstrated that MVA vaccines expressing AHSV VP2 and VP7 stimulated immunogenicity in ponies and another showed that MVA-VP2 vaccination provided successful protection against the disease and against viraemia (Alberca et al. 2014; Chiam et al. 2009; Calvo-Pinilla et al. 2014). In addition, Guthrie et al. (2009) developed a recombinant canarypox virus vectored (ALVAC®) vaccine co-expressing AHSV-4 VP2 and VP5 and this was shown to be successful in protective immunisation against a live virus challenge.

In 1998, a study by Wade-Evans *et al*. assessed insoluble AHSV VP7 crystals as a subunit vaccine using an established mouse model. After exposure to a lethal dose of AHSV-7, 80-100% of immunised mice survived in comparison to a 0-20% survival rate observed in non-immunised mice. Immunisation using denatured VP7 crystals or bacterial GST-VP7 fusion proteins as opposed to intact VP7 crystals resulted in lower levels of protection, suggesting that the conformation of VP7 crystals is important for protection. In addition, the duration of viraemia was highly reduced in immunised mice in comparison to non-immunised mice post-infection. However, the circulating antibody titres against AHSV VP7 were low (log_{10} titres less than 1.0) suggesting that protection was therefore unlikely to be as a result of an antibody-mediated immune response. The authors suggested that in the absence of neutralising antibodies cell-mediated immunity may enable cross-reactive protection (Wade-Evans et al. 1997). A more recent study by Bailey (2016) also demonstrated that VP7 crystals did not yield a favourable humoral response.

Virus-like particles (VLPs) have been considered as one of the most favourable alternatives to conventional vaccines and a major advancement in SUV development. There are presently four recombinant VLP based vaccines on the market: GlaxoSmithKline's Cervarix® and Merck and Co., Inc.'s Gardasil® for the human papillomavirus, and GlaxoSmithKline Engerix® and Merck and Co., Inc.'s Recombivax HB® for the hepatitis B virus (Kushnir et al. 2012; Zientara et al. 2015). VLPs usually include the structural viral proteins which have an innate ability to self-assemble. Furthermore, these VLPs mimic the native virus but do not contain the replicative transcription complex and are therefore non-pathogenic, lacking infectious material. They do however induce a strong humoral and cellular immune response as a result of the display of native conformations of diverse epitopes (Kushnir et al. 2012). In 1998 Maree et al. produced AHSV core-like particles (CLPs) in insect cells. However, this was a complex system involving the co-infection of two baculoviruses which expressed VP3 and VP7 separately, and only produced partial CLPs. In 2016 a further study was conducted by the same authors which involved assembling the major viral core and outer capsid proteins (VP2 and VP5) using a single recombinant baculovirus for co-synthesis of VP3 and VP7 to produce more affordable alternatives (Maree et al. 2016). While VLPs induce a stronger protective immune response than recombinant single-protein subunit vaccines, VLP vaccines may not be as cost-effective as they are more

complicated to produce involving the co-expression and assembly of viral structural proteins (VP2, VP3, VP5 and VP7) into virus-like structures, which often leads to problems in terms of reproducibility. This may cause further difficulties when upscaling, particularly as a result of the necessity for polyvalent vaccines which cover all nine serotypes (Maree et al. 2016). A more recent alternative which seems very promising is the generation of plant-produced AHSV VLPs which are likely to be more cost-effective to produce and scalable (Dennis 2019).

Another vaccine strategy is to create chimeric CLPs by displaying foreign epitopes on the surface of viral or multimeric particles. A prerequisite for this strategy is that chimeric particles need to assemble into stable CLPs. Both BTV and AHSV have been explored as foreign antigen presenting VLPs (Burroughs et al. 1994; Rutkowska et al. 2011). Rutkowska et al. originally investigated the possibility of using insoluble AHSV VP7 chimeric particles as a vaccine delivery system and then extended their study to incorporate soluble chimeric VP7 trimers. They reasoned that one could take advantage of the preferential formation of VP7 trimers during CLP assembly, and that these VP7 trimers may invoke a better humoral immune response than a single CLP. Their study determined that soluble chimeric VP7 proteins were able to form stable trimers and induce a strong humoral immune response, and that the neutralisation antibody titres resulting from the soluble fraction of VP7 was approximately ten times higher than that of the insoluble VP7 crystalline-particles (Rutkowska et al. 2011).

Furthermore, a reverse genetics approach has been utilised by some researchers generating ‘synthetic’ reassortments of AHSV serotypes. The Disabled Infectious Single Animal (DISA) vaccine which lacks NS3/NS3A (van de Water et al. 2015; van Rijn et al. 2018) and the Entry Competent Replication-Abortive (ECRA) vaccine using a VP6-defective AHSV strain in combination with in *trans* complementation of VP6 (Lulla et al. 2017; Lulla et al. 2016).

For an effective AHSV vaccine both a humoral and cellular immune response is needed. This has been shown to be essential in protective immunity against BTV (Andrew et al. 1995; Calvo-Pinilla et al. 2014; Jeggo et al. 1984). Many researchers have focused on the humoral immune response to AHSV (Alberca et al. 2014; Calvo-Pinilla et al. 2014; Castillo-Olivares et al. 2011; Chiam et al. 2009; Kanai et al. 2014; Manning et al. 2017; Calvo-Pinilla et al. 2018; Martinez-Torrecuadrada et al. 1996;

Bailey 2016). However, few have focused on the role of cellular immunity in protection against AHSV. Those that have shown both humoral and cellular immune responses, are based on pox viral vectors MVA expressing AHSV-4 VP2 and NS1 and canarypox virus expressing AHSV-4 VP2 and VP5 (ALVAC®). These candidate vaccines were shown to induce CD8 T-cell proliferation (Guthrie et al. 2009; Pretorius et al. 2016). In addition, a DNA vaccine encoding AHSV VP2 demonstrated a cytotoxic T-cell response (Romito et al. 1999).

1.4.3 Host Immune Responses and Vaccine Design

After pathogen infection, endogenous (heat shock proteins and nucleic acid damage) and exogenous (pathogen or adjuvant) cues alert the innate immune system to destroy the foreign antigen. These non-specific innate immune responses function within a few hours after infection and include the pattern recognition receptors (PRR) described in **Chapter 3** (Cui et al. 2014; Storni et al. 2005; Takeuchi and Akira 2010). PRRs recognise pathogen-associated molecular patterns (PAMPs) and trigger their associated signalling cascades leading to the production of various cytokines (**Chapter 3**) (Cui et al. 2014; Takeuchi and Akira 2009, 2010). If the pathogen is not destroyed by the quick acting innate responses, adaptive responses are triggered by PRR pathways (Storni et al. 2005). These adaptive responses include humoral immune responses i.e. B-cell receptor pathway activation and cell-mediated immune responses i.e. T-cell receptor pathway activation (Refer to **Chapter 3** for more detail) (Janeway et al. 2001; Savignac et al. 2010; Dorner and Radbruch 2007).

Viruses often have mechanisms which can evade or supress the immune system. For this reason, it is important that both humoral and cell-mediated immune responses are required for an effective AHSV vaccine. Furthermore the survival of vaccinated animals which demonstrate low antibody titres after a lethal challenge suggest that cell-mediated responses are important in AHSV immunity (Guthrie et al. 2009; Martinez-Torrecuadrada et al. 1996; Wade-Evans et al. 1997; Scanlen et al. 2002). Live vaccines generally induce strong T-cell responses. Whilst subunit vaccines, particularly soluble proteins, can often induce a humoral response and neutralising antibodies but rarely stimulate favourable T-cell responses (Storni et al. 2005). Furthermore, effective vaccines need to target antigen presenting cells (APCs) such as dendritic cells as these are well known T-cell activators. Soluble proteins do not

activate APCs and their immunogenicity is therefore low unless adjuvants are added (Storni et al. 2005).

1.4.4 Particulates and Quasi-Crystals as Vaccines

There is little research available on the use of protein crystals as vaccines, however there are numerous reasons why particulates may be favourable vaccine candidates. Firstly, due to the highly ordered and repetitive nature of protein crystals, immunologically important epitopes are likely to be more efficiently presented to the immune system as evidenced by comparative studies (Fehr et al. 1998; St Clair et al. 1999) and this is hypothesised to enhance B-cell and T-cell responses (**Chapter 3**) (St Clair et al. 1999; Bailey 2016; Storni et al. 2005; Rutkowska et al. 2011). Several studies have demonstrated that particulate antigen delivery systems induce Th1 and CTL responses similar to that of attenuated and inactivated viruses (Friede and Aguado 2005; Sharp et al. 2009; Storni et al. 2005).

Secondly, particulates are more effectively phagocytosed by APCs than soluble antigens and are therefore more efficient in presenting these to the adaptive immune system (Bachmann and Jennings 2010; Manolova et al. 2008; Snapper 2018; Vidard et al. 1996). Many particulate vaccine adjuvants have been shown to increase the dendritic cell uptake of antigens, increase IL-1 secretion and enhance cell-mediated immune responses (Sharp et al. 2009). APC presentation of particulates is covered in more detail in **Chapter 3**.

Other advantages include quasi-crystal stability and biodegradability (Bailey 2016). Furthermore, natural pathogens are particulate in nature and it therefore stands to reason that an effective vaccine would do well to mimic this characteristic (Storni et al. 2005).

1.4.5 AHSV VP7 Quasi-Crystals as a Potential Candidate Vaccine

AHSV VP7 is a highly immunodominant protein which has been demonstrated by high titres of anti-VP7 antibodies during natural AHSV infection (Bailey 2016). It is therefore widely used to identify AHSV infections using rapid diagnostic serological assays, enzyme-linked immunosorbent assays (ELISAs) and quantitative reverse-transcription polymerase chain reaction (RT-qPCR) assays (Maree and Paweska 2005; Martinez-

Torrecuadrada et al. 1996; Bailey 2016; Zientara et al. 2015). It is also serogroup-specific, with at least 98% amino acid similarity between serotypes, a trait which is very beneficial in vaccine design as it negates the need for a multivalent vaccine (Chuma et al. 1992; Williams et al. 1998; Bailey 2016).

An AHSV VP7 quasi-crystal vaccine would be simple to produce as it only relies on one structural protein for assembly and has the benefit of a highly ordered and repetitive quasi-crystal conformation. This repetitive display of epitopes is likely to enhance B-cell and T-cell immune responses (Bailey 2016; Friede and Aguado 2005; Rutkowska et al. 2011; St Clair et al. 1999; Storni et al. 2005). The closely related BTV VP7 has been shown to possess serotype-cross-reactive T-cell epitopes (Mertens 2004). Since AHSV VP7 is similar to BTV it may contain similar epitopes and comparably enhance the immune response to the virus (Martinez-Torrecuadrada et al. 1996).

Wade-Evans *et al.* (1997) speculated that the crystalline conformation of AHSV VP7 is important for inducing protection as VP7 crystals were more efficient at protecting mice against a live challenge when compared to soluble VP7. In contrast, other studies suggest that AHSV VP7 is more immunogenic when solubilised, however these studies are focused on the humoral response and did not investigate the cell-mediated response (Bailey 2016; Martinez-Torrecuadrada et al. 1996). AHSV challenge studies have demonstrated protection in animals with low antibody titres and no neutralising antibodies therefore suggesting other immune mechanisms such as cell-mediated immunity (Martinez-Torrecuadrada et al. 1996; Wade-Evans et al. 1997). For many years the main criteria for efficacious vaccines has been a humoral response and neutralising antibodies. However, the cell-mediated immune response may be as important in vaccine design.

Furthermore, AHSV VP7's intrinsic ability to aggregate and self-form crystalline structures can be exploited to produce large quantities of quasi-crystals to meet the high demands for vaccine production (Maree and Paweska 2005; St Clair et al. 1999).

1.5 Plant Expression Systems

In recent years, plant expression systems have received increasingly more attention as an alternative to the more traditional prokaryotic and eukaryotic cell culture platforms for vaccine production. Plant expression systems are advantageous as they are safer to produce, have a low risk of pathogen contamination and the literature suggests upstream processes are easily scalable and more cost-effective (Chen et al. 2013; Rybicki 2009; Mir-Artigues et al. 2019; Schillberg et al. 2019). In terms of upstream processes, the infrastructure and raw materials needed for plant expression systems are less expensive when compared to cell-based platforms, as plants can be grown in greenhouses and only require light, water and soil/ hydroponic medium, while cell-based systems require fermenters installed in dedicated facilities, sterile equipment, complex media and bioreactors. Furthermore, in terms of scalability, cell-based systems are restricted by the fermenter's capacity and production speed, while plant expression platforms can be increased by simply growing more plants (Mir-Artigues et al. 2019). However, downstream processes for protein purification can still be complicated and costly as plant-specific compounds such as phenols and toxic alkaloids (particularly in the case of *Nicotiana* plants) need to be removed before plant-produced recombinant proteins can be used as pharmaceuticals (Chen et al. 2013).

N. benthamiana is commonly used for the transient expression of recombinant proteins as it is a resilient species which easily withstands *Agrobacterium*-mediated-infiltration (agroinfiltration) and produces high yields of biomass (Chen et al. 2013). Agroinfiltration is an efficient gene-delivery technique where *Agrobacterium tumefaciens* is introduced into plants by syringe- or vacuum-infiltration (Chen et al. 2013; Maclean et al. 2007). In this technique, the natural plant pathogen *A. tumefaciens* has been manipulated to deliver genes of interest into plant host cells and induce transient expression of the required recombinant protein (Kapila et al. 1997; Maclean et al. 2007; Chen et al. 2013). Various expression vectors are used for agroinfiltration, including non-viral and plant-virus based vectors which have been integrated into modified *A. tumefaciens* plasmids (Chen et al. 2013; Regnard et al. 2010; Rybicki 2009). *Agrobacterium*-mediated-infiltration and plant expression vectors are covered further in **Chapter 2**.

The current technology surrounding plant-produced pharmaceuticals is well developed and many examples of successfully produced plant-derived antibodies and proteins exist (Paul and Ma 2011; Lomonossoff and D'Aoust 2016). Plant-produced VLP candidate vaccines for porcine circovirus (Gunter et al. 2019), AHSV (Dennis et al. 2018) and influenza (Pillet et al. 2019) have been shown to elicit strong immune responses in mice, horses and humans respectively. And the aforementioned VLP influenza vaccine candidate produced by Medicago is presently in phase III clinical trials (https://clinicaltrials.gov/ct2/show/NCT03739112). Furthermore, a plant-produced swine fever virus (SWV) E2 subunit vaccine demonstrated complete protection in SWV challenged pigs (Laughlin et al. 2019). A plant-derived therapeutic enzyme for the lysosomal storage disorder (LSD), Gaucher's Disease, has been developed (Chen et al. 2013). And the lysosomal enzyme, beta-galactosidase, has been produced in moss as a therapeutic for LSDs such as Fabry disease (Shen et al. 2016). Many plant-produced therapeutics are in clinical trials such as the HIV neutralising human monoclonal antibody (P2G12) which is in phase I clinical trials (Ma et al. 2015) and a conjugated vaccine for treatment of B-cell follicular lymphoma (Tuse et al. 2015). Furthermore a plant-produced combination of monoclonal antibodies, ZMapp™, was shown to reverse severe Ebola virus symptoms (Qiu et al. 2014).

1.6 Conclusions

Repeated AHSV outbreaks in national and international AHS-free zones are reported to have devastating economic consequences. The presently used prophylactic vaccines have detrimental side-effects and a new inexpensive, safer, DIVA compliant alternative is therefore required.

The cell-mediated immune response to vaccines has generally been overlooked but increasing evidence has shown that it is essential for a successful AHSV candidate vaccine. AHSV VP7 is highly immunogenic and its quasi-crystal formation is likely to generate strong cell-mediated responses. Furthermore plant-produced AHSV VP7 quasi-crystals have the added benefits of plant production platforms in that they are safer, easily scalable and upstream cultivation is more cost-effective.

To the best of our knowledge this is the first attempt to express and purify AHSV VP7 quasi-crystals from *N. benthamiana* plants. And furthermore, the first time that the

humoral and cell-mediated immune responses to VP7 quasi-crystals have been investigated.

1.7 Project Aims and Objectives

This study aims to develop recombinant plant-produced AHSV-5 VP7 quasi-crystals for use as a potential candidate vaccine.

The first objective was to optimise the expression conditions of AHSV-5 VP7 in *N. benthamiana*. An AHSV-5 VP7-encoding gene cloned into two plant expression vectors (pEAQ-*HT* and pRIC3.0) was used for small-scale (<10 g) agroinfiltration of *N. benthamiana* plants. Time trials and comparison studies were carried out by AHSV-5 VP7 detection using SDS PAGE, western blotting and Coomassie staining. To this end the optimal parameters: expression vector, culture density (OD_{600}) and harvest day post-infiltration, were selected.

The second objective involved optimising the purification protocol and characterising VP7 quasi-crystals. Discontinuous gradient ultra-centrifugation was performed, and levels of plant produced VP7 protein detected by western blotting and Coomassie stained gels. Formation of VP7 quasi-crystals was confirmed by transmission electron microscopy (TEM) and concentrations quantified by gel densitometry.

The third objective was to investigate the intra-cellular formation of quasi-crystals by embedding AHSV-5 VP7 agroinfiltrated leaves and performing *in situ* TEM.

The final objective was to test the vaccine potential of plant-produced AHSV-5 VP7 quasi-crystals. This included assessing the stability of AHSV VP7 quasi-crystals at 4°C, -20°C and -80°C over a 28-week period and analysing their ability to induce an AHSV VP7-specific immune response (humoral and cell-mediated) in guinea pigs. Immunogenicity studies were carried out at the Research Animal Facility (RAF) at the University of Cape Town (UCT). Guinea-pig sera were analysed for anti-VP7 antibodies by western blotting to investigate the humoral immune response, and the cell-mediated immune response was considered by analysing the differential expression of immune related genes. This was accomplished by extracting spleen-derived RNA, RNA-sequencing, bioinformatics using the Illumina Basespace platform

and R (R Core Team 2018) was used to analyse the global immune response from DESeq2 results.

CHAPTER 2: EXPRESSION & PURIFICATION OPTIMISATION OF AHSV-5 VP7 QUASI-CRYSTALS

2.1 Introduction

VP7 is one of the major core structural proteins of the African horse sickness virus (AHSV), which forms 260 stable trimers and assembles into a highly-ordered lattice surrounding a thin scaffold of 120 copies of VP3. AHSV VP7 is essential for viral replication and holds the major serogroup-specific antigenic sites (Bekker et al. 2017). It is also a highly immunogenic protein and for this reason has been widely utilised in serological assays to identify infections and distinguish between *Orbivirus* serogroups (Maree and Paweska 2005; Martinez-Torrecuadrada et al. 1996). The trimeric particles of AHSV VP7 have been shown to be stable at room temperature in the presence of 10% (w/v) sodium dodecyl sulphate (SDS), revealing strong monomer-monomer interactions (Monastyrskaya et al. 1997; Rutkowska et al. 2011). These intermolecular contacts are likely due to disulphide bridges formed between Cys_{195} residues of interacting VP7 monomers, as recently discovered by Bekker *et al.* (2017). Additionally, the polar residues Arg_{255} and Lys_{123} have been highlighted as potential contributors to polymerisation (Bekker et al. 2017).

AHSV VP7 is a largely insoluble and hydrophobic protein consisting of a high amount of alanines (12.9%), prolines (6.6%), valines (10.9%), leucines (7.2%) and methionines (3.7%) as concluded by Basak *et al.* (1996) and Roy *et al.* (1991) and validated by the peptide property online tool ProtParam on the ExPASy bioinformatics resource portal (https://web.expasy.org/protparam/)) (Gasteiger et al. 2005). Rutkowska *et. al.* (2011) found less than 10% of AHSV WT VP7 in the soluble fractions following density gradient purification. And whilst the top domain has been resolved using x-ray crystallography, its insolubility has resulted in difficulties in resolving the bottom domain. Basak *et al*. (1996) and Rutkowska *et al.* (2011) have suggested that the residues Ala_{167} (top domain) and Leu_{345} (bottom domain) respectively play a role in AHSV VP7 insolubility. And Monastyrskaya *et al.* (1997) suggested that residues of the top domain are critical in the insolubility of AHSV VP7 when compared to the solubility of the closely related bluetongue virus (BTV) VP7.

During AHSV particle assembly, VP7 trimers inherently aggregate into large flat hexagonal quasi-crystals both during AHSV infection and *in vitro* (Maree et al. 2016; Rutkowska et al. 2011). Reported crystal sizes range from 100 nm to 25 µm (Burroughs et al. 1994; Chuma et al. 1992; Maree and Paweska 2005; Wall et al. 2017; Bailey 2016). A length of 250 µm has been reported by Chuma *et al.* (1992). Bailey *et al.* (2016) observed that crystal sizes generally range between 3-5 µm during natural AHSV infection or when AHSV VP7 is expressed by Modified vaccinia virus Ankara (MVA). Whilst expression using baculovirus seems to result in a wider distribution of sizes up to 25 µm. They speculated that this may be due to the regulatory mechanisms driving expression and that abnormally high expression levels could result in irregular crystal sizes (Bailey 2016).

Little is known about AHSV VP7 aggregation, crystal formation and its role in the virus life cycle (Rutkowska et al. 2011; Wall et al. 2017). It is possible that these crystals are just a by-product rather than a crucial component of the viral replication process (Burroughs et al. 1994). Some studies have suggested that the majority of VP7 may preferentially aggregate to form crystals as opposed to virions (Bekker et al. 2014; Maree et al. 1998) and that this may be a way for the virus to evade the host's immune system (Bailey 2016). However, this seems unlikely since the repetition of immunologically important epitopes in crystal formations is more likely to enhance immune responses (Friede and Aguado 2005; Rutkowska et al. 2011; St Clair et al. 1999). Bekker *et al*. (2017) recently highlighted the hydrophobic amino acids $Ile_{228,}$ Pro_{230} and Ala_{167} as potential contributors to the crystal formation of AHSV VP7; in earlier research by the same authors it was shown that intracellular aggregation is due to inherent properties of AHSV VP7 rather than influences by other AHSV proteins, cellular trafficking or degradation pathways (Bekker et al. 2014).

During AHSV infection, VP7 is a highly immunodominant antigen and for this reason it is broadly used in ELISAs as an AHSV diagnostic tool (Bailey 2016; Maree and Paweska 2005; Martinez-Torrecuadrada et al. 1996). Furthermore, cross-linking of immunogenic epitopes in AHSV VP7 crystalline particles is considered to induce B-cell and T-cell immune responses (Friede and Aguado 2005; Rutkowska et al. 2011; St Clair et al. 1999). Due to its immunogenicity, various researchers have sought to further characterise AHSV VP7 and examine its potential use in prophylactics and therapeutics. To this end it has been successfully expressed and purified using

recombinant baculovirus-infected Sf9 insect cells (Basak et al. 1996; Bekker et al. 2014; Chuma et al. 1992; Maree and Paweska 2005; Martinez-Torrecuadrada et al. 1996; Rutkowska et al. 2011; Wall et al. 2017) and BHK cells infected with bacterial GST-VP7 fusion protein (Wade-Evans et al. 1997). In recent years plant expression systems have received an increasing amount of attention as an alternative to mammalian, insect and bacterial cell culture systems. Largely because plants offer a more scalable and safer option when compared to these conventional systems (Chen et al. 2013). As mentioned previously, the most commonly used plant species for transient expression of recombinant proteins is *N. benthamiana* as it is resilient and grows rapidly thereby producing high yields of biomass (Chen et al. 2013).

Agrobacterium tumefaciens is a natural plant pathogen which induces tumour formation by stimulating cell division; this relationship has been manipulated to deliver genes of interest into selected plant hosts. *A. tumefaciens'* tumour-inducing (Ti) plasmid includes the transfer DNA (T-DNA) and virulence (*vir*) gene region. The *vir* gene products aid in processing and transporting T-DNA into the plant host cell's nucleus. Here the T-DNA is transcribed and translated using host cell enzymes. On the left and right boundaries of the T-DNA are two 25 bp direct repeats. The DNA positioned between these flanking repeats is tranferred into the plant nucleus and incorporated into the host's genomic DNA (Maclean et al. 2007; Zupan et al. 2000). However, many of these T-DNA copies are not integrated into the genome but rather re-circularise or remain as linear copies in the nucleus and are transiently expressed. Therefore, by modifying the Ti plasmid to replace tumour inducing genes in the T-DNA region with a gene of interest, transient expression of selected proteins can easily be produced by agroinfiltration (Chen et al. 2013). Transient expression, as opposed to stable transformation, is preferable as it is less time-consuming and can therefore produce recombinant proteins rapidly as opposed to the labour-intensive stable transformation technology (Lomonossoff and D'Aoust 2016).

As mentioned in **Chapter 1,** a variety of non-viral or plant-virus based expression vectors can be used for *Agrobacterium*-mediated-infiltration (Chen et al. 2013; Regnard et al. 2010; Rybicki 2009). Previous studies have demonstrated that AHSV-5 VP7 is effectively expressed in *N. benthamiana* using the pEAQ-*HT* and pRIC3.0 expression vectors (Dennis 2019). Having shown this, this study aimed to compare AHSV-5 VP7 quasi-crystal yields resulting from these two virus-based vectors. Both

the pEAQ-*HT* and pRIC3.0 vectors include origins of replication for *E. coli* (ColE1 ori) and *A. tumefaciens* (RK2 ori), and the transgene is inserted within the T-DNA borders and controlled by the Cauliflower mosaic virus (CaMV) 35S promoter (Regnard et al. 2010; Sainsbury et al. 2009).

More specifically, pEAQ-*HT* is a cowpea mosaic virus (CPMV)-based *hyper-trans* expression system which targets expression to the cytoplasm (Thuenemann et al. 2013). It includes the *nptII* gene for kanamycin resistance and TrfA, an essential replication locus for *A. tumefaciens*. In addition, P19, a suppressor of gene silencing, is included in the T-DNA region. P19 originates from the Tomato bushy stunt virus (TBSV) and has been shown to enhance recombinant protein yield (Sainsbury and Lomonossoff 2014; Sainsbury et al. 2009).

pRIC3.0 is a self-replicating plant expression vector based on a mild strain of the bean yellow dwarf virus (BeYDV), a ssDNA circular geminivirus which has been shown to result in high levels of cytoplasmic expression of recombinant proteins (Regnard et al. 2010). Regnard *et al.* (2010) reported that expression via the pRIC vector resulted in 50% more human papillomavirus subtype 16 major CP L1 (HPV-16 L1) and three- to seven-fold more enhanced green fluorescent protein (EGFP) and human immunodeficiency virus subtype C p24 (HIV-1 p24) antigen, when compared to expression by the non-replicating *A. tumefaciens* vector pTRAc. pRIC3.0 includes the *bla* gene for ampicillin/carbenicillin resistance. Within the borders of the *A. tumefaciens* T-DNA are the: BeYDV long intergenic region (LIR) which contains transcriptional promoters and the viral origin of replication, the BeYDV short intergenic region (SIR) which holds transcription termination signals, and the BeYDV *rep* gene which encodes the replication-associated genetic elements. After infiltration and entry into the host's nucleus, the T-DNA is released and re-circularises to form a dsDNA pRIC3.0 replicon. The viral genome replicates by means of rolling circle replication, using Rep and host cell replication proteins, thereby increasing expression of the gene of interest (Regnard et al. 2010).

Whilst plant expression systems have various advantages over the aforementioned conventional platforms, downstream purification processes can be complicated and costly (Chen et al. 2013). This chapter focuses on optimising the expression and purification process of AHSV-5 VP7 quasi-crystals from *N. benthamiana* in order to

produce favourable antigen yields and purity for immunogenicity studies (**Chapter 3**). The most commonly used method for purifying both soluble and insoluble AHSV VP7 from insect and mammalian cells, is sucrose density gradient ultracentrifugation (Basak et al. 1996; Chuma et al. 1992; Maree and Paweska 2005; Martinez-Torrecuadrada et al. 1996; Wall et al. 2017) and some researchers have reported using an additional caesium chloride (CsCl) density gradient (Burroughs et al. 1994; Wade-Evans et al. 1997). In density gradient purification, particles are separated by moving through a density gradient by means of centrifugal force until they reach the equivalent density in the surrounding medium (isopycnic point). Alternative methods used to purify AHSV capsid proteins include affinity chromatography and ammonium sulphate precipitation, however both methods seem to result in conformational alterations possibly due to included chaotropic agents (Martinez-Torrecuadrada et al. 1996; Monastyrskaya et al. 1997). In addition, Bailey *et al.* (2016) applied freeze-thaw cycles and filtration techniques to isolate and extract AHSV VP7 quasi-crystals. In this study density gradient ultracentrifugation was selected for purification as it is a well-known successful method for isolating virus particles. It is also more likely to preserve the conformation of AHSV VP7 quasi-crystals, a critical component in providing protection against a viral challenge, as suggested by Wade-Evans *et al.* (1997). Iodixanol was selected as the preferred density gradient medium as it is non-ionic, non-toxic to cells and metabolically inert and therefore unlikely to affect the conformational integrity of particles. Iodixanol also has the added advantage of low viscosity, low osmolarity and most importantly it is sterile and therefore safer than sucrose for vaccine preparations (Ford et al. 1994).

2.2 Materials & Methods

2.2.1 Constructs

The constructs pRIC3.0-AHSV5-VP2, -VP3, -VP5, -VP7 and pEAQ-AHSV5-VP2, -VP3, -VP5 and -VP7 were kindly provided by S. Dennis, a member of the Biopharming Research Unit (BRU) at the Department of Molecular and Cell Biology (MCB), University of Cape Town (UCT). Consensus gene sequences (GenBank accession numbers shown in Addendum A) were codon optimised (OptimumGene™ codon optimization algorithm) for expression in *N. benthamiana* by S. Dennis and

synthesized by GenScript (Nanjing, China). The pEAQ-*HT* expression vector was provided by G. Lomonossoff (John Innes Centre, UK) and the pRIC3.0 expression vector by G. Regnard (BRU, MCB Department, UCT). S. Dennis electroporated the pRIC3.0-AHSV5-VP7 and pEAQ-AHSV5-VP7 plasmid constructs into *Agrobacterium tumefaciens* strains, GV3101 (containing the helper plasmid pMp90RK) and AGL1 (*A. radiobacter* AGL1-ATCC BAA-101) respectively as described by Maclean *et al.* (2007). These transformed *Agrobacterium* were acquired from the culture collection of the BRU, MCB Department, UCT and streaked onto lysogeny broth (LB) agar plates [1.0% tryptone, 0.5% yeast extract, 0.5% NaCl, 1.5% agar, pH 7.0] which had been supplemented with the appropriate antibiotics (AGL1: kanamycin 50 µg/ml, carbenicillin 25 µg/ml and GV3101::pMp90RK: kanamycin 30 µg/ml, carbenicillin 50 µg/ml, rifampicin 50 µg/ml). Liquid cultures were then grown in LB [1.0% tryptone, 0.5% yeast extract, 0.5% NaCl, pH 7.0] with gentle agitation at 220 rpm O/N at 28°C and glycerol stocks stored at -80°C.

Gene inserts from AGL1/ pEAQ-AHSV5 constructs were confirmed via colony PCR and inserts from GV3101::pMp90RK/ pRIC3.0-AHSV5 were confirmed after DNA extraction and PCR using KAPA Taq DNA polymerase (KAPA Biosystems). The primer sequences used were as follows:

pEAQ-*HT* forward: 5'-TTCTTCTTCTTGCTGATTGG-3'
pEAQ-*HT* reverse: 5'-CACAGAAAACCGCTCACC-3'
pRIC3.0 forward: 5'-CATTTCATTTGGAGAGGACACG-3'
pRIC3.0 reverse: 5'-GAACTACTCACACATTATTCTGG-3'

The pEAQ-AHSV5 constructs' PCR profile consisted of an initial denaturation step at 95°C for 5 min, 30 cycles of denaturation at 95°C for 30 sec, annealing at 51°C for 30 sec, extension at 72°C for 3.5 min and a final extension step at 72°C for 7 min. The PCR profile used for pRIC-AHSV5 constructs included one cycle of initial denaturation at 95°C for 3 min, 30 cycles of denaturation at 95°C for 30 sec, annealing at 59°C for 30 sec, extension at 72°C for 3.5 min and a final extension at 72°C for 4 min.

2.2.2 *Agrobacterium* Inoculum Preparation for Infiltration of Recombinant AHSV-5 VP7 in *N. benthamiana* Leaves

2.2.2.1 Agrobacterium inoculum preparation for small-scale (<10 g) syringe-infiltration

Cultures of recombinant pEAQ-AHSV5-VP2, -VP3, -VP5 & -VP7 and pRIC3.0-AHSV5-VP2, -VP3, -VP5 & -VP7 *A. tumefaciens* cells (AGL1 and GV3101 respectively) were grown to exponential phase as described by Maclean *et al.* (2007) for small-scale (<10 g) syringe-infiltration. Pre-cultures were grown by placing 1 ml glycerol stock into 10 ml LB which had been supplemented with the appropriate antibiotics for each *Agrobacterium* strain, as per **2.2.1**. In addition, 2 mM magnesium sulphate ($MgSO_4$) was added to prevent clumping and the pre-cultures were then incubated O/N at 28°C with gentle agitation (220 rpm).

Cultures were then upscaled. Pre-cultures were used to inoculate 50 ml Luria-Bertani broth (LBB) [0.25% tryptone, 1.25% yeast extract, 0.50% NaCl, 10 mM 2-morpholinoethanesulfonic acid (MES), pH 5.6] which had been supplemented with the antibiotics specified in **2.2.1** and 2 mM $MgSO_4$. Once again, these cultures were incubated O/N at 28°C with gentle agitation (220 rpm).

The inoculum was prepared by diluting cultures to the required optical density (OD_{600}) in resuspension solution [10 mM MES, 10 mM $MgCl_2.6H_2O$, pH 5.6]. 200 µM acetosyringone was added to the diluted cultures which were incubated for 1 hour at room temperature to allow for expression of the *vir*-genes prior to infiltration. Phenolics such as acetosyringone, which are naturally secreted by wounded dicotyledonous plants, assist in inducing the expression of *vir* genes (Chen et al. 2013; Maclean et al. 2007)

2.2.2.2 Agrobacterium inoculum preparation for medium to large-scale (10 g <) vacuum-infiltration

Pre-cultures containing recombinant pRIC3.0-AHSV5-VP2, -VP3, -VP5 and -VP7 constructs were prepared as per **2.2.2.1**, however cultures were upscaled to a greater volume. 50 ml pre-cultures were used to inoculate 500 ml LBB which had been supplemented with the appropriate antibiotics (as noted in **2.2.1**) and 2 mM $MgSO_4$.

In addition, these cultures were induced O/N with 20 µM acetosyringone at 28°C with gentle agitation (220 rpm).

Subsequently, the inoculum for AHSV-5 capsid protein co-expression via vacuum-infiltration was prepared as per **2.2.2.1** at an OD_{600} of 0.5**.**

2.2.3 Agroinfiltration and Optimisation of AHSV-5 VP7 Transient Expression in *N. benthamiana*

2.2.3.1 Determination of optimal expression conditions: Expression vector comparison, and co- vs single-infiltration

Four- to five-week-old *N. benthamiana* plants were syringe-infiltrated, using a blunt-ended syringe, on the abaxial side of the leaf with the inoculum prepared in **2.2.2.1**. An inoculum optical density of 0.5 at 600 nm was selected for this experiment, as previous research by S. Dennis (BRU, MCB Department, UCT) had shown this to be the optimal OD_{600} for AHSV-5 VLP expression and assembly in *N. benthamiana*. Two plants per vector (pEAQ-AHSV5 and pRIC3.0-AHSV5) were co-infiltrated with recombinants VP2: VP3: VP5: VP7 at a ratio of 1: 1: 1: 1. In addition, a further two plants per construct were infiltrated with AHSV-5 VP7 recombinants alone. Plants were grown at 22-25°C under 16-h/ 8-h light/dark cycles until day of harvest. Four leaves (two from each plant) per parameter were harvested 3 days post-infiltration (dpi). pEAQ-*HT* and pRIC3.0 empty vectors were used as negative controls and were infiltrated at an OD_{600} of 0.5.

Crude extracts were prepared by combining the harvested leaves with phosphate-buffered saline (PBS) [10 mM $Na_2HPO_42H_2O$, 137 mM NaCl, 2.7 mM KCl, 2 mM KH_2PO_4, pH 7.4] at a 1:3 (w/v) ratio and homogenised using a pestle and mortar. The extracts were then filtered through one layer of Miracloth™ (Merck, Darmstadt, Germany) and filtrate clarified by centrifugation at 15 900 x g/RCF (max) for 15 min using a benchtop Eppendorf® microcentrifuge 5424 (Merck, Darmstadt, Germany). The supernatant was then prepared for SDS-PAGE analysis by adding 5x sample application buffer [2%SDS, 100 mM Tris-Cl (pH 7.5), 2 mM EDTA, 52% glycerol, 4.3% 2-mercaptoethanol, 0.1% bromophenol blue] and heat denatured at 95°C for 5 min. The total soluble protein (TSP) concentrations were quantified using a NanoDrop 1000

Spectrophotometer (Thermo Fisher Scientific, Massachusetts, USA) at 280 nm and equal amounts of total protein were loaded into each lane. This was selected as the best method for quantification as Maree and Paweska (2005) found that the Bradford assay yielded values of approximately one-tenth of the actual concentration when compared to OD measurements (A280) and values estimated from SDS-PAGE gels using the LumiAnalystTM software. The authors speculated that this may result from reduced binding of the dye to the surface of AHSV VP7 trimers (Maree and Paweska 2005).

2.2.3.2 Determination of optimal expression conditions: Optical density selection and time trials

Four- to five-week-old *N. benthamiana* plants were syringe-infiltrated as per **2.2.3.1** with the inoculum prepared in **2.2.2.1** at an OD_{600} of 0.3, 0.5 and 0.8 to ascertain the optimal optical density for AHSV-5 VP7 protein expression. Six plants were co-infiltrated with pEAQ-AHSV5 recombinants VP2: VP3: VP5: VP7 at a ratio of 1: 1: 1: 1, of which two plants were used per OD_{600} (0.3, 0.5 and 0.8). These co-infiltration ratios and optical density replicates were repeated for the pRIC3.0-AHSV5 recombinants. In addition, a time trial was performed to determine the optimal harvest day for the maximum protein yield. This was done by harvesting three leaves per parameter on 3, 5 and 7 dpi. Negative controls and crude extracts were prepared as per **2.2.3.1.**

2.2.4 Agroinfiltration and Optimisation of AHSV-5 VP7 Quasi-Crystal Purification by Density Gradient Ultracentrifugation

2.2.4.1 Standard density gradient purification using the established optimal parameters

Four- to five-week-old *N. benthamiana* plants, grown at 22-25°C under 16-h/8-h light/dark cycle, were vacuum-infiltrated using a vacuum of 100 kPa with the inoculum prepared in **2.2.2.2** at the selected optical density of 0.5 at 600 nm. Since it was shown that the pRIC3.0-AHSV5 vector seemed to yield greater protein expression, plants were co-infiltrated with pRIC3.0-AHSV5 recombinants VP2: VP3: VP5: VP7 at a ratio

of 1: 1: 1: 1. The pRIC3.0 empty vector was used as a negative control and infiltrated at an OD_{600} of 0.5.

Infiltrated leaves were harvested at 3 dpi, weighed (±13.5 g per gradient) and either used immediately or frozen at -80°C. *N. benthamiana* leaves were combined with PBS, pH 7.4, at a 1:2 (w/v) ratio and 1x Complete protease inhibitor cocktail (Roche, Basel, Switzerland) was added per 50 ml volume of PBS. The extract was then thoroughly homogenised using the T25 digital Ultra-Turrax® blender (IKA®, Staufen, Germany) and incubated for 1 h at 4°C with gentle agitation. The homogenate was filtered through one layer of Miracloth™ (Merck, Darmstadt, Germany) and subsequently clarified by centrifugation at 23 300 x g/RCF (max) for 15 min at 4°C using the Beckman Avanti® J-25 High Speed Centrifuge (Beckman Coulter, Brea, CA). Twenty-seven ml of the clarified supernatant was then removed and placed onto a discontinuous iodixanol (Optiprep™; Sigma-Aldrich, St Louis, Missouri) gradient.

The iodixanol solutions were diluted in PBS to produce the desired concentrations and underlaid to create a 12 ml discontinuous step gradient (2 ml-20%, 2 ml-30%, 3 m-40%, 3 ml-50%, 2 ml-60%). The gradient was subsequently ultracentrifuged at 174 900 x g/RCF (max) for 2 h at 4°C in a SW 32 Ti rotor (Beckman Coulter, Brea, CA). Twelve x 1 ml fractions were then collected from the bottom of the tube and 28 µl of each were loaded onto a 10% SDS-polyacrylamide gel. Following this, Coomassie blue staining and western immunoblot analyses were performed.

2.2.4.2 Concentrating AHSV-5 VP7 quasi-crystals using an iodixanol cushion and low-speed centrifugation during clarification

Agroinfiltration and purification methods in **2.2.4.1** were repeated with the following adjustments:

Infiltrated *N. benthamiana* leaves were harvested at 5 dpi to increase maturation time. Fresh leaves were weighed (± 6.5 g per cushion) and combined with PBS at a 1:5 (w/v) ratio. Protease inhibitor cocktail was included as per **2.2.4.1.** Centrifugation speed during crude extract clarification was reduced to 1200 x g/RCF (max) for 10 min to decrease the potential loss of AHSV-5 VP7 quasi-crystals in the pellet. Subsequently, 32.5 ml of the clarified supernatant was then removed and placed onto

a 5 ml-25% and 1 ml-60% iodixanol cushion (**Figure 2.1**(1)). The cushion was ultracentrifuged at 174 900 x g/RCF (max) for 3 h at 4°C in a SW 32 Ti rotor (Beckman Coulter, Brea, CA). Previous research has shown the density of AHSV-5 VP7 quasi-crystals to be 1.31 g/ml (Burroughs et al. 1994), whilst the density of 60% iodixanol is ±1.32 g/ml and 25% iodixanol is 1.13 g/ml (https://www.axis-shield-density-gradient-media.com/V01.pdf). Applying a 25% and 60% iodixanol solution should theoretically concentrate AHSV-5 VP7 quasi-crystals at the 25% and 60% interface. After ultracentrifugation, six 400 µl fractions were collected (**Figure 2.1**(2)) and pooled with their respective replicates from a second cushion (**Figure 2.1**(3)). The resultant 800 µl fractions were diluted to a concentration of <25% iodixanol (**Figure 2.1**(4)) before placing onto six separate 30-60% iodixanol step gradients (750 µl volumes at 10% increments) (**Figure 2.1**(5)). The gradient was then centrifuged at 235 300 x g/RCF (max) for 3.5 h at 4°C in a SW 55 Ti rotor (Beckman Coulter, Brea, CA). Four 750 µl fractions were then collected, visible gradient bands aspirated, remaining pellets resuspended and remaining sample above the 30% iodixanol layer collected from each gradient. Twenty-eight µl samples of each of these were loaded onto a 10% SDS-polyacrylamide gel for analysis. Fractions from gradients originating from cushion fractions three and four were selected for Coomassie blue staining, western immunoblotting (**2.2.5**) and TEM analysis (**2.2.6**) as these are situated at the 25/60% cushion interface.

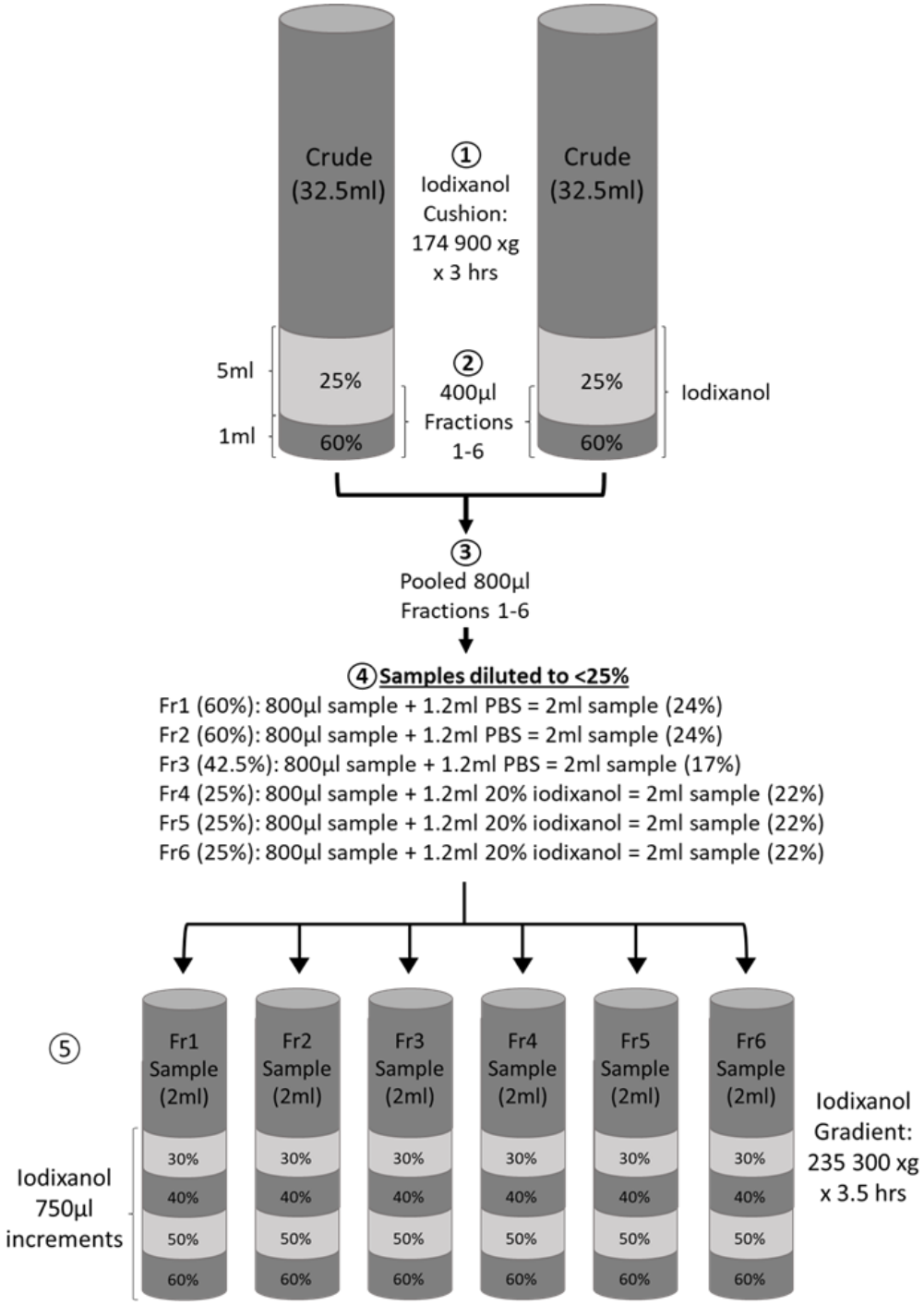

Figure 2.1: Iodixanol cushion and density gradient purification process to concentrate AHSV-5 VP7 quasi-crystals. The iodixanol percentages are indicated on each layer in the images and in brackets in step (4). Crude: Clarified supernatant, PBS: Phosphate-buffered saline, Fr: Fraction.

2.2.4.3 Increasing AHSV-5 VP7 trimer-trimer interactions via buffer pH adjustments

Agroinfiltration and purification methods in **2.2.4.1** were repeated with the following adjustments:

Plants were infiltrated with recombinant pRIC3.0-AHSV5-VP7 constructs alone. Infiltrated leaves were harvested at 7 dpi, fresh leaves weighed (±11 g per cushion) and combined with PBS, pH 7.4, or 0.2 M Tris-HCl, pH 8, at a 1:3 (w/v) ratio. To clarify the filtrate, it was centrifuged at 1200 x g/RCF(max) for 15 min at 4°C (**Figure 2.2**(1)) and the subsequent supernatant centrifuged at 23 300 xg/RCF(max) for 30 min (**Figure 2.2**(2)) using the Beckman Avanti® J-25 High Speed Centrifuge (Beckman Coulter, Brea, CA). Supernatant (33 ml), originating from ±11 g biomass, was transferred to a 6 ml-50% iodixanol cushion (39 ml centrifuge tube) (**Figure 2.2**(3)); and 3 ml of the resuspended pellet, originating from 14 g biomass, was transferred to a 2 ml-50% iodixanol cushion (5 ml centrifuge tube) (**Figure 2.2**(4)). A 50% iodixanol layer was selected as its density was considered to be sufficient to exclude a greater amount of lower density particles while concentrating AHSV-5 VP7 quasi-crystals (1.31 g/ml density) into this layer or into concentrated pellets. The density of 50% iodixanol was calculated to be ±1.27 g/ml when using both diluent alternatives: PBS and 0.2 M Tris-HCl. The 39 ml centrifuge tubes were placed into the SW 32 Ti rotor and 5 ml tubes into the SW 55 Ti rotor (Beckman Coulter, Brea, CA). These were centrifuged at 174 900 x g/RCF (max) and 124 400 x g/RCF (max) respectively for 4 h at 4°C. Six x 1 ml (39 ml centrifuge tubes) and 4 x 500 µl (5 ml centrifuge tubes) fractions were then collected. Samples of the crude pre- and post- 1200 x g/RCF (max) spin were collected and the resuspended pellets from both cushions sampled. Twenty-two µl of each sample was loaded onto a 10% SDS-polyacrylamide gel. Following this Coomassie blue staining and western immunoblot analyses were performed.

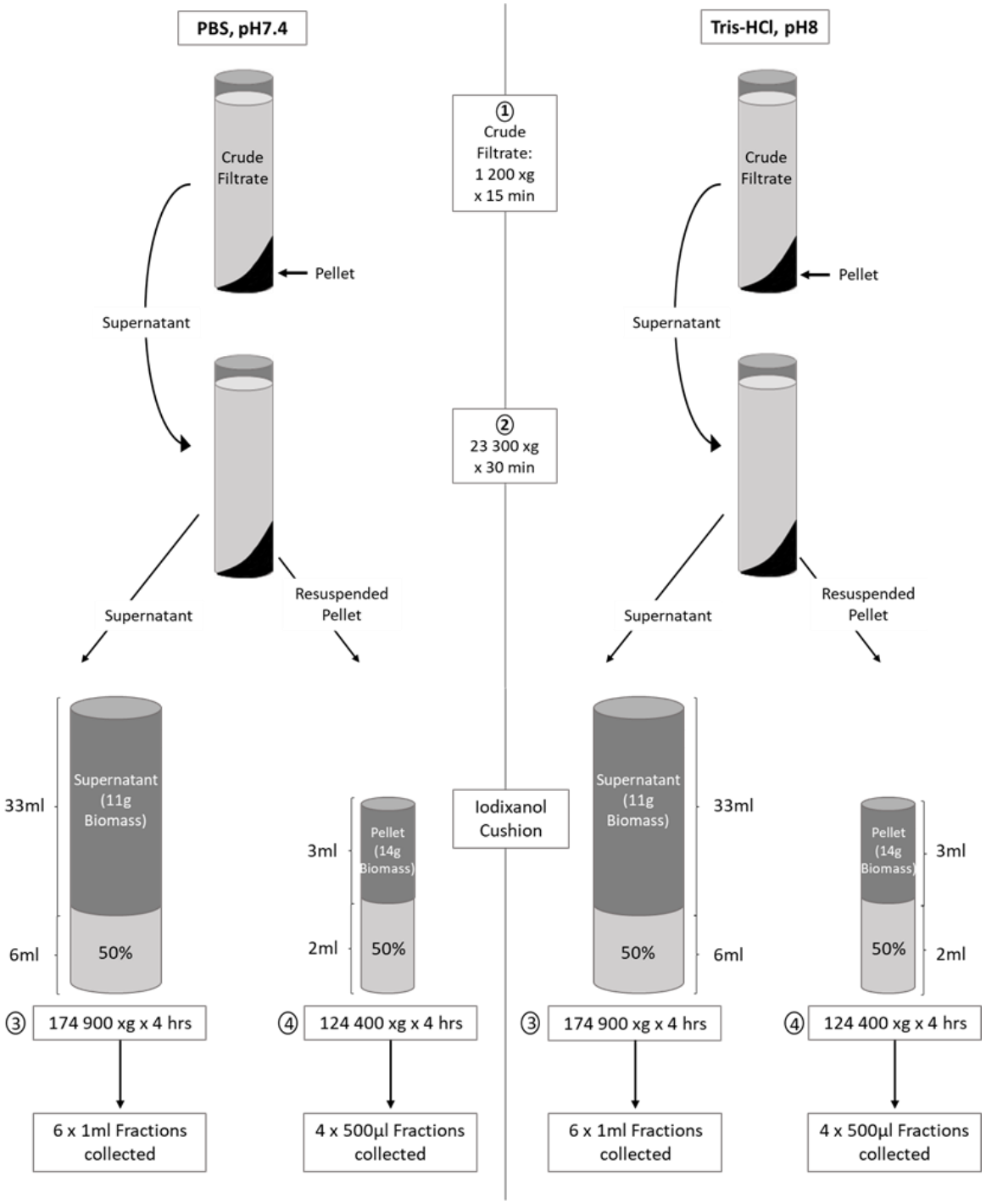

Figure 2.2: Purification process for PBS, pH 7.4, and 0.2 M Tris-HCl, pH 8, comparison. Original biomass from which each sample was derived is indicated on the sample layer. 50%: Iodixanol percentage used.

2.2.4.4 Increasing AHSV-5 VP7 quasi-crystal yield using low-speed differential and density gradient centrifugation

Agroinfiltration and purification methods in **2.2.4.1** were repeated with the following adjustments:

Plants were infiltrated with recombinant pRIC3.0-AHSV5-VP7 constructs alone. Infiltrated leaves were harvested at 6 dpi and combined with 0.2 M Tris-0.15 M NaCl, pH 8 (including protease inhibitor), at a 1:3 (w/v) ratio. The filtrate was initially clarified by centrifugation at 1200 x g/RCF (max) for 10 min and a subsequent second spin at 3000 x g/RCF (max) for 35 min at 4°C using the Beckman Avanti® J-25 High Speed Centrifuge (Beckman Coulter, Brea, CA). The pellet, originating from ±20 g biomass, was then resuspended in 1.5 ml, placed onto a discontinuous sucrose gradient (1.4 ml-40%, 1.4 ml-50% and 0.8 ml-68%) and spun at a low speed of 17 500 x g/RCF (max) for 1 h at 4°C in the SW 55 Ti rotor (Beckman Coulter, Brea, CA). Sucrose solutions, prepared in 0.2 M Tris-0.15 M NaCl, were used during this experiment in order to reduce costs during optimisation. After ultracentrifugation, 5 x 800 µl fractions were collected and dialysed against 0.2 M Tris-0.15 M NaCl and further samples collected and analysed as per **2.2.4.3**.

2.2.4.5 Sucrose- and iodixanol density gradient conversion

Agroinfiltration and purification methods in **2.2.4.1** were repeated with the adjustments made in **2.2.4.4**, and the sucrose gradient was replicated as per **2.2.4.4.** In contrast, the iodixanol step gradient was converted to 1.4 ml-30% (1.18 g/ml), 1.4 ml-40% (1.22 g/ml) and 800 µl-60% (1.32 g/ml) to produce the equivalent sucrose densities using the equation: $D=\frac{Vd+V_1\,d_1}{V+V_1}$, where D= density of mixture; V= volume of iodixanol stock solution; d= density of iodixanol stock solution; V_1= volume of diluent; d_1= density of diluent (https://www.axis-shield-density-gradient-media.com/V01.pdf). The rotor and ultracentrifugation protocols were used and performed as per **2.2.4.4.**

2.2.4.6 Increasing AHSV-5 VP7 quasi-crystal yields for immunogenicity studies

Agroinfiltration and purification methods in **2.2.4.1** were repeated with the adjustments made in **2.2.4.5.** Additional alterations to the protocol were made to produce a more stable gradient resulting in a purer product and to increase the yield of AHSV-5 VP7 quasi-crystals. The biomass was doubled, producing a pellet originating from ±40 g biomass. This pellet was resuspended in 2.5 ml of 0.2 M Tris-0.15 M NaCl and placed onto an iodixanol gradient adjusted to: 500 µl-30%, 1 ml-36%, 800 µl-40% and 400 µl-50%. A 1 ml 36% iodixanol layer was included to avoid contamination of the 40% iodixanol layer by plant proteins; and the 60% iodixanol layer was adjusted to a 50% layer as few AHSV-5 VP7 quasi-crystals were observed in the 60% layer. The ultracentrifugation protocol remained as per **2.2.4.4,** however the centrifugation time was adjusted to 3.5 h to increase the probability of AHSV-5 VP7 quasi-crystals reaching their isopycnic point. After ultracentrifugation, 3 x 500 µl fractions were collected and analysed as per **2.2.4.3**.

2.2.5 SDS-PAGE, Coomassie Staining and Western Immunoblot Analysis

Crude extracts and purified samples were combined with 5x SDS sample application buffer [2%SDS, 100 mM Tris-Cl (pH 7.5), 2 mM EDTA, 52% glycerol, 4.3% 2-mercaptoethanol, 0.1% bromophenol blue] and heat-denatured for 5 min at 95°C. Eight µl of the Colour Prestained Protein Standard, Broad Range (11–245 kDa) (New England Biolabs, Ipswich, MA), was used as a molecular weight marker and sample volumes of between 25 µl and 35 µl were loaded onto 10% SDS-PAGE-gels and electrophoresed in a Bio-Rad Mini-Protean® Tetra Cell System (Bio-Rad, Irvine, CA) at 120 volts for approximately 2 h.

In order to analyse the purity qualitatively and to quantify the concentration of AHSV-5 VP7 protein, gels were stained with Coomassie® Brilliant Blue G-250 staining solution (Merck, Darmstadt, Germany) O/N, destained O/N with a destaining solution [45% methanol, 10% glacial acetic acid and 45% dH_2O] and rinsed in distilled water.

For protein quantification, purified AHSV-5 VP7 protein and bovine serum albumin (BSA) (Sigma-Aldrich, St Louis, Missouri) standards (0.250, 0.125, 0.060, 0.030,

0.015 mg/ml) were run on the same 10% Coomassie stained SDS-PAGE gel and AHSV-5 VP7 concentrations estimated using a BSA standard curve. The SynGene Genius bio-imaging system was used to visualise and document gels and GeneTools (Synoptics, Cambridge, UK) or Image Studio™ Lite (Li-Cor®, Nebraska, USA) software was used to quantify gel bands. The fresh weight (FW) yield was calculated using the equation: $FW\ yield = \frac{C \times V}{B}$, where C= final concentration quantified using a BSA standard curve as explained above; V= volume of the fraction being analysed; B= total biomass used.

For western immunoblot analysis, transfers of SDS PAGE-gels were carried out onto HyBond™ C Extra nitrocellulose membranes (AEC-Amersham, Gauteng, South Africa) using a Trans-blot®_Semi-dry transfer cell (Bio-Rad, Irvine, CA) at 15 volts for 1.25 h. Membranes were then blocked with blocking buffer (5% non-fat dairy milk (NFDM) and PBS-T (1 x PBS and 0.1% Tween®-20 (Sigma Aldrich, St Louis, MO)) for 30 min, after which they were probed O/N at 4°C with polyclonal anti-AHSV5-VLP guinea-pig serum primary antibody (BRU, MCB Department, UCT) which was prepared in blocking buffer at a 1:5000 dilution. After four 15 min washes with blocking buffer, membranes were then probed for 1 h at 35°C with the goat anti-guinea-pig IgG alkaline phosphatase-conjugated secondary antibody (Sigma-Aldrich, St Louis, Missouri) which was diluted in blocking buffer to a 1:5000 dilution. After four 15 min washes in PBS-T, proteins were detected with 5-bromo-4-chloro-3-indoxyl-phosphate (BCIP) and nitroblue tetrazolium (NBT) (BCIP/NBT 1-component, KPL, SeraCare, Milford, MA), substrates for alkaline phosphatase.

2.2.6 Transmission Electron Microscopy

Carbon-coated copper grids with a mesh size of 200 were made hydrophilic by glow discharging at 25 mA for 30 sec using an EMS Glow Discharge Unit. Within 24 hours after glow discharging, 20 µl sample droplets of crude plant extract or purified fractions were placed on top of the carbon-coated grids for 10 min (Maree and Paweska 2005). Thereafter, grids were washed carefully by placing them beneath three 20 µl droplets of sterile water and carefully blotted onto filter paper. These were then negatively stained by placing grids below a 20 µl droplet of 2% uranyl acetate for 30 sec and set down onto filter paper to slowly absorb the excess stain. Careful consideration was

taken not to dehydrate the grids before staining, as rapid dehydration has been shown to result in a decrease in AHSV-5 VP7 quasi-crystal detection (Maree and Paweska 2005). Samples were observed using a Tecnai 20 transmission electron microscope (TEM).

2.2.7 Fixing, Dehydration and Embedding of Agroinfiltrated Leaf Sections for *In Situ* TEM

N. benthamiana leaves were agroinfiltrated with recombinant pRIC-AHSV5-VP7 cultures by vacuum-infiltration as per **2.2.2.2.** Leaves were harvested on 5 dpi and a leaf cutting of approximately 3 cm x 3 cm was removed by scalpel blade in a petri dish in the presence of 2.5% glutaraldehyde diluted in 0.1M phosphate buffer [20 mM NaH2PO4, 80 mM Na2HPO4, pH 7.4]. The leaf cutting was then soaked in 2.5% glutaraldehyde for 72 h at 4°C. After this, the sample was divided into 1 mm x 3 mm fragments in the presence of 2.5% glutaraldehyde and incubated in this solution over a 48-h period at 4°C. The leaf fragments were then washed three times for 5 min each in 0.1 M phosphate buffer (pH 7.4) and following this fixed in one part 2% osmium tetroxide and one part 0.2 M phosphate buffer [40 mM NaH2PO4, 160 mM Na2HPO4, pH 7.4] for 1 h. After this, fragments were washed twice for 5 min each with 0.1 M phosphate buffer (pH 7.4) and a further two washes were carried out for 5 min each using sterile water.

After fixation, an ethanol dehydration series was performed, leaf fragments were incubated in 30%, 50%, 70%, 80%, 90%, 95% ethanol for 5 min each and finally placed in 100% ethanol for 10 min. The final 100% ethanol incubation step was repeated twice. Subsequently, leaf fragments were dehydrated in 100% acetone for 10 min and this was also repeated twice.

Following dehydration, leaf fragments were mixed at room temperature for 24 h in 1:1 acteone: Spurr's resin (Agar Scientific, Essex, UK) mixture. After this the fragments were mixed at room temperature in a 75%, 87.5% and 100% Spurr's resin (diluted with 100% acetone where necessary) for 4 h, 24 h and 4 h respectively. This was then replaced once again by 100% Spurr's resin and incubated for 72 h at room temperature. Finally, the fragments were embedded in 100% Spurr's resin and incubated for 24 h at 60°C. The embedded leaf samples were then cut into ultrathin

leaf sections with a diamond knife and placed onto copper grids with a mesh size of 200. These grids were stained with 2% uranyl acetate for 10 min and subsequently washed with 20 µl sterile water droplets five times for 15 sec each. Grids were blotted dry and placed onto lead citrate in a CO_2 free environment for 10 min. These were then washed thoroughly with sterile water and blotted dry on filter paper. Samples were observed using a Technai G2 TEM.

2.3 Results

2.3.1 Transient Expression of AHSV-5 VP7 in *N. benthamiana*

2.3.1.1 Determination of optimal expression conditions: Expression vector comparison and co- vs single-infiltration

To optimise the expression conditions for AHSV-5 VP7 in *N. benthamiana*, yields produced by expression vectors pRIC-3.0 and pEAQ-*HT* were compared. Additionally, a co-expression (AHSV-5 VP2, VP3, VP5 and VP7) tactic was explored to ascertain whether other AHSV capsid proteins influence the expression levels of AHSV VP7 and/or trimer formation. Previous research involving the closely related BTV, found that VP3 has an effect on BTV VP7 trimer lattice formation and intracellular distribution, in that BTV VP7 only associates with virus inclusion bodies in the presence of VP3 and forms no morphological structures in its absence (Bekker et al. 2014; Kar et al. 2007; Loudon and Roy 1991). Furthermore, the successful production of AHSV VP7 quasi-crystals via co-expression (AHSV-5 VP2, VP3, VP5 and VP7) was previously demonstrated by a member of the BRU (data not shown).

N. benthamiana leaves were syringe-infiltrated as per **2.2.3.1**, and 3 days post-infiltration (dpi) crude extracts were prepared as per **2.2.3.1.** Three dpi was chosen as the initial harvest day as AHSV-5 VP7 expression in *N. benthamiana* was previously demonstrated as early as 3 dpi by Dennis *et al.* (2018). Equal amounts of TSP were loaded into each well of the SDS PAGE gel (**2.2.5**) and the expression levels of AHSV-5 VP7 using the pRIC-3.0 and pEAQ-*HT* vectors were compared. VP7 forms very stable trimers and even after the addition of SDS sample application buffer and heat denaturation at 95°C for 5 min both monomers and trimers are observed after SDS PAGE and western immunoblotting (**2.2.5**). After western blot analysis

(**Figure 2.3**), AHSV-5 VP7 monomer bands (37 kDa) were found to be similar in terms of intensity when comparing the pRIC3.0 and pEAQ-*HT* vectors. However, in comparison to all other combinations, stronger AHSV-5 VP7 trimer bands (135 kDa) were detected in the crude extract after co-infiltration with pRIC-AHSV5-VP2, -VP3, -VP5 and -VP7 recombinants (pRIC3.0 - Co).

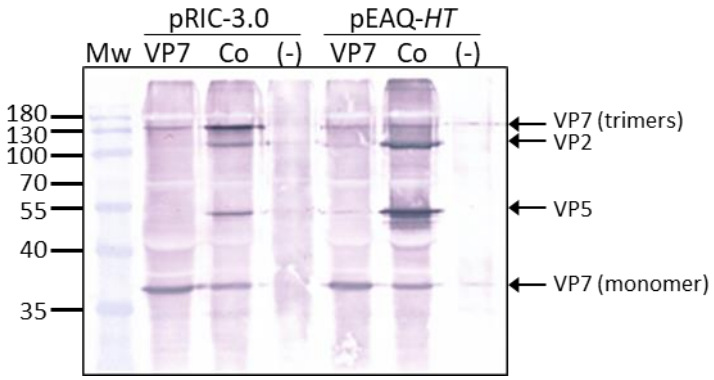

Figure 2.3: Comparison of expression vectors, pRIC3.0 and pEAQ-*HT*, and co-infiltration (AHSV-5 VP2, VP3, VP5 and VP7) vs single-infiltration (AHSV-5 VP7). Western immunoblot analysis of AHSV-5 VP7 expression and monomer (37 kDa) and trimer (135 kDa) protein accumulation on 3 dpi. An inoculum culture OD_{600} of 0.5 was used during syringe-infiltration. For analysis equal amounts of protein were added to each lane. Mw: NEB molecular weight marker (sizes displayed in kDa), VP7: Crude leaf extract from plants expressing AHSV-5 VP7, Co: Crude leaf extract from plants co-expressing AHSV-5 VP2, VP3, VP5 and VP7, (-): Negative control- pRIC3.0 and pEAQ-HT empty vector crude leaf extract. Arrows indicate the positions of AHSV-5 VP2 (123 kDa), VP5 (57 kDa), VP7 monomer (37 kDa) and VP7 trimer (135 kDa).

2.3.1.2 Determination of optimal expression conditions: Selection of optical density and harvest day post-infiltration

To further optimise the expression conditions for AHSV-5 VP7 in *N. benthamiana*, the expression vectors pRIC-3.0 and pEAQ-*HT* were compared once again, along with a comparison of optical densities and harvest day post-infiltration. Since it was shown in **2.3.1.1** that co-infiltrated plants (AHSV5-VP2, -VP3, -VP5 and -VP7) accumulated a higher yield of AHSV VP7 protein, evident by strong VP7 trimer bands (135 kDa) (**Figure 2.3**), plants were co-infiltrated in the experiments to follow.

N. benthamiana leaves were syringe-infiltrated with inoculum prepared in **2.2.2.1**. Optical densities of 0.3, 0.5 and 0.8 at 600 nm were compared **(2.2.3.2)** and leaves were subsequently harvested on 3, 5 and 7 dpi as per **2.2.3.2** to determine the optimal harvest day for the maximum protein yield**.** As shown in **Figure 2.4**, all *N. benthamiana* plants showed signs of necrosis and chlorosis by 5 dpi after syringe-infiltration. However, plants co-infiltrated with pEAQ-*HT* recombinants demonstrated higher levels of necrosis by 5 dpi when compared to those co-infiltrated with pRIC3.0 recombinants.

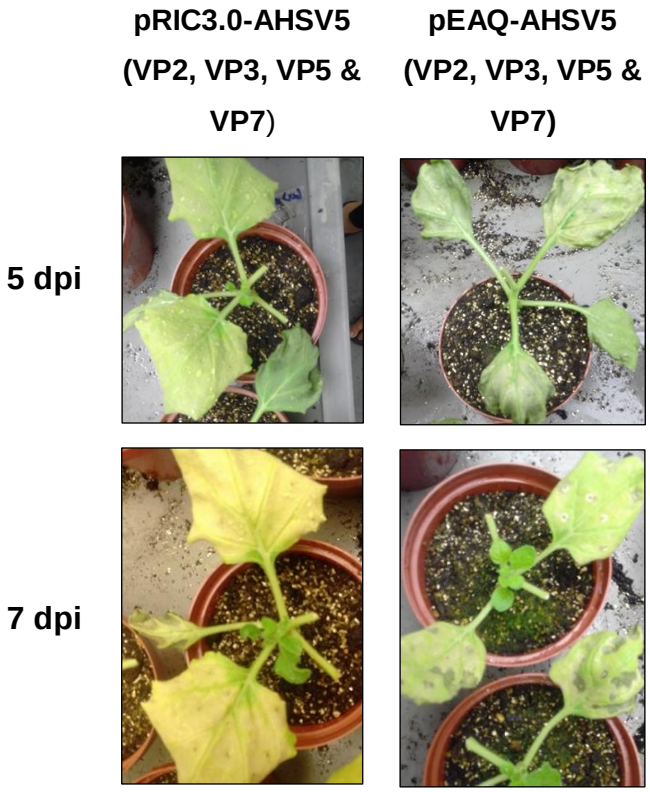

Figure 2.4: Physiological conditions at 5 dpi and 7 dpi after syringe infiltration. *N. benthamiana* leaves were co-infiltrated (AHSV-5 VP2, VP3, VP5 and VP7) with pRIC3.0 or pEAQ-*HT* recombinants at an OD_{600} of 0.5 (OD_{600} 0.3 and 0.8 not shown).

When comparing the co-infiltration inoculum optical densities 0.3, 0.5 and 0.8 and their effects on AHSV-5 VP7 expression levels: The western immunoblots in **Figure 2.5.a and b** show qualitatively similar levels of AHSV-5 VP7 monomer expression and trimer formation across the varying optical densities, with the exception of expression levels shown at 3 dpi using the pRIC3.0 expression vector (**Figure 2.5.b**). At 3 dpi higher

levels of pRIC-AHSV-5 VP7 protein expression were shown when using a 0.5 OD_{600} as opposed to an OD_{600} of 0.3 or 0.8, evident in the intensity of the trimer band (135 kDa). When qualitatively assessing the expression vector and harvest day effects on AHSV-5 VP7 expression by visual comparison: AHSV-5 VP7 monomer and trimer band intensity seemed relatively similar across all harvest days when using both the pEAQ (**Figure 2.5.a**) and pRIC (**Figure 2.5.b**) expression vectors with a marginal increase in trimer band intensity on 5 dpi using the pRIC3.0 vector. In contrast, the lowest level of AHSV-5 VP7 expression and trimer formation was observed on 3 dpi using the recombinant pRIC3.0 vector (**Figure 2.5.b**). Unfortunately, in this experiment, the optimal harvest day was a very qualitative assessment, as the 3 dpi, 5 dpi and 7 dpi samples were not on the exact same western immunoblot. However, every attempt was made to follow the protocol (**2.2.5**) for each immunoblot in the exact same manner and to avoid inconsistencies.

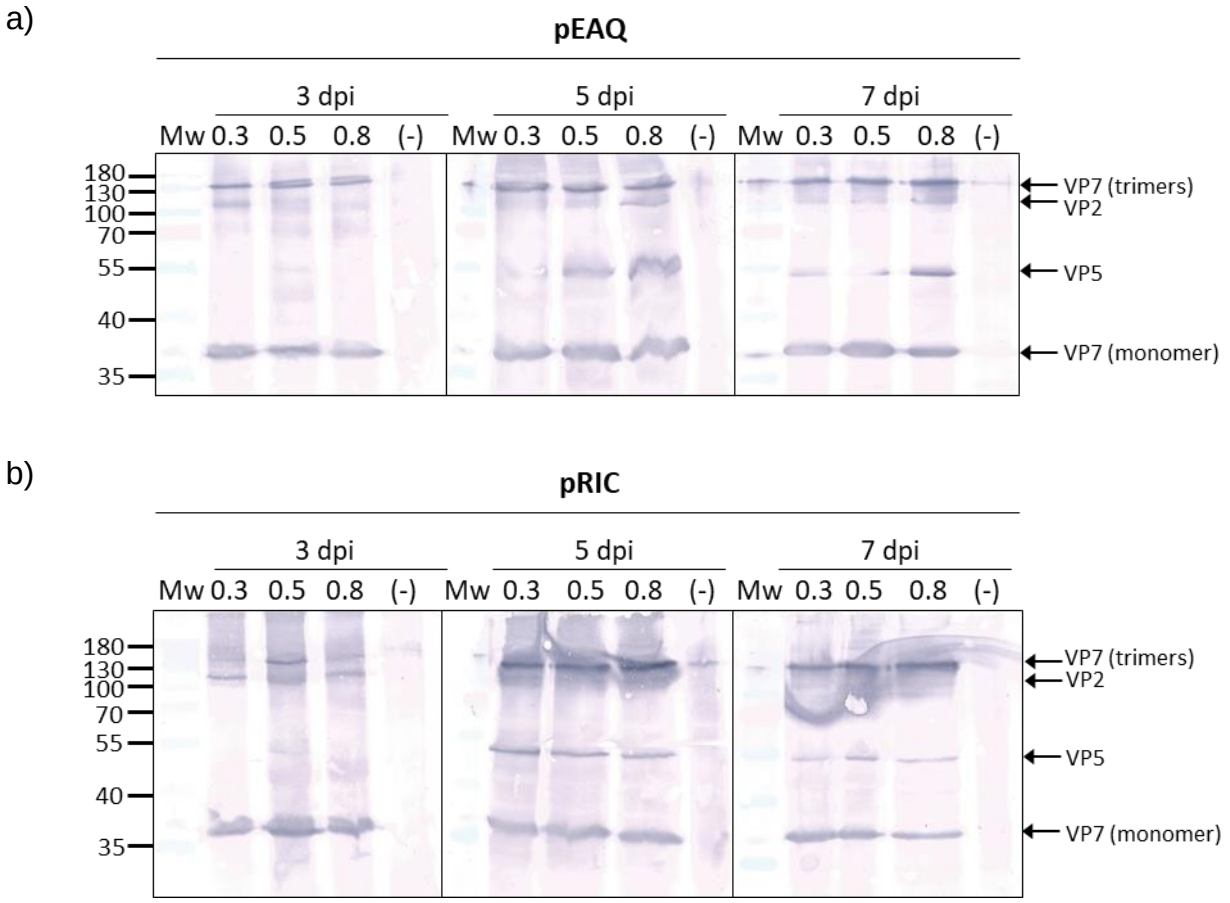

Figure 2.5: Comparison of expression vectors, optical density at 600 nm and harvest day. (a) and (b) Western immunoblot analysis of pEAQ-AHSV5 (a) and pRIC-AHSV5 (b) VP7 expression and monomer (37 kDa) and trimer (135 kDa) protein accumulation on 3 dpi, 5 dpi and 7 dpi. *N. benthamiana* leaves were co-infiltrated (AHSV-5 VP2, VP3, VP5 and VP7) by syringe using an OD_{600} of 0.3, 0.5 or 0.8. For analysis equal amounts of protein were added to each lane. Mw: NEB molecular weight marker (sizes displayed in kDa), dpi 3-7: Days post infiltration, 0.3-0.8: Inoculum culture OD_{600} used, (-): Negative control - pRIC3.0 and pEAQ-HT empty vector crude leaf extract. Arrows indicate the positions of AHSV-5 VP2 (123 kDa), VP5 (57 kDa), VP7 monomer (37 kDa) and VP7 trimer (135 kDa).

2.3.2 Purification of AHSV-5 VP7 Quasi-Crystals by Density Gradient Ultracentrifugation

2.3.2.1 Standard density gradient purification using the established optimal parameters

Having established the optimal parameters for AHSV-5 VP7 protein expression in *N. benthamiana* to be: (1) the expression vector pRIC3.0-AHSV5, (2) co-infiltration using AHSV5-VP2, -VP3, -VP5 and -VP7, (3) 0.5 OD_{600} and (4) day 3 as the optimal harvest day post-infiltration, these conditions were used to scale-up production and develop a purification protocol for AHSV-5 VP7 quasi-crystals. A co-infiltration tactic was pursued at this stage as results from **Figure 2.3** suggested that higher yields of AHSV VP7 protein may accumulate in co-infiltrated plants. And the optimal harvest day of 3 dpi was selected as high levels of necrosis and chlorosis were observed after 3 dpi in previous experiments (**Figure 2.4**).

The initial density gradient purification performed was a relatively standard procedure used by members of the BRU for purifying AHS virus-like-particles (AHSV VLPs). Agroinfiltration, density gradient purification and ultracentrifugation were carried out as per **2.2.4.1**.

As seen in **Figure 2.6.a,** the iodixanol gradient layers stratified well after ultracentrifugation and the 20% and 30% iodixanol layers in combination were sufficient to trap the majority of contaminating plant proteins (fractions 10-12). Western immunoblot analysis of the fractions (**Figure 2.6**.**b**) revealed AHSV-5 VP7 monomer and trimer bands in the crude extract (Cr) and fractions 5-12, with band intensity increasing in higher fractions. No AHSV-5 VP7 quasi-crystals were observed in any of the 12 fractions during TEM analysis. However, CLPs were observed in fraction 6 (40% iodixanol) (**Figure 2.6**.**c**). Additionally, a band of approximately 50 kDa was noted but this was also present in the negative control and therefore likely to be a plant protein.

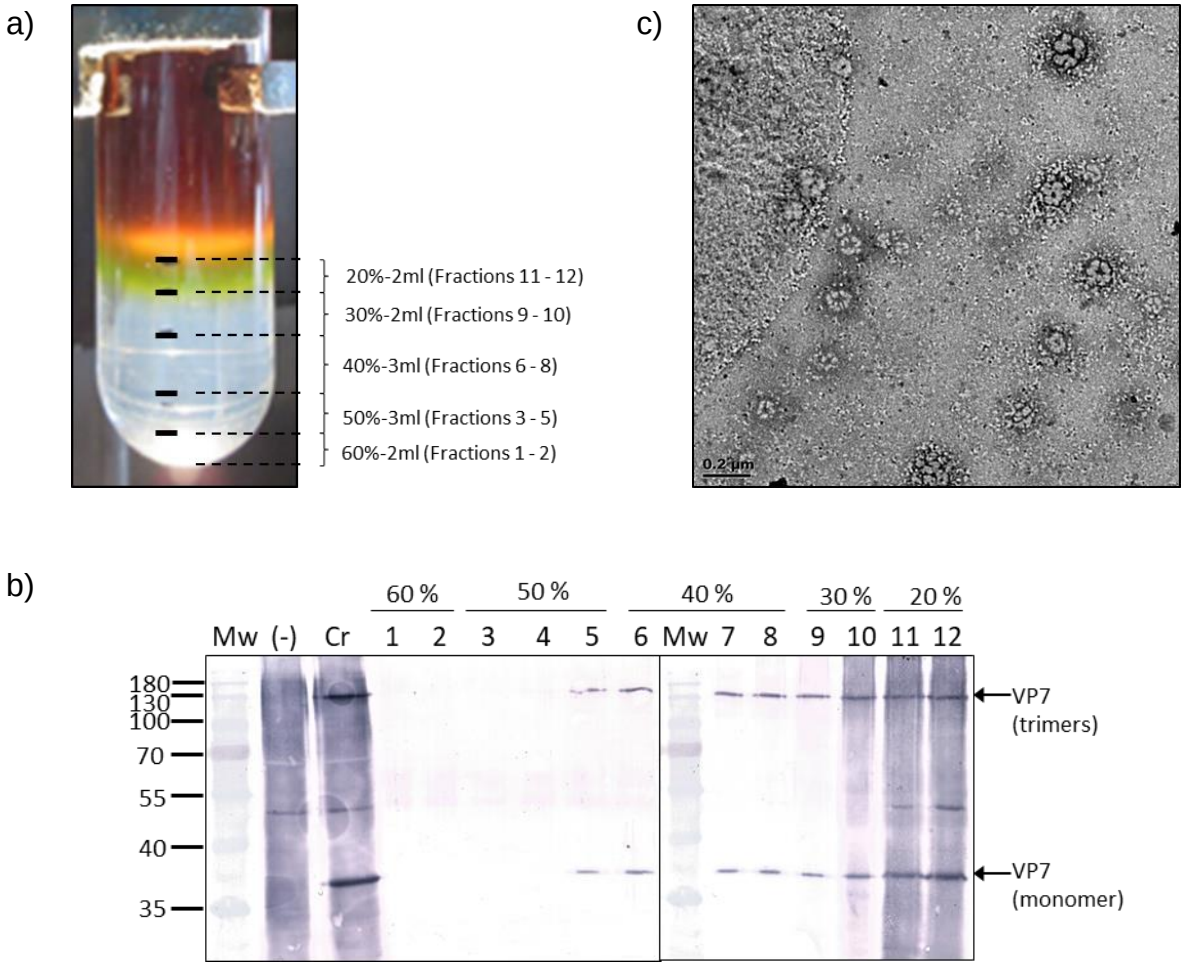

Figure 2.6: Initial iodixanol density gradient and ultracentrifugation method to optimise AHSV-5 VP7 quasi-crystal purification. (a) Image displaying the 20-60% iodixanol step gradient after ultracentrifugation. *N. benthamiana* plants were co-infiltrated with AHSV-5 VP2, VP3, VP5 and VP7 and the inoculum culture OD_{600} 0.5 used for vacuum-infiltration. Crude leaf extracts were prepared from leaves harvested on 3 dpi. Black lines denote the change in iodixanol percentage. Iodixanol layers and corresponding fractions displayed. (b) Western immunoblot analysis of AHSV-5 VP7 expression and monomer (37 kDa) and trimer (135 kDa) protein accumulation. For analysis equal sample volumes of 28 µl were added to each lane. Mw: NEB molecular weight marker (sizes displayed in kDa), (-): Negative control - pRIC3.0 empty vector crude leaf extract, Cr: Crude leaf extract before density gradient purification from plants co-expressing AHSV-5 VP2, VP3, VP5 and VP7, 1-12: Fractions from iodixanol step gradient with corresponding iodixanol layers (20-60%) indicated above. Arrows indicate the positions of AHSV-5 VP7 monomer and VP7 trimer. (c) TEM image of CLPs observed in iodixanol gradient fraction 6 (40% iodixanol). Scale bar: 0.2 µm.

2.3.2.2 Concentrating AHSV-5 VP7 quasi-crystals using an iodixanol cushion and low-speed centrifugation during extract clarification

Results from **2.3.2.1** indicated that after ultracentrifugation the majority of available AHSV-5 VP7 was in soluble form. It was therefore suspected that due to its highly insoluble nature, the insoluble VP7 quasi-crystals were being lost in the pellet in high-speed differential spins during crude extract clarification and only soluble VP7 remained after purification.

In order to concentrate AHSV-5 VP7 protein and potentially increase crystal formation a 25/60% iodixanol cushion was used prior to the discontinuous step gradient (30-60%) as per **2.2.4.2**. Furthermore, a lower initial spin (1200 xg/RCF (max)) was used to remove contaminants from the filtrate as crystal loss was suspected in the pellet when using high speed spins (23 300 xg/RCF (max)). Once again a co-infiltration tactic was used (AHSV-5 VP2, VP3, VP5 and VP7), as results from **Figure 2.3** suggested that co-infiltrated plants may accumulate a higher yield of AHSV-5 VP7 protein. *N. benthamiana* plants co-expressing AHSV-5 VP2, VP3, VP5 and VP7 showed no signs of necrosis three days after vacuum-infiltration and were therefore harvested on 5 dpi to increase the maturation time (**Figure 2.7**).

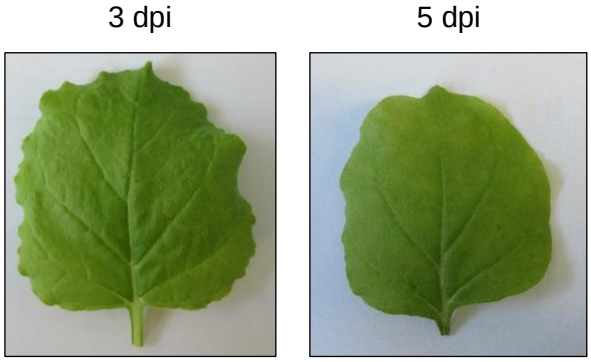

Figure 2.7: *N. benthamiana* leaf physiology at 3 dpi and 5 dpi after vacuum-infiltration. Plants co-infiltrated with recombinant pRIC3.0-AHSV5-VP2, -VP3, -VP5 and -VP7 at an OD_{600} of 0.5.

As shown in **Figure 2.8**, the iodixanol cushion and gradient layers separated well, and the 25% iodixanol cushion layer (**Figure 2.8.a**) and 30% iodixanol gradient layer

(**Figure 2.8.b and c**) seemed sufficient to trap the majority of plant crude extract. Clear white bands were observed in the 40% layers of both iodixanol gradients (**Figure 2.8.b and c**) resulting from the cushion fractions 3 and 4 i.e. the 25/60% iodixanol interface (**Figure 2.8.a**).

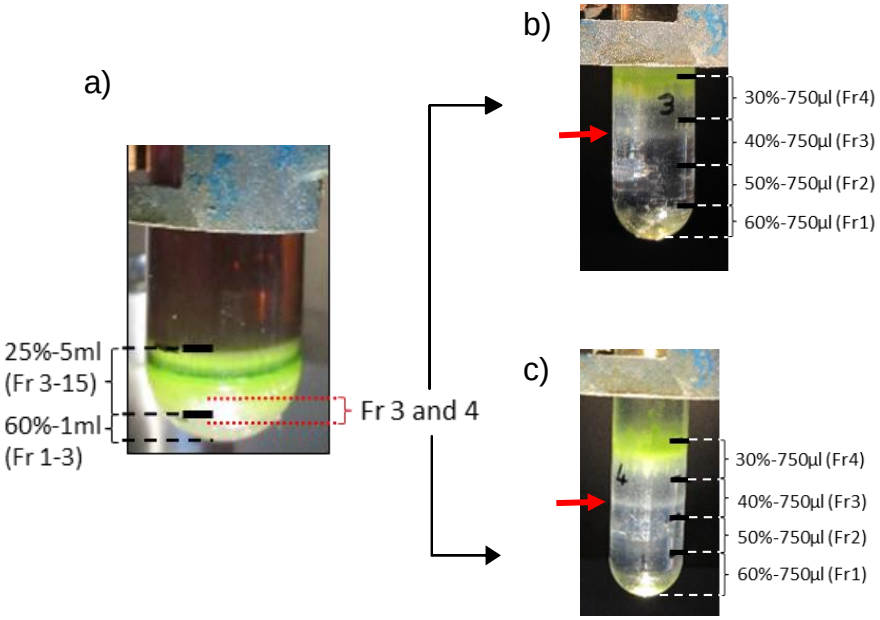

Figure 2.8: Iodixanol cushion and density gradient ultracentrifugation to optimise AHSV-5 VP7 quasi-crystal purification. (a) Image displaying the 25% and 60% iodixanol cushion after ultracentrifugation. Crude extract was prepared from *N. benthamiana* plants co-expressing AHSV-5 VP2, VP3, VP5 and VP7. The inoculum culture OD_{600} for vacuum-infiltration was 0.5 and leaves were harvested on 5 dpi. Red lines represent the boundaries of fractions 3 and 4. (b) Fraction 3, 30%-60% iodixanol density gradient after ultracentrifugation. (c) Fraction 4, 30%-60% iodixanol density gradient after ultracentrifugation. Black lines denote the change in iodixanol percentage and red arrows the observed bands which were subsequently aspirated. Iodixanol concentrations, volumes and corresponding fractions displayed. Fr: Fractions.

Western immunoblot analysis of the iodixanol cushion and gradient shown in **Figure 2.8**, revealed strong AHSV-5 VP7 monomer and trimer bands in the iodixanol cushion fractions 3 (C-Fr3) and 4 (C-Fr4) **(Figure 2.9.a and b)**. In the subsequent iodixanol gradients, light AHSV-5 VP7 monomer and trimer bands were present in the aspirated bands (B) where AHSV-5 VP7 was expected to concentrate, whilst stronger

bands were observed in the 30% and 40% iodixanol gradient layers. Little to no bands were observed in the 50% and 60% layers or the resuspended gradient pellet (P). Coomassie staining in **Figure 2.9.c and d** revealed higher levels in the 30% and 40% layers of cushion fraction 3 (**Figure 2.9.c**). While AHSV-5 VP7 trimer bands were observed in western immunoblots (**Figure 2.9.a and b**), no trimer bands were observed in Coomassie stained gels (**Figure 2.9.c and d**).

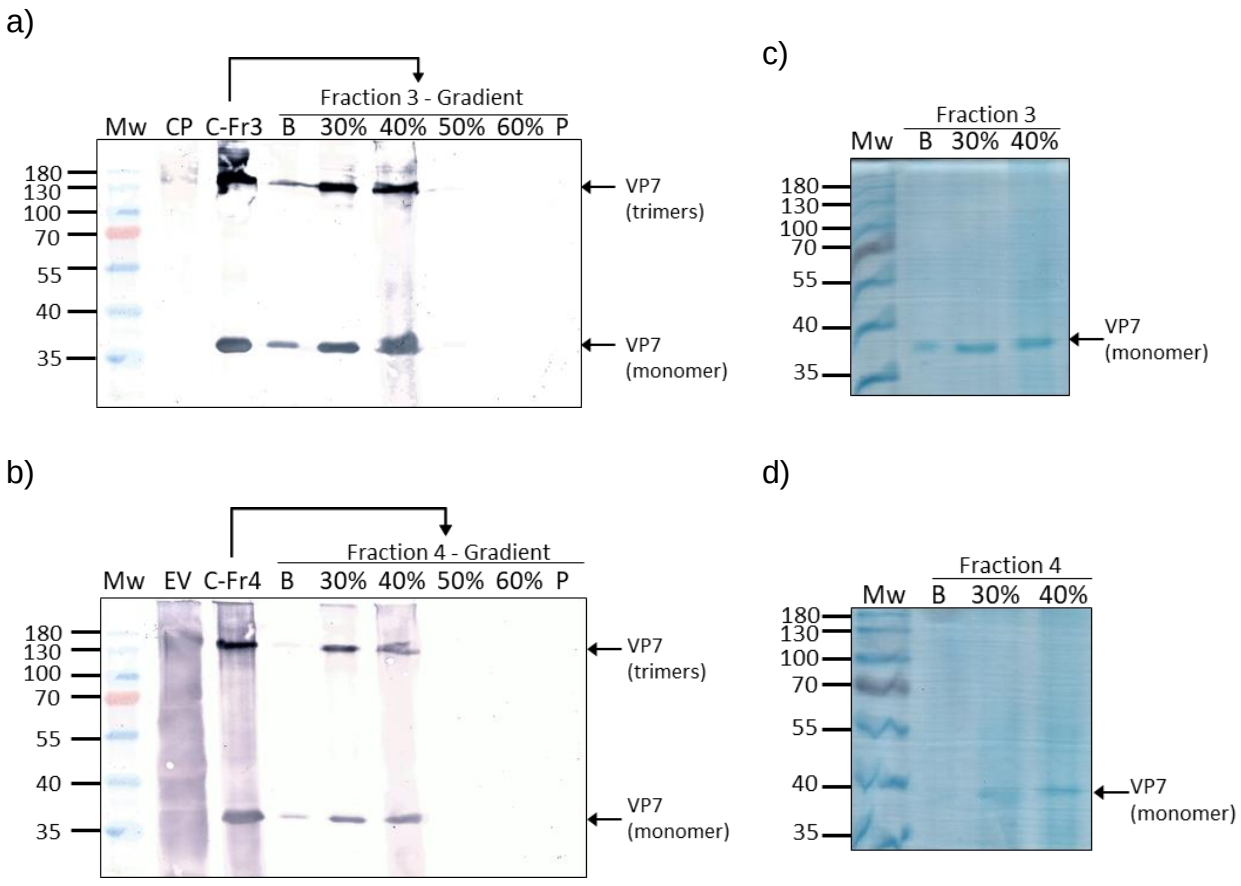

Figure 2.9: Analysis of AHSV-5 VP7 expression after co-infiltration, and purification by means of an iodixanol cushion and density gradient purification. (a) and (b) Western immunoblot analysis of iodixanol cushion fraction 3 (a) and fraction 4 (b), and resultant 30%-60% density gradient fractions. (c) and (d) Coomassie stained SDS-PAGE gels of iodixanol cushion fraction 3 (c) and fraction 4 (d) after density gradient ultracentrifugation. Equal sample volumes of 28 µl were added to each lane. Arrows indicate the positions of AHSV-5 VP7 monomer (37 kDa) and VP7 trimer (135 kDa). Mw: NEB molecular weight marker (sizes displayed in kDa), CP: Iodixanol cushion pellet, C-Fr3: Fraction 3 of iodixanol cushion, C-Fr4: Fraction 4 of iodixanol cushion, EV: Negative control - pRIC3.0 empty vector crude leaf extract, B: Aspirated band from 30-60% iodixanol density gradient, P: Resuspended pellet from 30-60% iodixanol density gradient, 30-60%: Iodixanol concentrations.

Figure 2.10 shows AHSV-5 VP7 quasi-crystals observed during TEM analysis in the aspirated band from the 40% iodixanol gradient layer originating from cushion-fraction 3 (Lane 3 (labelled B) in **Figure 2.9.a**). Few crystals were observed, one of approximately 300 nm in size shown on the left of **Figure 2.10** and one unclear

crystal formation of ±650 nm on the right of **Figure 2.10**. Despite the presence of strong AHSV-5 VP7 monomer and trimer bands in the 30-40% iodixanol layers after western immunoblot analysis (**Figure 2.9**) no AHSV-5 VP7 quasi-crystal formations were observed in these gradient layers, only CLPs (data not shown).

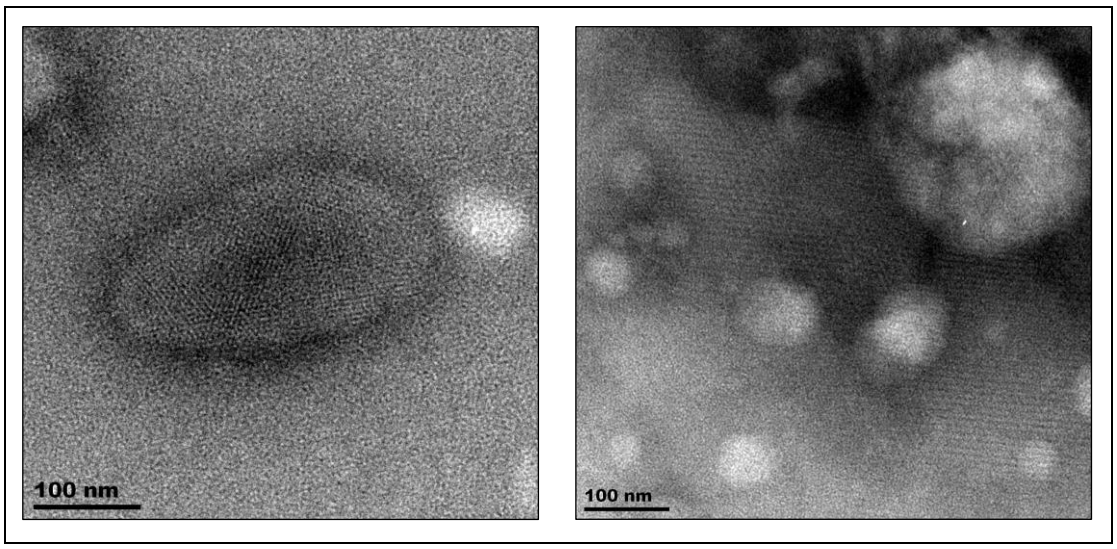

Figure 2.10: TEM images of AHSV-5 VP7 quasi-crystals in the aspirated gradient band (40% iodixanol layer) using fraction 3 from the iodixanol cushion. *N. benthamiana* plants were co-infiltrated with AHSV-5 VP2, VP3, VP5 and VP7. Scale bar: 100 nm.

2.3.2.3 Increasing AHSV-5 VP7 trimer-trimer interactions via buffer pH adjustments

Results from **2.3.2.2** suggested that most of the purified AHSV-5 VP7 was once again in soluble form as it was observed in the higher gradient fractions (**Figure 2.9**). Samples were therefore assessed at every step during the protocol to detect the relative loss of AHSV-5 VP7 protein during low-speed spins and in the resultant pellet as only the supernatant had been used in previous experiments during gradient purification. In addition, a single-infiltration using the recombinant pRIC3.0-AHSV5-VP7 construct alone was pursued and this strategy's impact on quasi-crystal yields investigated.

Furthermore, it was suspected that PBS (pH 7.4) was not a favourable buffer for enhancing VP7 trimer-trimer interactions. Previous research has suggested that the forces involved in AHSV VP7 trimer-trimer interactions are likely hydrophobic and

electrostatic (Bekker et al. 2017). The buffer pH range of Tris-HCl (pH 7.2-9.0) is higher than that of PBS (pH 5.8-8.0) and was therefore used as a comparison to investigate whether an increase in pH may increase trimer-trimer interactions and promote crystal formation. A higher pH as opposed to lower pH was investigated as previous researchers have reported successful AHSV VP7 crystal formation at pH 8 (Maree and Paweska 2005) Agroinfiltration and density gradient purification was carried out as per **2.2.4.3.**

Figure 2.11 shows the 50% iodixanol cushions using PBS, pH 7.4 (**Figure 2.11.a and b**) and 0.2 M Tris-HCl, pH 8 (**Figure 2.11.c and d**) as the buffers. The 50% iodixanol layer remained clear after centrifugation when using the resuspended crude pellet (**Figure 2.11.a and c**) and supernatant (**Figure 2.11.b and d**) and the majority of plant crude extract was trapped above this layer.

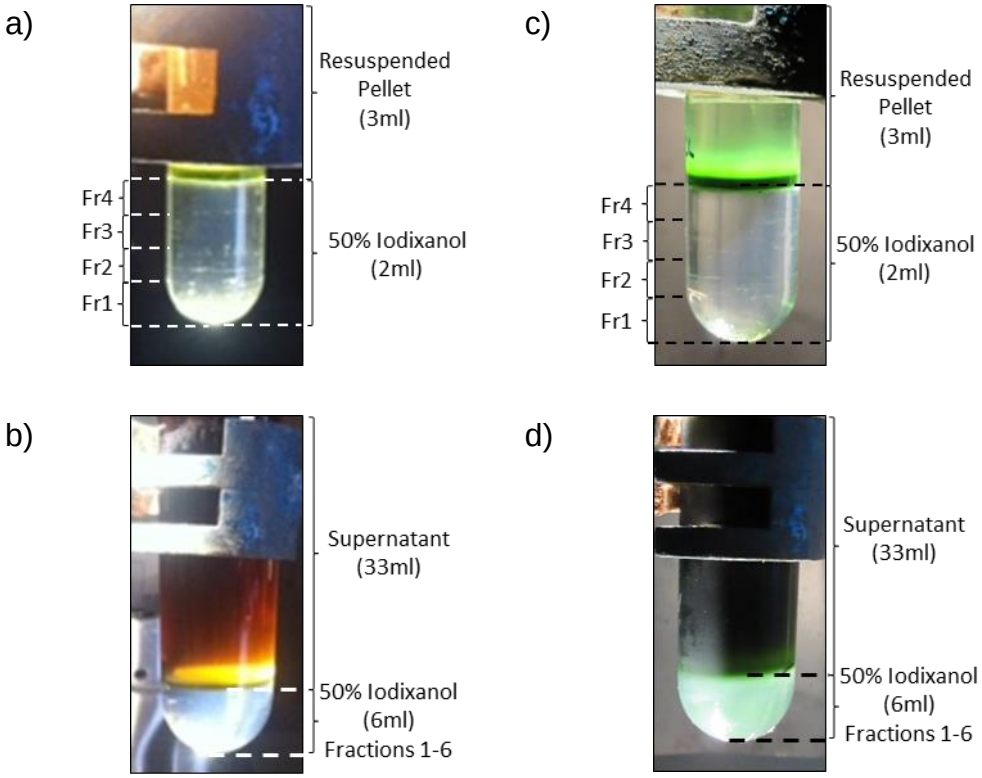

Figure 2.11: Iodixanol cushion and density gradient ultracentrifugation: Comparison of buffers PBS, pH 7.4 (a and b) and 0.2 M Tris-HCl, pH 8 (c and d) for AHSV-5 VP7 quasi-crystal purification. Images display the 50% iodixanol cushions after ultracentrifugation, using the resuspended crude pellet (a and c) and supernatant (b and d). Crude extract was prepared from *N. benthamiana* plants expressing AHSV-5 VP7 alone. The inoculum culture OD_{600} for vacuum-infiltration was 0.5 and leaves were harvested on 5 dpi. Dotted lines denote the 50% iodixanol boundary (b and d). Iodixanol volumes and fractions are displayed next to the figure. Fr: Fractions.

Figure 2.12.a and b display western immunoblot analysis of samples prepared from cushions shown in **Figure 2.11a and b** using PBS, pH 7.4, and **Figure 2.12.c and d** demonstrate western immunoblots of samples from cushions **Figure 2.11.c and d** using 0.2 M Tris-HCl buffer, pH 8. In **Figure 2.12.a**, western immunoblot analysis revealed strong AHSV-5 VP7 monomer and trimer bands in the crude before (Cr1) and after the initial low-speed spin of 1200 x g/RCF (max) (Cr2) when using PBS, pH 7.4 as the buffer of choice. In addition, strong bands were observed in the supernatant (S) after the 23 300 x g/RCF (max) spin and little was observed in the resuspended pellet (Crude-P) (**Figure 2.12.a**). In **Figure 2.12.a and b**, AHSV-5 VP7

monomer and trimer bands were only apparent in the higher fractions of the cushion when using both the pellet (Pellet Cushion – 3/4 and R) and supernatant (Supernatant Cushion – 5, 6 and R). In **Figure 2.12.c,** western immunoblot analysis revealed strong AHSV-5 VP7 monomer and trimer bands in the crude before (Cr1) and after the initial low speed spin of 1200 x g/RCF (max) (Cr2). Little was observed in the supernatant (S) and resuspended pellet (Crude-P) after the 23 300 x g/RCF (max) spin (**Figure 2.12.c**). In addition, in **Figure 2.12.c**, strong AHSV-5 VP7 monomer and trimer bands were apparent in the resuspended pellet of the cushion when using the crude pellet for purification (Pellet Cushion – P), while little was observed in the remaining sample (Pellet Cushion – R). In contrast, in **Figure 2.12.d,** monomer and trimer bands were only apparent in fraction 6 and the remaining sample of the cushion when using the supernatant (Supernatant Cushion – 6 and R).

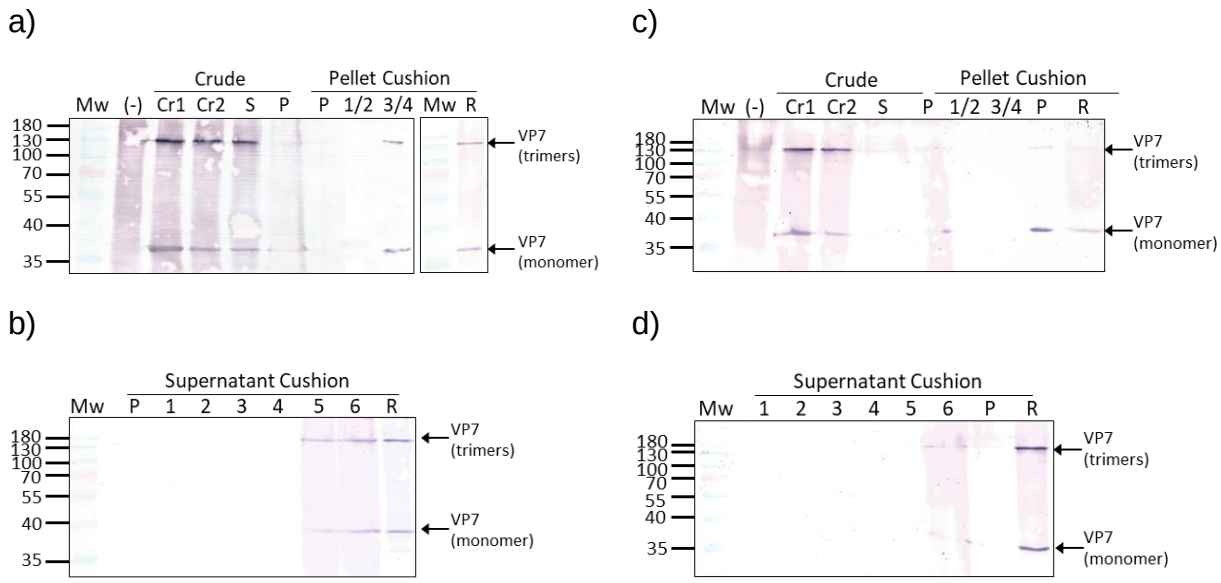

Figure 2.12: Western immunoblot analysis and comparison of buffers: PBS, pH 7.4 (a and b) and 0.2M Tris-HCl, pH 8 (c and d), for AHSV-5 VP7 purification. (a) and (c) Western immunoblot analysis of the crude plant extract and 500 µl fractions 1-4 from the 50% iodixanol cushion using the resuspended crude pellet. (b) and (d) Western immunoblot analysis of 1 ml fractions 1-6 from the 50% iodixanol cushion using the crude supernatant. Equal sample volumes of 22 µl were added to each lane. Arrows indicate the positions of AHSV-5 VP7 monomer (37 kDa) and VP7 trimer (135 kDa). Mw: NEB molecular weight marker (sizes displayed in kDa), (-): Negative control - pRIC3.0 empty vector crude leaf extract, Cr1: Crude plant extract before 1200 x g/RCF(max) centrifugation, Cr2: Crude plant extract after 1200 x g/RCF(max) centrifugation, S: Supernatant, P: Resuspended pellet, 1/2: Fractions 1 and 2 combined, 3/4: Fractions 3 and 4 combined, R: Remaining sample above the cushion after ultracentrifugation, 1-6 (supernatant cushion): Fractions 1-6.

Coomassie staining analysis of samples prepared from cushions shown in **Figure 2.11** are shown in **Figure 2.13**. This revealed marginally stronger bands in the crude supernatant after the 1200 x g/RCF (max) (Cr2) spin and crude pellet (Crude-P) when using the 0.2 M Tris-HCl buffer, pH 8 (**Figure 2.13.b**), as opposed to PBS, pH 7.4 (**Figure 2.13.a**). In addition, when using PBS, pH 7.4, as a buffer (**Figure 2.13.a**), an AHSV-5 VP7 monomer band was observed in the pooled third and fourth fraction of the cushion when using the crude pellet for purification (Pellet Cushion – 3/4). In contrast to this, when using 0.2 M Tris-HCl, pH 8 (**Figure 2.13.b**), an AHSV-5 VP7 monomer band was observed in the resuspended pellet of the cushion when using the

crude pellet for purification (Pellet Cushion – P). Very little evidence of AHSV-5 VP7 bands were observed in the cushion originating from the supernatant when considering both buffer options (**Figure 2.13.a and b**).

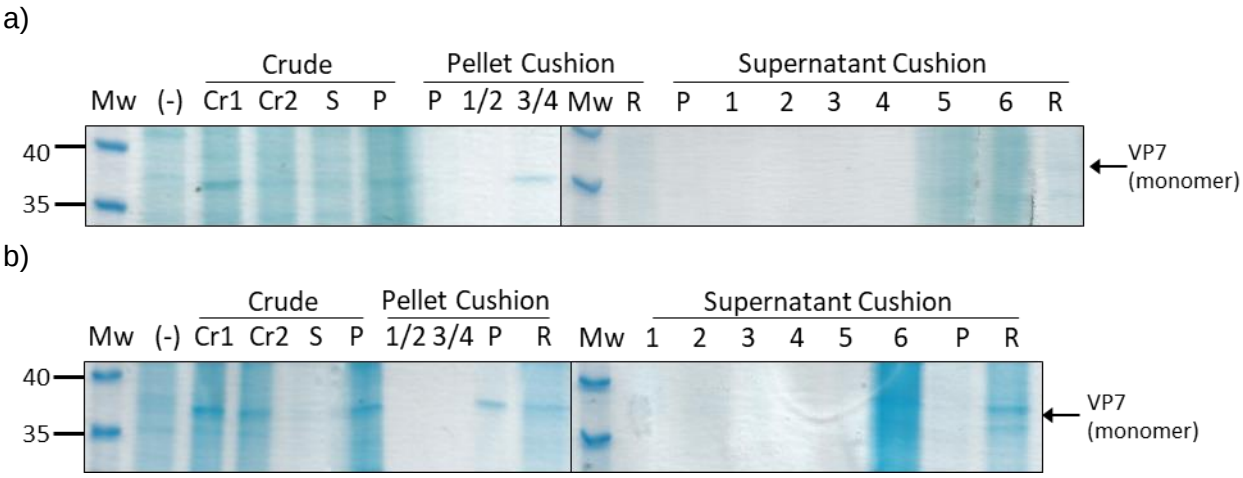

Figure 2.13: Comparison of buffers (a) PBS, pH 7.4, and (b) 0.2 M Tris-HCl, pH 8, for AHSV-5 VP7 expression using iodixanol density gradient purification. *N. benthamiana* plants were infiltrated with AHSV-5 VP7 alone (a) and (b) Coomassie stained SDS-PAGE gels of the crude plant extract, 500 µl fractions 1-4 from the 50% iodixanol cushion using resuspended crude pellet, and 1 ml fractions 1-6 from the 50% iodixanol cushion using crude supernatant. Equal sample volumes of 22 µl were added to each lane. The arrow indicates the position of AHSV-5 VP7 monomer (37 kDa). Mw: NEB molecular weight marker (sizes displayed in kDa), (-): Negative control - pRIC3.0 empty vector crude leaf extract, Cr1: Crude plant extract before 1 200 x g/RCF(max) centrifugation, Cr2: Crude plant extract after 1 200 x g/RCF(max) centrifugation, S: Supernatant, P: Resuspended pellet, 1/2: Fractions 1 and 2 combined, 3/4: Fractions 3 and 4 combined, R: Remaining sample above the cushion after ultracentrifugation, 1-6 (supernatant cushion): Fractions 1-6.

Figure 2.14 demonstrates the presence of AHSV-5 VP7 quasi-crystal formations during TEM observation in the crude extract after the 1200 x g/RCF (max) spin (Cr2) (**Figure 2.14.a**) and in the pellet after the 23 300 x g/RCF (max) spin (Crude-P) (**Figure 2.14.b**) when using PBS buffer. **Figure 2.14.b**, suggests degradation of quasi-crystal structure. Interestingly, no crystals were observed in the crude extract (Cr2) when using 0.2 M Tris-HCl, however the observation of crystal formations may have been impeded by the presence of large quantities of crude plant debris. No other crystal formations were noted in any other cushions and their fractions.

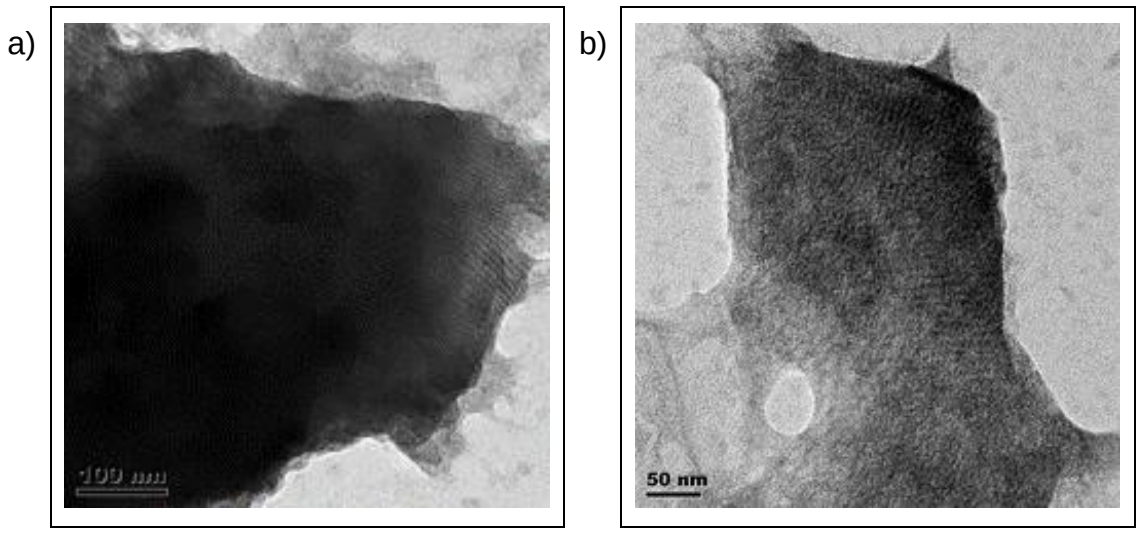

Figure 2.14: TEM images indicating crystal formations in the crude extract after 1200 x g/RCF (max) spin **(a)** and after the 23 300 x g/RCF (max) spin **(b)** using PBS buffer. *N. benthamiana* plants were infiltrated with AHSV-5 VP7 alone. Scale bar: 100 nm **(a)** and 50 nm **(b)**

2.3.2.4 Increasing AHSV-5 VP7 quasi-crystal yield using low-speed differential and density gradient centrifugation

The presence of AHSV-5 VP7 quasi-crystals in the crude but lack thereof after high-speed spins suggested possible disassembly of these crystalline-particles. It was therefore decided to investigate whether low-speed spins of crude filtrate and during density gradient purification may prevent degradation and promote the assembly of AHSV-5 VP7 quasi-crystals. It was also suspected that greater amounts of AHSV-5 VP7 quasi-crystals may reside in the resuspended pellet as opposed to supernatant and the protocol was therefore adjusted as per **2.2.4.4**. Briefly, this protocol included initial clarification of the crude extract by low-speed centrifugation at 1200 x g/RCF (max). After a second low-speed spin at 3000 x g/RCF (max) the resultant pellet was then used for density gradient purification and spun at a low speed spin of 17 500 x g/RCF (max). In addition, sodium chloride was included in the buffer i.e. 0.2 M Tris-0.15 M NaCl, to mimic physiological conditions and increase its ionic strength. A sucrose gradient was used for further optimisation in order to reduce costs as iodixanol is an expensive medium.

After agroinfiltration with AHSV-5 VP7 alone as per **2.2.4.4,** *N. benthamiana* plants showed no signs of necrosis five days after vacuum-infiltration and were therefore harvested at 6 dpi to increase maturation time and potentially promote further crystal formation (**Figure 2.15**).

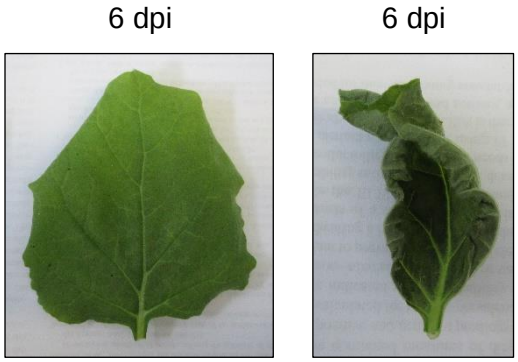

Figure 2.15: *N. benthamiana* leaf physiology at 6 dpi after vacuum-infiltration. The images above show the variability in physiology of different leaves from the same plant at 6 dpi. Plants infiltrated with recombinant pRIC3.0-AHSV5- VP7 alone at an OD_{600} of 0.5 showed no signs of necrosis on 5 dpi and were therefore harvested on 6 dpi.

As shown in **Figure 2.16**, the gradient layers separated well, and the 40% and 50% sucrose layers in combination seemed sufficient to trap the majority of thick plant crude extract from the resuspended pellet. This resulted in a clean 68% layer.

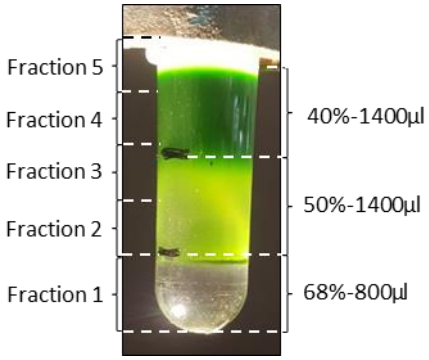

Figure 2.16: Optimising AHSV-5 VP7 quasi-crystal purification using 0.2 M Tris-0.15 M NaCl, pH 8, buffer and low speed density sucrose gradient ultracentrifugation. Image displaying the 40, 50 and 68% sucrose step gradient after ultracentrifugation, using resuspended crude pellet. Crude extract was prepared from *N. benthamiana* plants expressing AHSV-5 VP7 alone. The inoculum culture OD_{600} for vacuum-infiltration was 0.5 and leaves were harvested at 6 dpi. White lines denote the change in sucrose percentage and corresponding fractions.

In **Figure 2.17.a**, a qualitative western immunoblot analysis of the gradient displayed in **Figure 2.16** revealed strong AHSV-5 VP7 monomer and trimer bands in all the crude samples and gradient fractions, with marginally stronger bands in fractions 1 and 2. A quantitative analysis via Coomassie staining in **Figure 2.17.b**, agreed with these findings and revealed relatively clean and strong AHSV-5 VP7 monomer bands in fractions 1, 2 and 3.

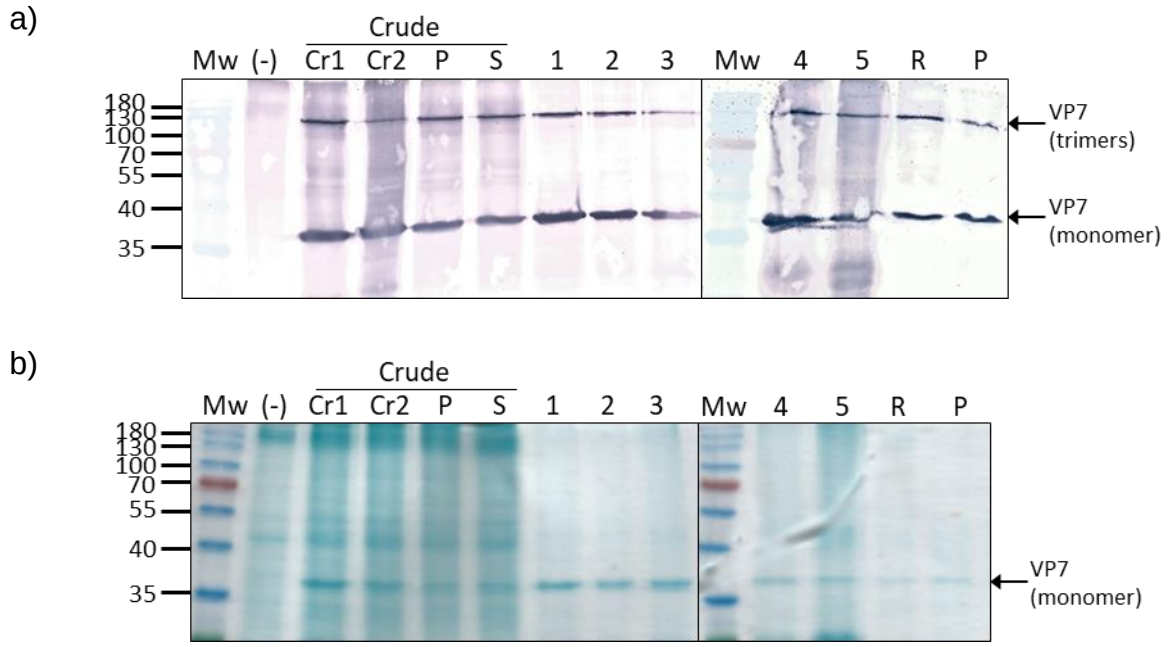

Figure 2.17: Analysis of AHSV-5 VP7 expression after sucrose gradient purification. (a) Western immunoblot analysis and (b) Coomassie stained SDS-PAGE gels of crude extract and 40, 50 and 68% sucrose density gradient fractions (1-5). Equal sample volumes of 22 µl were added to each lane. *N. benthamiana* plants infiltrated with AHSV-5 VP7 alone. Arrows indicate the positions of AHSV-5 VP7 monomer (37 kDa) and VP7 trimer (135 kDa). Mw: NEB molecular weight marker (sizes displayed in kDa), (-): Negative control - pRIC3.0 empty vector crude leaf extract, Cr1: Crude plant extract before 1200 x g/RCF (max) centrifugation, Cr2: Crude plant extract after 1200 x g/RCF (max) centrifugation, P: Resuspended pellet, S: Supernatant, R: Remaining sample above the cushion after ultracentrifugation, 1-5: Fractions 1-5.

Samples resulting from the gradient shown in **Figure 2.16** were analysed via TEM. **Figure 2.18.a and b** show clear well-structured AHSV-5 VP7 crystal formations of approximately 200 nm in fraction 1 after TEM observation. **Figure 2.18.c and d** show larger crystal conglomerates in fraction 2, however not as clean as in fraction 1. Fewer crystals and more plant extract was observed in fraction 3 (**Figure 2.18.e**).

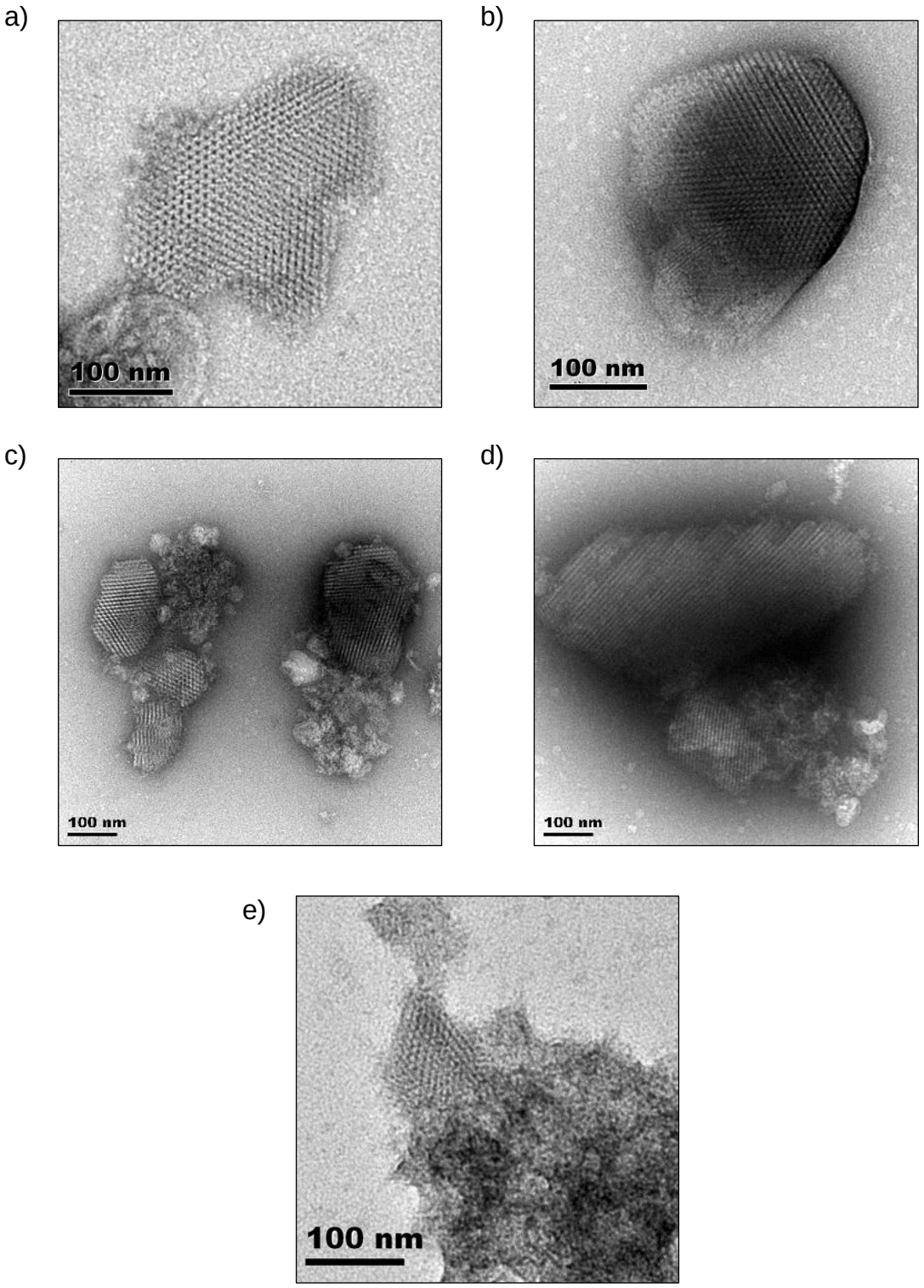

Figure 2.18: TEM images indicating AHSV-5 VP7 crystal formations after density gradient ultracentrifugation, (a) and (b) in fraction 1/ 68% sucrose, (c) and (d) in fraction 2/ 50% sucrose and (e) in fraction 3/ 40-50% sucrose. *N. benthamiana* plants infiltrated with AHSV-5 VP7 alone. Scale bar: 100 nm.

2.3.2.5 Sucrose- and iodixanol density gradient conversion

The successful sucrose gradient needed to be converted to an iodixanol alternative. Iodixanol is safe to use in animals and when compared to sucrose is a preferable substitute for vaccine preparation. Sucrose is easily contaminated and needs to be extracted before the vaccine can be used. Agroinfiltration and density gradient purification was therefore carried out as per **2.2.4.5**. *N. benthamiana* plants were infiltrated with AHSV-5 VP7 alone. **Figure 2.19** shows that fraction 1 and 2 of the iodixanol gradient were clean and that the 30% iodixanol layer seemed sufficient to obstruct the crude plant extract from falling into lower iodixanol layers. A clear white band was observed between the 40% and 60% layers.

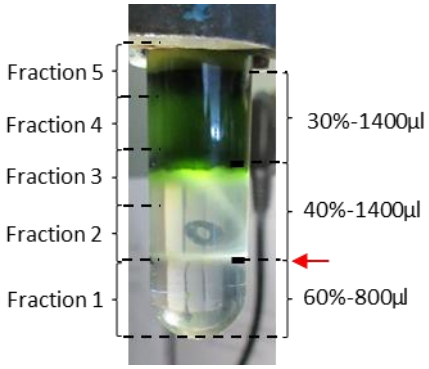

Figure 2.19: Iodixanol density gradient conversion. Image displaying the 40, 50 and 68% iodixanol step gradient after ultracentrifugation, using resuspended crude pellet. Crude extract was prepared from *N. benthamiana* plants expressing AHSV-5 VP7 alone. The inoculum culture OD_{600} for vacuum-infiltration was 0.5 and leaves were harvested on 6 dpi. Black lines denote the change in iodixanol percentage and corresponding fractions and red arrows indicate the observed bands which were subsequently aspirated.

Figure 2.20.a demonstrates a western immunoblot analysis of the fractions removed from the iodixanol gradient above (**Figure 2.19**). Strong monomer and trimer bands were observed in the lanes where the aspirated band (B) (40/60% interface) was loaded and fractions 2, 3 and 4. Lighter bands were observed in fractions 1, 5 and 6 and very faint bands in the resuspended pellet (P). Coomassie staining revealed higher concentrations of AHSV-5 VP7 in the aspirated band and fractions 2, 3 and 4, however fraction 4 was heavily contaminated (**Figure 2.20.b**). Unfortunately, gel

quantification as per **2.2.5** revealed low concentrations of AHSV-5 VP7: 2.39 µg/ml in the aspirated band (B) and 12.70 µg/ml in fraction 2 and a total of 0.52 µg/g FW yield (FW yield calculated as per **2.2.5**).

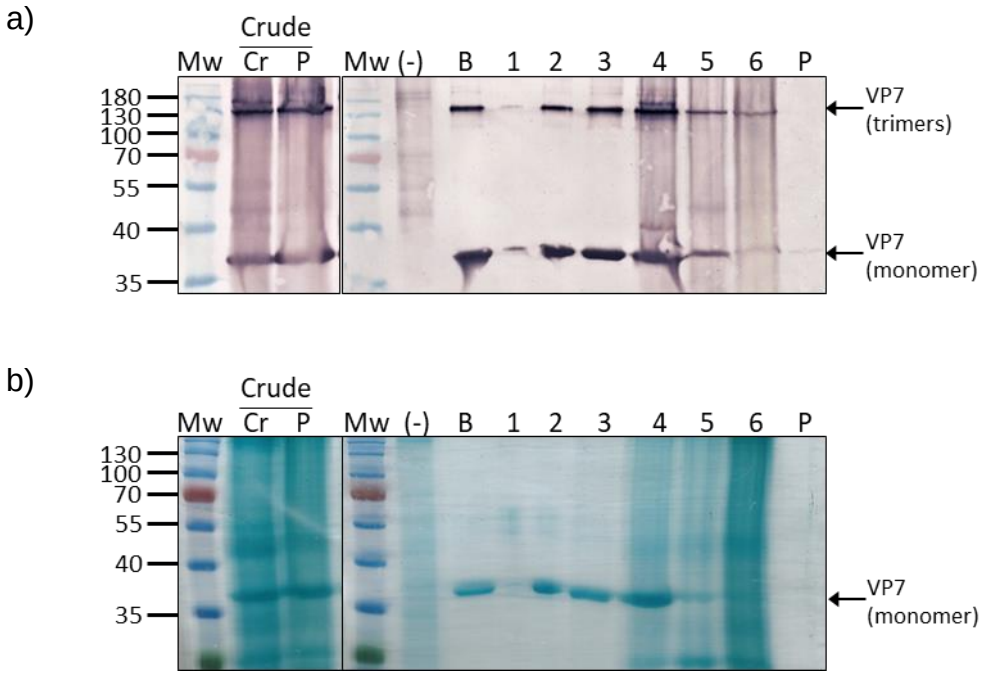

Figure 2.20: Analysis of AHSV-5 VP7 expression after iodixanol density gradient conversion. (a) Western immunoblot analysis and (b) Coomassie stained SDS-PAGE gels of crude extract and 30, 40 and 60% iodixanol density gradient fractions (1-6). Equal sample volumes of 22 µl were added to each lane. *N. benthamiana* plants were infiltrated with AHSV-5 VP7 alone. Arrows indicate the positions of AHSV-5 VP7 monomer (37 kDa) and VP7 trimer (135 kDa). Mw: NEB molecular weight marker (sizes displayed in kDa), Cr: Crude plant extract before 1200 x g/RCF (max) centrifugation, P: Resuspended pellet, (-): Negative control - pRIC3.0 empty vector crude leaf extract, B: Aspirated band at 40/60% interface, 1-6: Fractions 1-6.

In **Figure 2.21**, TEM was used to observe crystals in the fractions removed from the iodixanol gradient in **Figure 2.19**. Well-structured large crystal formations ranging from 600 nm to 800 nm were seen in the aspirated band (**Figure 2.21.a**) and fraction 3 (**Figure 2.21.b**). The conversion from sucrose to an iodixanol gradient alternative was

therefore successful, however AHSV-5 VP7 quasi-crystals resided in higher fractions than expected after ultracentrifugation.

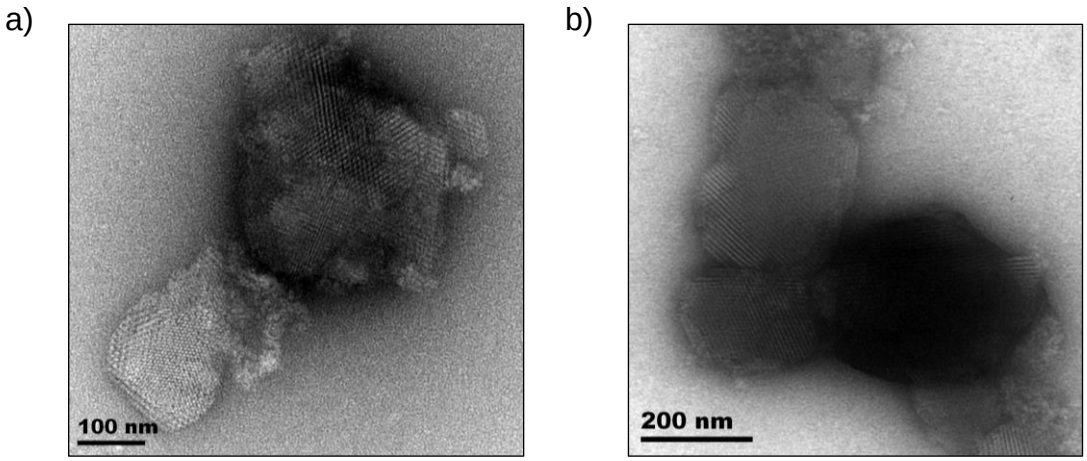

Figure 2.21: TEM images of AHSV-5 VP7 quasi-crystals after density gradient ultracentrifugation. (a) Crystals in aspirated band at 40/60% interface. (b) Crystals in fraction 3/ 30-40% layer. *N. benthamiana* plants infiltrated with AHSV-5 VP7 alone. Scale bar: 100 nm (a) and 200 nm (b).

2.3.2.6 Increasing AHSV-5 VP7 quasi-crystal yields for immunogenicity studies

Although large VP7 crystals were viewed in the previous experiment, gel densitometry revealed low protein concentrations of AHSV-5 VP7 – too low for use as doses for a vaccine. Attempts were therefore made to increase these yields by increasing biomass, adjusting gradient layers and increasing ultracentrifugation time in order to increase the probability of particles reaching their isopycnic point.

Agroinfiltration and purification was carried out as per **2.2.4.6**. *N. benthamiana* plants were infiltrated with AHSV-5 VP7 alone. **Figure 2.22** shows that the 30% and 36% iodixanol layers in combination seemed sufficient to obstruct the crude extract from falling into lower layers allowing fractions 1 and 2 to remain clean.

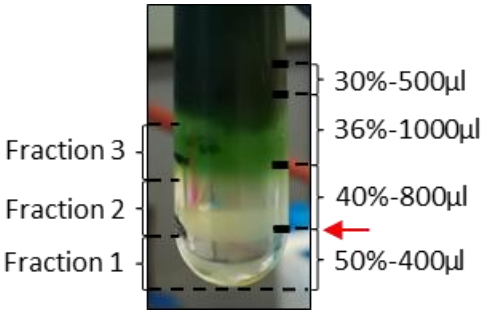

Figure 2.22: Iodixanol density gradient purification of AHSV-5 VP7 quasi-crystals. Image displaying the 30-50% iodixanol step gradient after ultracentrifugation, using resuspended crude pellet. Crude extract was prepared from *N. benthamiana* plants expressing AHSV-5 VP7 alone. The inoculum culture OD_{600} for vacuum-infiltration was 0.5 and leaves were harvested on 5 dpi. Black lines denote the change in iodixanol percentage and corresponding fractions and the red arrow indicates observed bands.

Coomassie staining, in **Figure 2.23**, revealed high concentrations of AHSV-5 VP7 protein with very little plant contaminants observed. Gel densitometry showed concentrations of 213.16 µg/ml in fraction 2 and 2.66 µg/g FW yield (FW yield calculated as per **2.2.5**). Unfortunately, fraction 1 showed signs of bacterial contamination and was therefore not analysed further and not used for vaccine purposes.

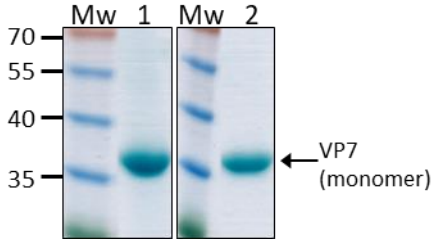

Figure 2.23: Analysis of AHSV-5 VP7 expression after iodixanol density gradient purification. Coomassie stained SDS-PAGE gels of fraction 1 (40/50% iodixanol) and 2 (40% iodixanol). Equal sample volumes of 22 µl were added to each lane. Arrow indicates the positions of AHSV-5 VP7 monomer (37 kDa). Mw: NEB molecular weight marker (sizes displayed in kDa), 1: Fraction 1, 2: Fraction 2.

TEM of fraction 2, showed many well-structured large AHSV-5 VP7 quasi-crystal formations ranging from 500 nm to 1 µm (**Figure 2.24).**

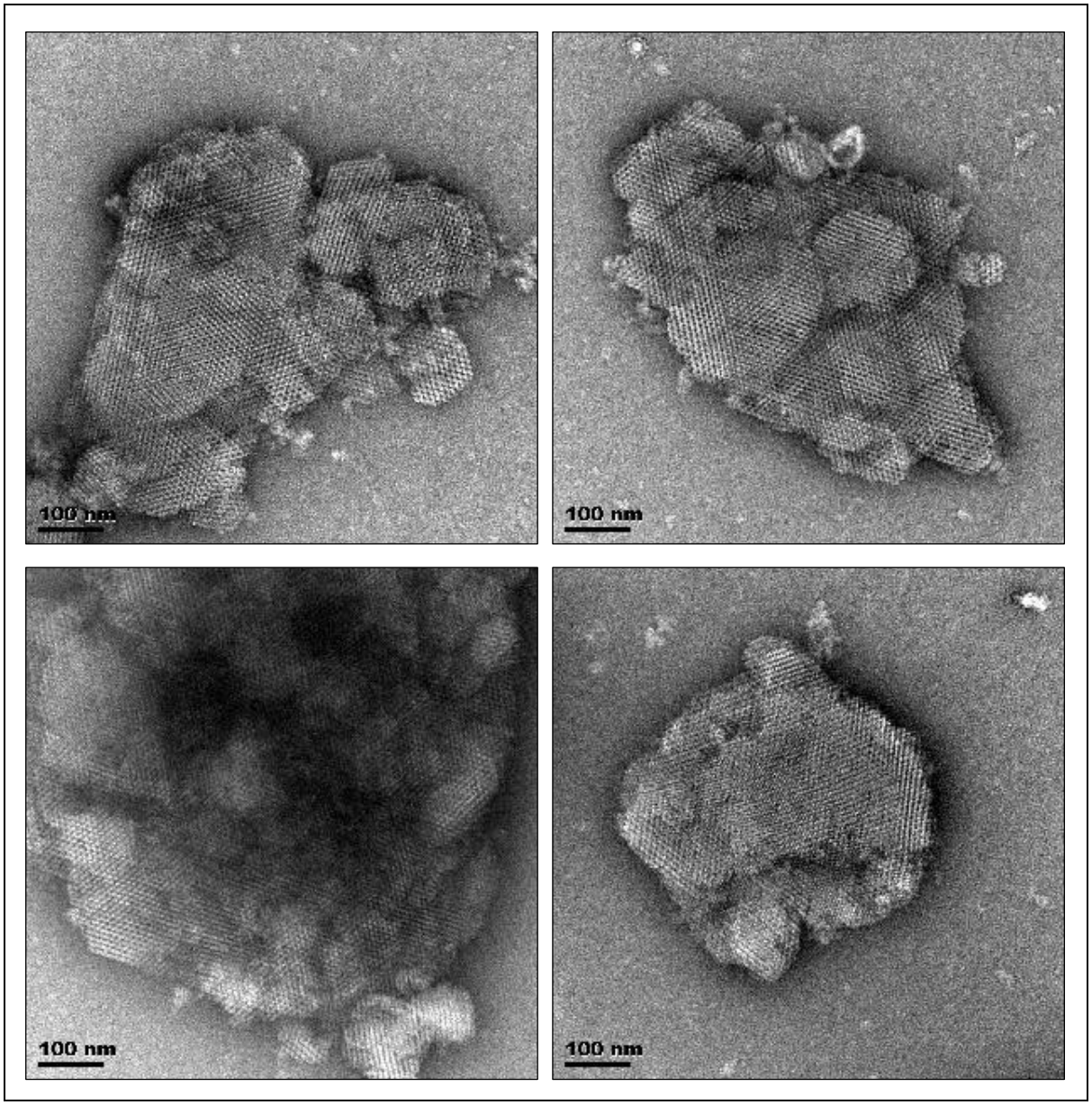

Figure 2.24: TEM images of AHSV-5 VP7 quasi-crystals after iodixanol density gradient purification. 500 µl fractions stored at -20°C. Crystals observed in fraction 2/ 40% iodixanol. *N. benthamiana* plants infiltrated with AHSV-5 VP7 alone. Scale bar: 100 nm.

2.3.3 *In Situ* TEM of Recombinant pRIC-AHSV5-VP7 Agroinfiltrated *N. benthamiana* Leaves

In situ TEM was performed in an attempt to confirm that AHSV-5 VP7 quasi-crystals were forming inside *N. benthamiana* leaves and not as a result of favourable physiological conditions which may arise during the purification process. *N. benthamiana* plants were agroinfiltrated with recombinant pRIC3.0-AHSV5-VP7 alone, harvested on 5 dpi, fixed, embedded and sectioned for *in situ* TEM as per **2.2.7**. Whilst fixation of cellular structures seemed to be satisfactory and *A. tumefaciens* was observed (**Figure 2.25**), no AHSV-5 VP7 quasi-crystals were observed *in situ*.

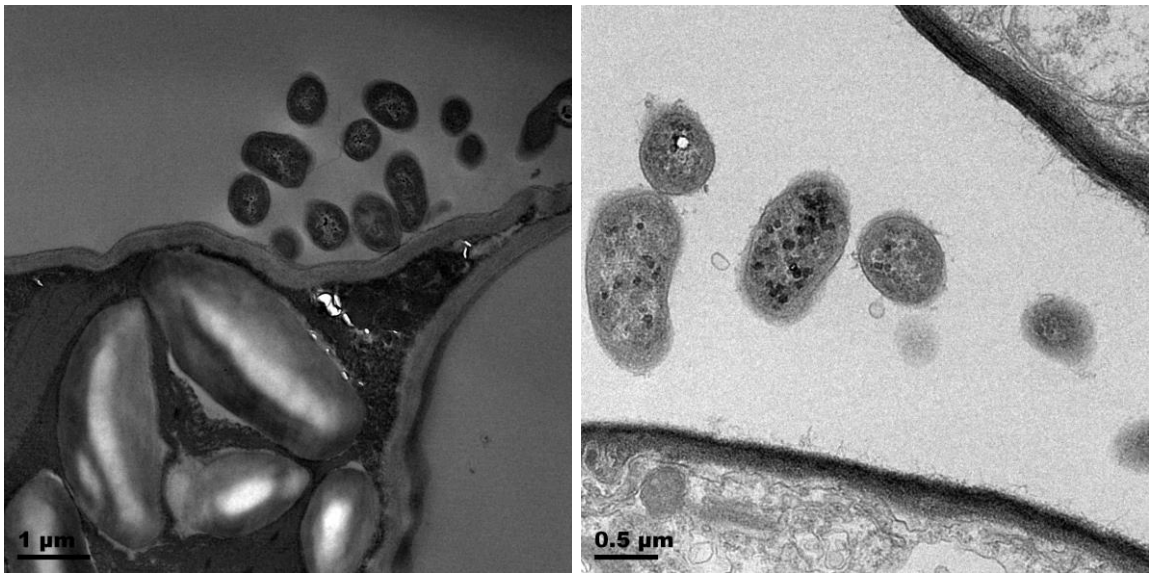

Figure 2.25: *In situ* TEM images of *A. tumefaciens* in *N. benthamiana* leaves. Left: Unstained grids, Right: Grids prepared with 2% uranyl acetate and lead citrate. Scale bars: 1 µm (left) and 0.5 µm (right).

2.4 Discussion

To test the immunogenicity of AHSV-5 VP7 quasi-crystals an optimised purification protocol was required to produce sufficient antigen yields and purity for animal studies. Many researchers have expressed and purified AHSV VP7 using the conventional mammalian and insect expression systems (Basak et al. 1996; Bekker et al. 2014; Burroughs et al. 1994; Chuma et al. 1992; Maree and Paweska 2005; Martinez-Torrecuadrada et al. 1996; Rutkowska et al. 2011; Wade-Evans et al. 1997; Wall et

al. 2017). In contrast, this study aimed to express and purify AHSV-5 VP7 quasi-crystals from *N. benthamiana*, as the literature suggests that plant expression systems may hold various advantages over the more conventional expression platforms (Chen et al. 2013; Mir-Artigues et al. 2019; Rybicki 2019; Schillberg et al. 2019).

The successful expression of AHSV-5 VP7 in *N. benthamiana* using the pRIC3.0 and pEAQ-*HT* vectors was confirmed by western immunoblot using a polyclonal anti-AHSV5-VLP guinea-pig antiserum. To optimise the expression conditions of VP7, recombinant protein yields resulting from pRIC3.0 and pEAQ-*HT* were compared. AHSV-5 VP7 was expressed on its own and co-expressed with AHSV-5 VP2, VP3 and VP5 in order to ascertain whether other AHSV capsid proteins may affect the expression levels of AHSV VP7. Interestingly, after qualitative assessment via SDS PAGE and western immunoblotting, higher levels of AHSV VP7 trimers were noted when *N. benthamiana* leaves were co-infiltrated with AHSV-5 VP2, VP3, VP5 and VP7 using the pRIC3.0 vector. The co-expressed capsid proteins may have a positive effect on VP7 trimer formation. Studies focusing on the closely related BTV, have found that BTV VP3 affects the intracellular distribution of VP7 and trimer lattice formation (Bekker et al. 2014; French and Roy 1990; Kar et al. 2007). Furthermore, the increase in expression levels suggested by the strong trimer bands observed in **Figure 2.3** lane 2 (pRIC3.0 - Co), when utilising the self-replicating plant expression vector pRIC3.0, may result from an increase in gene expression by rolling circle replication mentioned in **2.1** (Regnard et al. 2010). However, the difference in expression levels may also result from leaf variability.

The vector comparison was therefore repeated and included comparisons on optical densities and harvest days. Overall when considering the expression and protein production of AHSV-5 VP7, this experiment revealed relatively similar expression levels when using both expression vectors, OD_{600} readings and harvest days. A slight difference of higher expression levels was noted when using the pRIC3.0 vector and harvesting at 5 dpi. Based on the increase in AHSV-5 VP7 protein expression using the pRIC3.0 vector and co-infiltration (AHSV-5 VP2, VP3, VP5 and VP7) observed in **Figure 2.3**, the pRIC3.0 vector and co-expression tactic were selected for the purification experiments to follow. Furthermore, an OD_{600} of 0.5 and harvest day at 3 dpi were selected as the optimal parameters for purification experiments. Three dpi was selected as the optimal harvest day despite observing higher yields at 5 dpi as

plants were shown to have deteriorated rapidly after syringe-infiltration by this day. Additionally, an OD_{600} of 0.5 was used since higher yields of VP7 were observed at 3 dpi when using the pRIC3.0 vector (**Figure 2.5.b**). It is important to note that the analysis by western immunoblotting was a qualitative assessment, as a quantitative assessment via Coomassie staining and gel densitometry was difficult to perform on crude extracts.

The first protocol used to purify out AHSV-5 VP7 quasi-crystals was a relatively standard procedure used by members of the BRU for purifying AHSV VLPs. PBS, pH 7.4, was used as the buffer of choice and high-speed differential centrifugation (23 300 x g/RCF (max)) was used to extract contaminants. The subsequent crude supernatant was used for density gradient purification and high-speed density gradient ultracentrifugation (174 900 x g/RCF (max)) performed. Unfortunately, after TEM analysis of gradient fractions, no evidence of AHSV-5 VP7 quasi-crystals was apparent in any of the fractions. CLPs alone were observed as seen in **Figure 2.6.c,** and western immunoblot analysis revealed VP7 monomer and trimer bands (37 kDa and 135 kDa respectively) in the higher fractions (5-12) (**Figure 2.6.b**). Suggesting that after ultracentrifugation the majority of available AHSV-5 VP7 was in soluble form. Hence, it was suspected that due to its insolubility VP7 quasi-crystals were being lost in the pellet during high-speed differential spins and clarification.

Considering these findings, the differential centrifugation speeds were reduced to 1200 x g/RCF (max) and an iodixanol cushion was used to concentrate AHSV-5 VP7 at the 25/60% iodixanol interface. Additionally, the harvest day was increased to 5 dpi allowing an increase in potential crystal maturation time, as vacuum-infiltrated plants seemed relatively healthy by 5 dpi. Due to the aforementioned protocol adjustments a few small crystals were observed by TEM in the aspirated gradient band (40% iodixanol layer) which originated from the 25/60% layer of the iodixanol cushion. Additionally, many CLPs were seen in the 30/40% gradient layer originating from the 25/60% layer of the iodixanol cushion. Once again most of the available AHSV-5 VP7 was observed in the higher fractions suggesting that mostly the soluble form was present.

In light of the previous findings, it was suspected that PBS (pH 7.4) was not a suitable buffer for enhancing VP7 trimer-trimer interactions. Assembly of BTV-10 VP7 crystals

and rotavirus nucleocapsid protein, VP6, hexagonal lattices are pH dependent (Monastyrskaya et al. 1997; Sabara et al. 1987). And Bekker *et al* (2017) reported that hydrophobic and electrostatic interactions are likely to influence trimer-trimer interactions which can be affected by ionic strength and pH. 0.2 M Tris-HCl (pH 8) was therefore selected which has been utilized by various researchers when attempting to isolate and purify AHSV-5 VP7 crystals from insect cells (Bailey 2016; Burroughs et al. 1994; Maree et al. 2016). In addition, a single-infiltration with AHSV-5 VP7 alone was used for further experiments. For subsequent experiments the initial low-speed differential centrifugation step was retained, a second differential spin was included (23 300 x g/RCF (max)), and both the supernatant and pellet resulting from the 23 300 x g/RCF (max) spin were used for purification using a 50% iodixanol cushion After western immunoblot analysis of fractions from the 50% iodixanol cushion little loss of VP7 protein was observed after the low-speed spin (1200 x g/RCF (max)) when using both buffers. However, when using 0.2 M Tris-HCl, there seemed to be an increase in protein loss after the second spin (23 300 x g/RCF (max))**.** Additionally, when using 0.2 M Tris-HCl, the majority of AHSV-5 VP7 was observed in the higher fractions when using the supernatant for purification, and in the pellet when using the pellet for purification. In contrast, when using PBS, VP7 was only observed in the higher fractions of both the pellet- and supernatant-cushion. These results suggest that higher quantities of insoluble AHSV-5 VP7 are present when using 0.2 M Tris-HCl, pH 8. However, VP7 quasi-crystals were not observed in any of the fractions after ultracentrifugation. Crystal formations were observed in the crude extract before and after the 23 300 x g/RCF (max) spin and the latter showed signs of degradation suggesting that high-speed spins may damage the crystalline-structure. A finding that was also reported by Maree and Paweska (2005).

Based on the previous findings, 0.2 M Tris, pH 8, seemed to increase trimer-trimer interactions and was therefore used for further optimisation experiments. However, 150 mM sodium chloride was included to mimic physiological conditions and increase ionic strength. In addition, low-speed differential centrifugation (1200 x g/RCF (max)) was retained, the resuspended-pellet after 3000 x g/RCF (max) spin was used for density gradient purification, and the ultracentrifugation speed was reduced to 17 500 x g/RCF (max). Furthermore, sucrose gradients were used for further optimisation to reduce costs, and maturation time was increased as limited necrosis

and chlorosis was observed on plant leaves 5 dpi so harvest day could be extended to 6 dpi. After western immunoblot analysis, AHSV-5 VP7 was observed in all gradient fractions and Coomassie staining showed higher concentrations in the lower fractions (**Figure 2.17**) displaying an increase in the insolubility of AHSV-5 VP7. This was confirmed by the observation of many well-formed quasi-crystals in fraction 1 (68%) and fraction 2 (50%) during TEM (**Figure 2.18**). However, while these crystals retained the crystal lattice they did not resemble the flat hexagonal formations reported by others (Basak et al. 1996; Chuma et al. 1992; Maree et al. 2016; Rutkowska et al. 2011). In addition, they were relatively small when compared to previous research (Burroughs et al. 1994; Chuma et al. 1992; Maree and Paweska 2005; Wall et al. 2017; Bailey 2016) ranging in size from 200-700 nm and forming conglomerates of various shapes. This may be a consequence of using plant expression systems. Interestingly, similar structural changes were observed by Rutkowska *et al.* (2011) when using a mutated version of AHSV VP7 which included an epitope of the foot-and-mouth disease virus (FMDV). However, despite the differences in crystal shape, the protocol adjustments seemed favourable for crystal-formation. These findings in conjunction with previous observations gave support to the hypothesis that high-speed spins may damage quasi-crystals, 0.2 M Tris-0.15 M NaCl, pH 8, strengthens VP7 trimer-trimer interactions, and a low-speed spin of 3000 x g/RCF (max) seems sufficient to isolate VP7 crystals in the pellet for further purification steps.

The penultimate step was to convert the successful sucrose step gradient into an iodixanol alternative. Optiprep^{TM} iodixanol is a preferable gradient medium for vaccine preparation as it is sterile, while sucrose is notoriously easy to contaminate. After conversion to iodixanol, analysis by western immunoblot and Coomassie staining demonstrated higher concentrations of AHSV-5 VP7 in the lower fractions, except for fraction 1, and observation by TEM revealed VP7 quasi-crystals in fraction 3 of the iodixanol gradient (**Figure 2.21**). Unfortunately, quantification by gel densitometry revealed low protein concentrations (2.39 µg/ml in the aspirated band (B) and 12.70 µg/ml in fraction 2 and a total of 0.52 µg/g FW yield).

In order to increase AHSV-5 VP7 crystal concentrations, the biomass was increased, and ultracentrifugation time was increased to 3.5 hours to allow more crystals to reach their isopycnic point. In addition, the gradient layers were adjusted to shift the crystals to a lower fraction. As a result, many well-formed quasi-crystals were observed in

fraction 1 (40/50%) and 2 (40%) and after gel densitometry, concentrations of 213.16 µg/ml and 2.66 µg/g FW yield were achieved in fraction 2. 10-50 µg in 400 µl (max) was needed for guinea-pig immunogenicity experiments, hence the concentrations were adequate to commence with these studies.

To confirm that AHSV-5 VP7 quasi-crystals were assembling in *N. benthamiana* leaves and not in vitro as a result of an ideal physiological environment created during the extraction process, leaves were agroinfiltrated with recombinant pRIC3.0-AHSV5-VP7, fixed on 5 dpi, embedded, leaf-ultra-sections prepared and *in situ* TEM performed. However, while *A. tumefaciens* was observed, no evidence of AHSV-5 VP7 quasi-crystals was seen. The typical pH for tobacco plant cell cytoplasm is between 7.5 and 7.8 which may decrease in response to abiotic stress such as agroinfiltration (Martiniere et al. 2013; Urbanowski 2012; Grosse-Holz et al. 2018). Interestingly, when using PBS, pH 7.4, in the purification process mostly the soluble version of AHSV-5 VP7 was present, therefore low pH cytosolic conditions may impede trimer-trimer formations. Future studies should include immunogold labelling for TEM to aid in AHSV VP7 quasi-crystal observation.

In conclusion, AHSV-5 VP7 was successfully expressed and VP7 quasi-crystals produced in *N. benthamiana.* The expression vectors pEAQ-*HT* and pRIC3.0 were compared and since pRIC3.0 resulted in higher yields of AHSV-5 VP7 it was selected as the optimal expression vector. Additionally, 6 dpi was established as the optimal harvest day to increase quasi-crystal maturation time. High amounts of VP7 quasi-crystals were present in the pellet after low-speed differential centrifugation and the resuspended pellet was suitable for density gradient purification. 0.2 M Tris-0.15 M NaCl, pH 8, increased trimer-trimer interactions and high-speed ultracentrifugation was found to destroy quasi-crystals. An FW yield of approximately 2.66 µg/g of plant-produced AHSV-5 VP7 quasi-crystals was achieved and this was considered satisfactory as previous researchers have reported yields of approximately 0.0025 ng/cell (Burroughs et al. 1994), 0.03 ng/cell (Chuma et al. 1992) and 0.5 ng/cell (Maree and Paweska 2005) when using recombinant baculovirus-infected Sf9 insect cells.

For the purposes of this study, density gradient ultracentrifugation was considered a successful method for AHSV VP7 quasi-crystal purification, however, future work

should seek a more scalable alternative such as depth filtration and tangential flow cytometry, as density gradient ultracentrifugation can be tedious particularly when upscaling and requires expensive equipment (Dennis 2019). To our knowledge this is the first time that AHSV VP7 quasi-crystals have been expressed using a plant expression platform.

CHAPTER 3: TESTING THE IMMUNOGENICITY OF AHSV-5 VP7 QUASI-CRYSTALS AS A CANDIDATE VACCINE

3.1 Introduction

AHSV VP7 is a highly immunogenic protein and its immunodominance has been widely utilised in serological assays to identify infections and distinguish between *Orbivirus* serogroups (Maree and Paweska 2005; Martinez-Torrecuadrada et al. 1996). AHSV VP7 is highly conserved within its serogroup with greater than 98% amino acid identity between the nine serotypes, and has been established as the group-specific antigen (Chuma et al. 1992; Williams et al. 1998). In vaccine design, this similarity between serotypes is a favourable characteristic as it negates the need for a multivalent vaccine.

As mentioned previously, another advantageous characteristic of AHSV VP7 quasi-crystals is the highly ordered repetitive conformation which results in the repetition of immunologically important epitopes thereby potentially enhancing humoral and cell-mediated immune responses (Bailey 2016; Friede and Aguado 2005; Rutkowska et al. 2011; St Clair et al. 1999; Storni et al. 2005). A study by St Clair et al. (1999) demonstrated that cross-linking human serum albumin crystals for vaccine delivery resulted in a 6 to 10-fold increase in antibody titres raised in Sprague–Dawley rats. AHSV VP7's intrinsic ability to aggregate and self-form crystalline structures can therefore be utilised to produce large quantities of cross-linked quasi-crystals to meet the demand for vaccine production (Maree and Paweska 2005; St Clair et al. 1999).

Furthermore, particulates are more efficiently processed by antigen presenting cells (APC) than soluble antigens (Snapper 2018; Vidard et al. 1996). Antigens larger than 200-500 nm need to be transported from peripheral tissues to lymphoid organs by APCs resulting in T-cell activation. Smaller antigens, 20-200 nm, freely enter the lymphatic system and activate B-cell responses (Bachmann and Jennings 2010; Manolova et al. 2008; Snapper 2018; Vidard et al. 1996). Particulates have been utilised in many antigen delivery systems and various studies have shown that dendritic cell uptake of particles enhances the production of interleukins stimulating innate and cellular immune responses. More specifically, some of these antigen delivery systems have been shown to induce T-helper (Th)1 and cytotoxic T-

lymphocyte (CTL) responses (Friede and Aguado 2005; Sharp et al. 2009; Storni et al. 2005). Dendritic cells and macrophages are the most important APCs for activation of T-cell responses (Bachmann and Jennings 2010). Dendritic cells efficiently phagocytose particulates of less than 0.5 µm, whilst macrophages process particles less than ±5 µm (Foged et al. 2005; Hirota and Ter 2012; Yue et al. 2010). In a recent study by Bailey et al. (2016) VP7 crystals did not yield a favourable humoral response and this was speculated to be due to large antigen sizes often exceeding 5 µm. In contrast, plant-derived quasi-crystals produced in this study (**Chapter 2**) tend to range from 50 nm to 1000 nm which we hypothesise to be satisfactory to yield both humoral and cell-mediated responses.

The role of humoral immunity to AHSV infection has been relatively well studied. However, cell-mediated immunity has been overlooked. The survival of vaccinated animals after a lethal viral challenge but void of sufficient humoral responses and neutralising antibodies for protection suggest that cell-mediated responses are paramount in AHSV immunity (Guthrie et al. 2009; Martinez-Torrecuadrada et al. 1996; Wade-Evans et al. 1997). The importance of cell-mediated immunity against the closely related Bluetongue virus (BTV) has been established and BTV NS1, NS3, VP2, VP5 and VP7 CTL epitopes have been described (Andrew et al. 1995; Jeggo et al. 1984; Wade-Evans et al. 1997). AHSV VP7 has been hypothesised to have T-cell epitopes similar to that of BTV VP7 (Martinez-Torrecuadrada et al. 1996). And research by Pretorius et al (2016) has demonstrated that innate, humoral and cell-mediated immune responses were induced in horses after AHSV infection (Pretorius et al. 2016). Furthermore, another study detected proliferating CD8 T-cells in peripheral blood mononuclear cells (PBMC) obtained from horses after infection by attenuated AHSV-4. The cytotoxicity of these CD8 T-cells was tested using the fluorescent antigen-transfected target cells-cytotoxic T lymphocytes (FATT-CTL) assay. VP1, VP2, VP4, VP7 and NS3 antigen-specific CD8 T-cells resulted in cell lysis which suggested that CTL immune responses are important in protection against AHSV (Faber et al. 2016).

Cell-mediated immune responses are activated by the fast-acting innate immune system. Pattern recognition receptors (PRR) such as the membrane bound: Toll-like receptors and C-type lectin receptors, and the cytoplasmic: NOD-like receptors and RIG-I-like receptors, recognise pathogen-associated molecular patterns (PAMPs).

This initiates signalling cascades leading to the production of cytokines by infected cells and PBMCs (Cui et al. 2014; Takeuchi and Akira 2009, 2010). Cytokines include interferons (IFNs), chemokines, tumour necrosis factors and interleukins (IL) that regulate and mediate inflammatory and immune responses to pathogens (Justiz Vaillant and Qurie 2019). Activation of B-cell receptor pathways cause B-cell proliferation and differentiation into antibody secreting plasma cells or memory B-cells (Janeway et al. 2001; Savignac et al. 2010; Dorner and Radbruch 2007). The antibody isotypes IgM, IgG and IgA are important for controlling viral infection and either opsonise or neutralise the virus or activate the complement system (**Figure 3.1**). B-cells can also act as APCs to naive T-cells (Dorner and Radbruch 2007). After antigens have been processed and presented by APCs they are presented on MHC-I or MHC-II which stimulate CD8 and CD4 T-cells respectively (**Figure 3.1**). The former activates CTLs mediating cell lysis by cytotoxic granules and the latter activates Th1, Th2 and Th17 cells which further regulate B-cell production, upregulate macrophages and further activate CTLs (Alberts et al. 2002; Dorner and Radbruch 2007; Janeway et al. 2001).

Interferons are an important part of the antiviral immune response, they stimulate macrophages and natural killer (NK) cells, induce apoptosis in infected cells and increase the production of major histocompatibility complexes, MHC-I and MHC-II (Morris 1988; Samuel 2001). In particular, type-I interferons play a pivotal role in antiviral studies and IFN1-alpha and -beta have been shown to be important for immunity against BTV and AHSV (Castillo-Olivares et al. 2011; Pretorius et al. 2016; Schroder et al. 2004). Chemokines are attractants of T-cells, monocytes and granulocytes. The chemokine CX3CL1, activated by interferon-gamma and tumour necrosis factor-alpha, is an important chemoattractant to cytotoxic effector lymphocytes as its receptor CX3CR1 is expressed on NK cells and CTLs (Pretorius et al. 2016; Umehara et al. 2004; Wojdasiewicz et al. 2014). Interleukins are a large group of proteins which are involved in regulating both the innate and adaptive immune responses (**Figure 3.1**). Interleukins involved in adaptive immunity include, IL-1 which activates macrophages, B-cells, T-cells and stimulates T-cell IL-2 production. IL-2 induces proliferation and differentiation of T-cells, B-cells, NK cells and CTL activation. Furthermore, IL-21 is produced by CD4 T-cells and various interleukins are produced by Th2 cells (IL-4, IL-5, IL-10, IL-13, IL-19 and IL-31), Th17 cells (IL-9, IL-17 and

IL-26), NKT-cells (IL-9 and IL-13) and NK cells (IL-21). The interleukins, IL-10, IL-12 and IL-18 are responsible for the induction of Th1 cells. IL-28 stimulates cell presentation of viral antigens to CD8 T-cells and IL-5 activates CD8 T-cell proliferation (Justiz Vaillant and Qurie 2019).

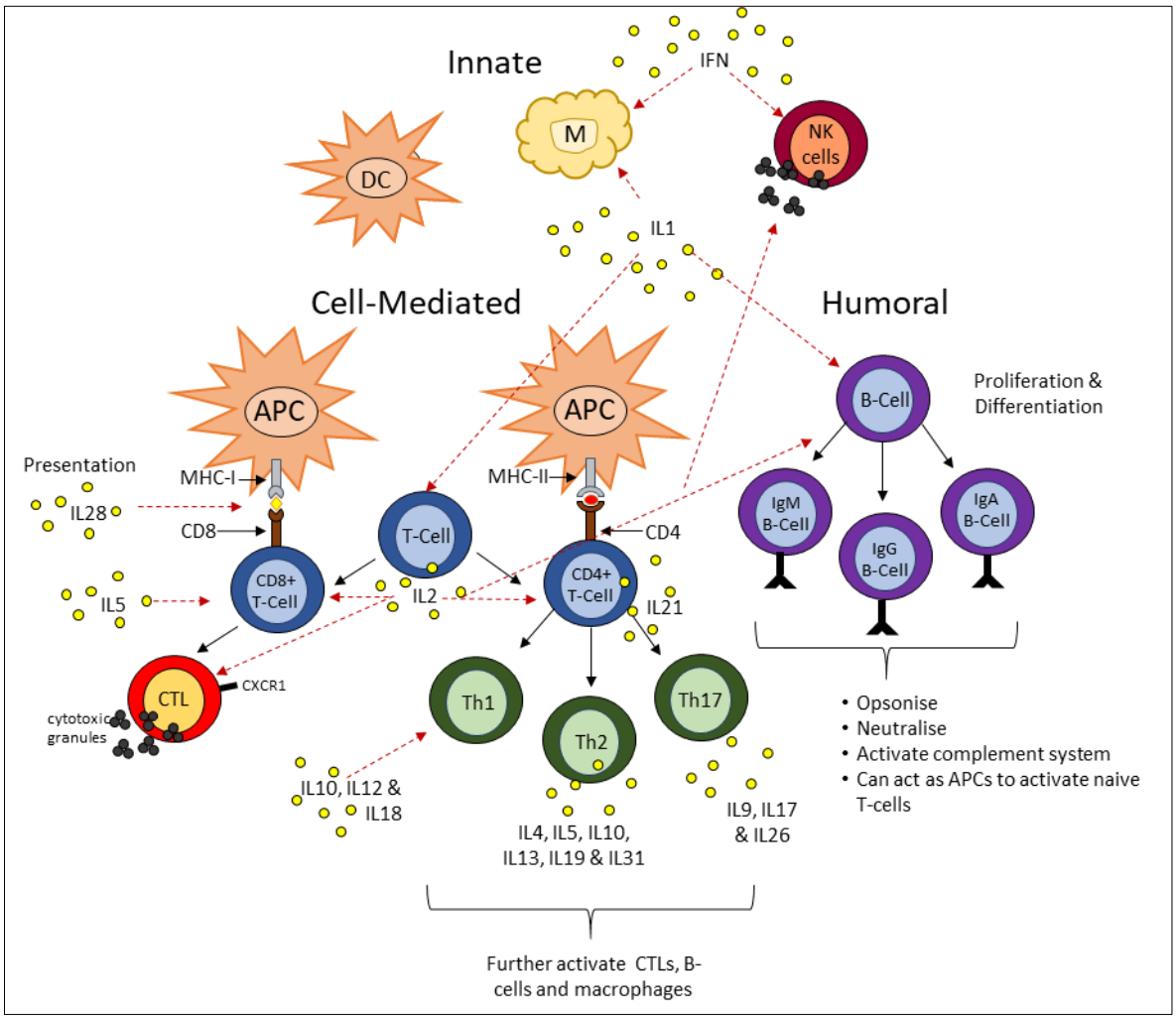

Figure 3.1: Simplified representation of cell-mediated and humoral responses, and associated interleukins. The presentation of epitopes via MHC-I and -II to CD8+ and CD4+ T-cells is represented. Additionally, differentiation into CTLs and Th1, Th2 and Th17 cells are depicted as well as their associated interleukins. Yellow dots represent cytokines. Black arrows signify proliferation and differentiation, and red arrows depict activation. DC: Dendritic cells; M: Macrophages; NK: Natural Killer; APC: Antigen presentation cell; MHC: Major histocompatibility complex; CTL: Cytotoxic T-cells; Th: T-helper; IL: Interleukin; IFN: Interferons; Ig: Immunoglobulin.

In order to investigate the cell-mediated immune response to AHSV VP7 quasi-crystals, RNA sequencing (RNA-seq) of spleen-derived mRNA was used to assess the guinea-pig transcriptome post-vaccination with AHSV-5 VP7 quasi-crystals. RNA-seq is a powerful technique used to perform genome-wide transcriptome profiling. It is a highly sensitive tool and is preferred over array-based technologies to capture global expression profiles and provide more precise results. RNA-seq has been widely used in differential gene expression analyses and is therefore considered a good tool for studying the immune transcriptome profile (Anamika et al. 2016).

We therefore tested the humoral and cell-mediated immune response to AHSV-5 VP7 quasi-crystals using western immunoblotting and RNA-seq transcriptome profiling. Furthermore, we assessed the stability of AHSV VP7 quasi-crystals to examine the viability of the candidate vaccine.

3.2 Materials & Methods

3.2.1 Assessing AHSV-5 VP7 Quasi-Crystal Stability

AHSV-5 VP7 crystals were purified as per **2.2.4.6** respectively. A 1100 µl volume (58 µg/ml) of purified AHSV-5 VP7 quasi-crystals was removed and aliquoted into 21 x 50 µl (2.9 µg per 50 µl) samples. Seven aliquots were stored at 4°C, -20°C and -80°C (**Figure 3.2**). AHSV-5 VP7 quasi-crystals were then examined one day post-purification (pp) and 2-, 4-, 8-, 12-, 16-, 20- and 28-weeks pp. Of the 50 µl volume stored, 15 µl was removed and assessed using a Tecnai 20 transmission electron microscope (TEM) as per **2.2.6** and 35 ul was removed for western immunoblot and Coomassie staining analysis as per **2.2.5**.

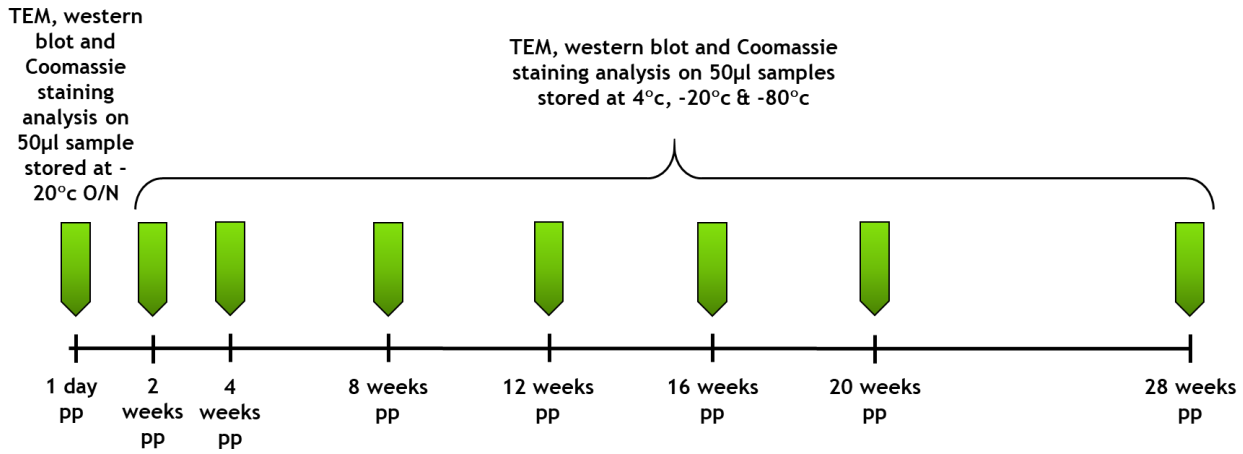

Figure 3.2: AHSV-5 VP7 quasi-crystal stability assessment timeline. Samples were analysed at 2-, 4-, 8-, 12-, 16-, 20- and 28-weeks post-purification (pp) via TEM, western immunoblot and Coomassie staining analysis.

3.2.2 AHSV-5 VP7 Quasi-Crystal Vaccine Preparation for Immunogenicity Studies

In order to prepare the primary AHSV VP7 inoculum and booster for guinea-pig immunogenicity studies, AHSV-5 VP7 was expressed and quasi-crystals purified under sterile conditions using the methods described in **2.2.4.6**. The control inoculum was produced in the exact same manner as the AHSV VP7 inoculum, however an empty pRIC3.0 expression vector was used for infiltration. Quantification was carried out as per **2.2.5**. To examine the ASHV VP7 and control inocula preparations for contamination, samples were streaked onto lysogeny broth (LB) agar plates [1.0% tryptone, 0.5% yeast extract, 0.5% NaCl, 1.5% agar, pH 7.0] and incubated O/N at 27°C. Additionally, endotoxin levels were quantified by means of the ToxinSensor™Chromogenic LAL Endotoxin Assay Kit (Genscript Biotech Corporation, Piscataway, USA). The primary AHSV VP7, booster and control inocula were all stored at -20°C until required and 25 µl samples were removed on the day of vaccination to re-assess sterility and concentration levels as per **2.2.5.** Directly preceding vaccination, 5% Montanide™ PET Gel A adjuvant (Seppic, Paris, France) was added to the inocula under sterile conditions.

3.2.3 Guinea-Pig Immunogenicity Study

In the absence of the ideal animal model i.e. horses, guinea-pigs were selected as a suitable substitute as they have previously demonstrated a favourable humoral response to AHSV, similar to that of horses (Lelli et al. 2013b). The guinea-pig immunogenicity study took place in the Research Animal Facility (RAF) at the University of Cape Town (UCT) and was approved by the Faculty of Health Sciences (FHS) Animal Ethics Committee (AEC), UCT (FHS AEC ref no.: 016/019). All procedures were carried out by a trained animal technologist, Mr Rodney Lucas (Registration no: SAVC L03/5973), who also performed the daily welfare monitoring of all animals. Ten female guinea-pigs (*Cavia porcellus*) of the Hartley strain and approximately 12-weeks-old (480-590 g) were acquired for this study. Five guinea-pigs per group were considered a suitable number of biological replicates for RNA-sequencing experiments as per the 'ENCODE Guidelines and Best Practices for RNA-Seq' and (https://genohub.com/next-generation-sequencing-guide/#replication). Guinea-pigs were randomly assigned into control (C1-5) and experimental (X1-5) groups and housed together in large pens including the appropriate materials for bedding and enrichment. Following transport to RAF UCT, guinea-pigs were given time to acclimatise to their new environment for at least ten days before the experiment commenced.

On day 0 and prior to primary inoculation, 100 µl pre-bleeds were drawn from each of the ten guinea-pigs (**Figure 3.3**). Five guinea-pigs (X1-5) were then subcutaneously injected with the primary inoculum using a 23 G needle and a further five injected with the control (C1-5) described in **3.2.2**. Each guinea-pig received a total volume of 400 µl dispensed as 100 µl injections at four sites. Each 400 µl experimental sample contained 35.13 µg of purified AHSV-5 VP7 quasi-crystals (**3.2.2**). On day 13 the experimental guinea-pigs (n=5) were subcutaneously injected with a 400 µl booster which contained 26.87 µg of purified AHSV-5 VP7 quasi-crystals, prepared as described in **3.2.2** (**Figure 3.3**)**.** Control guinea-pigs (n=5) were also injected with a 400 µl preparation prepared in the same way as the booster but void of AHSV-5 VP7 as per **3.2.2**. The subcutaneous route of injection was selected as it is considered the preferred route of administration due to slow rates of absorption and reduced distress to the animal. Following subcutaneous injection, dendritic cells have been found to be the primary APCs recruited and the C-type lectin, FC receptor and Toll-like receptor

pathways are more likely to be activated mediating T-cell responses (Fathallah et al. 2013). No signs of severe inflammation or infection were detected after the primary inoculation or booster at the injection sites. Animals were weighed on a weekly basis and both experimental and control guinea-pigs gained weight well throughout the experiment. On day 41 all guinea-pigs were exsanguinated whilst under a deep terminal anaesthesia using ketamine/xylazine, after which they were euthanised by a 1ml Potassium Chloride (1-2 mM/kg) cardiac puncture (**Figure 3.3**). Serum was separated from whole blood via centrifugation at 2000 xg/RCF (max) for 20 min by Mr Rodney Lucas. Randomisation was implemented when selecting guinea-pigs for the above procedures.

Spleens were extracted directly after euthanasia on day 41 by Mr Rodney Lucas and immediately cut into thin sections to produce a single dimension of less than 0.5 cm. Each spleen weighed ≤1 g and analogous sections were therefore placed in 5 ml RNA*later*™ stabilisation solution (Thermo Fisher Scientific, Massachusetts, USA) immediately to stabilise and preserve RNA. These samples were stored O/N at 4°C to allow the solution to thoroughly penetrate the tissue. After which the supernatant was removed, and spleen sections stored at -20°C until RNA extraction could be performed (**3.2.6.1**).

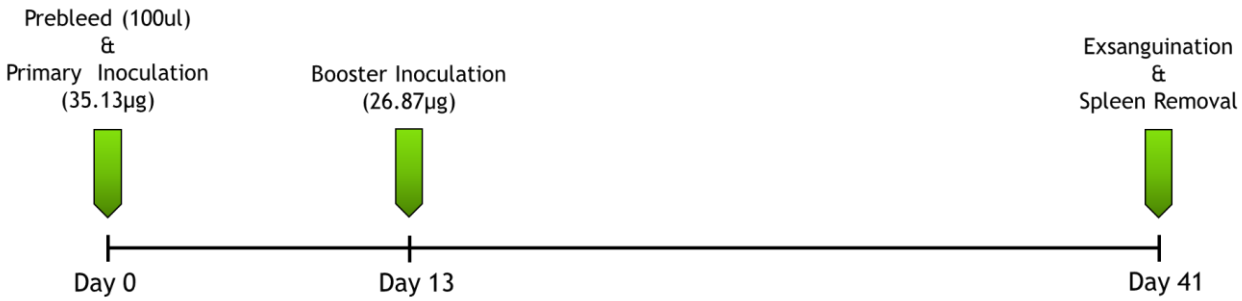

Figure 3.3: Guinea-pig immunogenicity study timeline. 100 µl pre-bleeds were removed on day 0, and primary and booster inoculations were performed on day 0 and day 13, respectively. Exsanguination and spleen removal were carried out on day 41.

3.2.4 Testing Neutralisation Capability of AHSV-5 VP7 Quasi-Crystals

Serum neutralisation tests (SNT) were performed by Ms Carina Lourens, Technologist at the Equine Research Centre, Department of Veterinary Tropical Diseases, University of Pretoria. Guinea-pig anti-AHSV-5 VP7 sera were assayed against AHSV serotype 4, 5 and 8, and the Onderstepoort Biological Product (OBP) vaccine was used as the positive control.

3.2.5 Analysis of Humoral Immune Response to AHSV-5 VP7 Quasi-Crystals

3.2.5.1 SDS PAGE and western immunoblot analysis of guinea-pig pre-bleeds and final-bleeds

Guinea-pig pre-bleed and final-bleed, control and experimental sera were used to detect purified AHSV-5 VP7 antigen (0.77 µg loaded per well). Purified AHSV-5 VP7 was prepared using the methods described in **2.2.4.6** and SDS PAGE carried out as per **2.2.5**. Western immunoblotting was performed as per **2.2.5** with a few alterations: After transfer and blocking of HyBond^{TM} C Extra nitrocellulose membranes (AEC-Amersham, Gauteng, South Africa) each lane was labelled, excised and placed into one of the allocated polyclonal anti-AHSV-5 VP7 guinea-pig sera (X1-5 or C1-5). The antigen detection capability of polyclonal anti-AHSV-5 VP7 guinea-pig sera were assessed at dilutions of 1:50 000 and 1:100 000.

As a positive control, polyclonal anti-AHSV-5 VLP guinea-pig serum previously used as the primary antibody for detection of AHSV-5 VP7 (**2.2.5**) at a 1:5000 dilution was used to detect AHSV-5 VP7 antigen. Additionally, various negative controls were used: (1) In order to assess secondary antibody contamination, no primary antibody was used and goat anti-guinea-pig IgG alkaline phosphatase-conjugated secondary antibody (Sigma-Aldrich, St Louis, Missouri) was used to detect AHSV-5 VP7 antigen at a dilution of 1:5000, (2) Final-bleed mouse sera (1:20 000) obtained from mice injected with a plant-produced vaccine control, prepared using the empty pRIC3.0 expression vector, were used to detect AHSV-5 VP7 antigen, (3) Plant-produced Shuni virus (SHUV) protein, kindly provided by Mr Matt Verbeek (BRU, MCB, UCT), was loaded as the antigen and probed with anti-AHSV-5 VP7 guinea-pig pre-bleed

(C2) and final-bleed (C2, X1 and X2) sera to assess non-specific binding, (4) The vaccine-control, prepared in the same way as the vaccine but void of AHSV-5 VP7, was loaded and probed with anti-AHSV-5 VP7 final-bleed (C2 and X1) guinea-pig sera to assess non-specific binding, (5) Polyclonal anti-foot and mouth disease virus (FMDV) guinea-pig serum, kindly provided by Mr Scott De Beer (BRU, MCB, UCT), was used as the primary antibody (1:2000) to detect AHSV-5 VP7 antigen, (6) A semi-crude preparation of AHSV-5 VP7 was used as the antigen and probed by anti-AHSV-5 VP7 final-bleed control guinea-pig (C2) serum to assess non-specific binding.

Furthermore, blocking buffer containing 3% bovine serum albumin (BSA) (Sigma-Aldrich, St Louis, Missouri) as opposed to 5% fat-free milk and the pre-absorption technique (**3.2.5.2**) was tested to increase specificity of the anti-AHSV-5 VP7 guinea-pig sera.

3.2.5.2 Pre-absorption with host cell proteins to increase binding specificity of anti-AHSV-5 VP7 guinea-pig sera

Six grams of leaf biomass was removed from healthy four-week-old *N. benthamiana* plants and combined with 20 ml 0.2 M Tris-0.15 M NaCl, pH 8. The mixture was thoroughly homogenised using the T25 digital Ultra-Turrax® blender (IKA®, Staufen, Germany) and placed at 4°C with gentle shaking for 30 min. The homogenate was then filtered through one layer of Miracloth™ (Merck, Darmstadt, Germany) and centrifuged at 1200 xg/RCF (max) for 10 min at 4°C using the Beckman Avanti® J-25 High Speed Centrifuge (Beckman Coulter, Brea, CA). To allow binding of plant proteins to the nitrocellulose, the supernatant was then transferred to a container possessing 5 x 5 cm pre-wet (dH_2O) HyBond™ C Extra nitrocellulose and incubated for 2 hrs at room temperature with gentle agitation. The plant extract was then removed and replaced with 15 ml anti-AHSV-5 VP7 guinea-pig serum diluted to 1:50 000, which allowed binding of non-specific anti-plant antibodies. This was incubated for 2 hrs at room temperature with gentle shaking and then stored O/N at -20°C until utilised in subsequent western immunoblots. The pre-absorption technique was repeated for all final-bleed experimental and control guinea-pig sera.

3.2.6 Transcriptome Profiling: Analysing the Cell-mediated Immune Response to AHSV-5 VP7 Quasi-crystals

3.2.6.1 RNA extraction & integrity analysis

15-20 mg of RNA*later*™ stabilised spleen tissue was placed in a 2 ml Eppendorf tube containing 600 µl of the RNeasy Mini Kit lysis buffer (Qiagen GmbH, Hilden, Germany). The lysis buffer included 1% β-Mercaptoethanol. A TissueLyser LT (Qiagen, Hilden, Germany) and stainless-steel beads were used to disrupt and homogenise the lysate. Total RNA was extracted from guinea-pig spleens (C1-5 and X1-5) using the RNeasy Mini Kit (Qiagen GmbH, Hilden, Germany) according to the manufacturer's instructions, and an on-column DNase digestion (Qiagen GmbH, Hilden, Germany) was used to remove genomic DNA contaminants. The resultant RNA was eluted in 60 µl RNase free water and 30 µl removed to assess RNA concentration and quality. The remaining 30 µl of eluted RNA, ranging from between 348.1-672.2 ng/µl, was combined with 90 µl E.Z.N.A. RNA Transport buffer (Omega Bio-tek, Georgia, USA) and couriered to Omega Bio-tek (Georgia, USA) at room temperature for RNA integrity analysis, library preparation, transcriptome sequencing and bioinformatics analyses.

RNA concentration was assessed using a NanoDrop 1000 Spectrophotometer (Thermo Fisher Scientific, Massachusetts, USA) at 260 nm and RNA quality quantified at the absorbance ratio 260/280 nm and 260/230 nm. A further assessment of RNA quality was performed by agarose gel electrophoresis. Samples were diluted in RNAse free H_2O to yield ±2 µg of RNA, combined with 6x DNA loading dye (Thermo Fisher Scientific, Massachusetts, USA), heat-denatured for 5 min at 65°C and subsequently snap cooled on ice until loading. 2 µl of O'GeneRuler™1 kb DNA ladder (Thermo Fisher Scientific, Massachusetts, USA) was used as a molecular weight marker, in the absence of the more appropriate RNA molecular weight marker. Sample volumes of 10 µl were loaded onto a 1% agarose gel including 3 µl ethidium bromide (EtBr) and electrophoresed at 60 volts for approximately 1.5 h. The 28S (5 kb) and 18S (1.9 kb) ribosomal subunit RNA bands were assessed as a proxy to ascertain the total RNA quality.

Furthermore, the RNA quantity, purity and integrity of all ten samples was assessed by Omega Bio-tek (Georgia, USA) using the bioanalyser, Agilent 2200 TapeStation System (Agilent, California, USA) and RNA ScreenTape (Agilent, California, USA). RNA samples with RIN (RNA integrity number) scores greater than 7.2 were selected for subsequent mRNA library preparation and RNA sequencing.

3.2.6.2 Transcriptome sequencing & bioinformatics analyses

RNA library preparation and sequencing were performed by Omega Bio-tek (Georgia, USA). At least 0.5 µg of starting total RNA was needed for library preparation and the Agilent 2100 TapeStation System (Agilent, California, USA) revealed between 5.91 µg to 21.68 µg of total RNA in our samples. The TruSeq Stranded mRNA Library Prep Kit (Illumina, California, United States) was used for mRNA library preparation as per manufacturer's instructions. RNA sequencing (RNA-seq) was performed using an Illumina HiSeq X high-throughput platform, sequencing ±40 million reads in 150 bp paired-end format per sample. Five guinea-pigs per group was considered a suitable number of biological replicates for RNA-seq experiments as per the 'ENCODE Guidelines and Best Practices for RNA-Seq' and (https://genohub.com/next-generation-sequencing-guide/#replication).

Bioinformatics analyses were performed by Omega Bio-tek (Georgia, USA) using the Illumina Basespace platform (https://basespace.illumina.com) and DESeq2 tool for mapping and differential gene expression analysis. Approximately 20.21-53.54 million 150 bp paired-end raw reads for each sample were imported, filtered and trimmed by removing adapter sequences and low-quality base reads using the BowTie short read aligner. The resultant high-quality reads were mapped to a reference genome (*Cavia* porcellus) using STAR in the Illumina RNA alignment App. Unfortunately, the *Cavia porcellus* genome was not available as a standard reference genome at the time of this study as the Mammalian Genome Project had only sequenced the guinea-pig genome to 2x coverage and was therefore only assembled to scaffold level. The existing scaffold genome was therefore used as a reference in combination with *de novo* transcriptome assembly by using the Illumina Basespace Custom Genome Builder App. Genes were annotated using GENCODE and DESeq2 results revealed an annotated gene count of 26 855. The total number of mapped reads for each transcript were determined and these were normalised to FPKM (fragments per

kilobase of exon model per million mapped reads). These normalised gene counts were then $\log^2$ transformed to observe proportional changes in the data. As mentioned, differential gene expression analysis was then performed on the experimental (n=5) and control (n=5) datasets by Omega Bio-tek (Georgia, USA) in Illumina Basespace (https://basespace.illumina.com) using the DESeq2 analysis tool (Love et al. 2014).

The DESeq2 model uses a generalized linear model (GLM) for differential expression analysis (Love et al. 2014) where:

$$K_{ij} \sim \mathrm{NB}(\mu_{ij}, a_i)$$

$$\mu_{ij} = s_j q_{ij}$$

$$\log^2(q_{ij}) = X_j . \beta_i$$

where:

- Counts $\boldsymbol{K_{ij}}$ for gene $\boldsymbol{i}$ sample $\boldsymbol{j}$ are modeled using a negative binomial distribution with fitted mean $\boldsymbol{\mu_{ij}}$ and a gene-specific dispersion parameter $\boldsymbol{a_i}$.
- The fitted mean is composed of a sample-specific size factor $\boldsymbol{s_j}$ and a parameter $\boldsymbol{q_{ij}}$ proportional to the expected true concentration of fragments for sample $\boldsymbol{j}$.
- The dispersion parameter $\boldsymbol{a_i}$ defines the relationship between the variance of the observed count and its mean value, which depends both on the size factor $\boldsymbol{s_j}$ and the covariate-dependent part $\boldsymbol{q_{ij}}$ (defined above).
- The coefficients $\boldsymbol{\beta_i}$ give the log2 fold changes for gene $\boldsymbol{i}$ for each column of the model matrix $\boldsymbol{X}$ (Love et al. 2014).

After normalisation and transformation, an annotated gene count of 7213 was tested for statistical significance by the DESeq2 model. The DESeq2 model uses the Wald test to test the statistical significance of differential expression, where the estimated

standard error of the $\log^2$ fold change (between the control and experimental group) is tested to see if it differs significantly from zero (Love et al. 2014). The DESeq2 model adjusts the Wald test p-values for multiple testing, taking into account the false discovery rate (FDR), using the procedure of Benjamini and Hochberg (Benjamini and Hochberg 1995) to calculate q-values (corrected p-values). Experimental and control 'regularised transformed gene counts/ expressed transcripts' were found to be significantly differentially expressed if the q-value (corrected p-value) ≤ 0.05. Three hundred and fifty genes were found to be significantly differentially expressed (DE) when compared to the control gene counts.

3.2.6.3 Global and cell-mediated immune response analyses

R (R Core Team 2018) was used to analyse the global immune response from the DESeq2 results, with the main focus being the cell-mediated immune response. Twenty two immune pathways and their related genes were accessed using the Kyoto Encyclopedia of Genes and Genomes (KEGG) (https://www.genome.jp/kegg/pathway.html) and Reactome pathway databases (https://reactome.org/PathwayBrowser/) (**Table 3.1**). Unfortunately, *Cavia Porcellus* was not one of the listed KEGG or Reactome organisms. The National Center for Biotechnology Information (NCBI) Taxonomy browser (https://www.ncbi.nlm.nih.gov/taxonomy) and Lifemap NCBI (http://lifemap-ncbi.univ-lyon1.fr/) were used to ascertain the closest living relative to *Cavia porcellus*. As a result, the *Heterocephalus glaber* and *Mus musculus* immune pathways from the KEGG and Reactome pathway databases respectively were used for further analyses.

Table 3.1: Innate and adaptive immune pathways and the respective categories and pathway databases used.

Analysed Immune Related Pathways	Database Categories	Pathway Database
Chemokine signalling pathway	Immune system	KEGG Pathway Database (https://www.genome.jp/kegg/pathway.html)
Natural killer cell mediated cytotoxicity		
Leukocyte transendothelial migration		

Fc gamma R-mediated phagocytosis		Organism: *Heterocephalus glaber*
NOD-like receptor signalling pathway		
Complement and coagulation cascades		
Platelet activation		
T cell receptor signalling pathway		
Th1 and Th2 cell differentiation		
Th17 cell differentiation		
IL-17 signalling pathway		
Antigen processing and presentation		
C-type lectin receptor signalling pathway		
Toll-like receptor signalling pathway		
RIG-I-like receptor signalling pathway		
Cytosolic DNA-sensing pathway		
B cell receptor signalling pathway		
Cytokine-cytokine signalling interaction	Signalling molecules and interactions	
Jak-STAT signalling	Signal transduction	
Ras signalling pathway		
Rap1 signalling pathway		
MHC-1 Processing and Presentation	Adaptive immune system	Reactome database (https://reactome.org/PathwayBrowser/) Organism: *Mus Musculus*

Ensembl and NCBI Entrez gene IDs were converted to gene symbol/name using the biomaRt package (Steffen Durinck 2009) in R (R Core Team 2018). Commonalities between gene symbols/name from the selected KEGG and Reactome immune pathways and the 350 significantly differentially expressed genes were examined using R (R Core Team 2018). 30 of the *Cavia Porcellus* innate and adaptive immune response pathway genes were found to be significantly differentially expressed, 8.6% of the 350 significantly differentially expressed genes. Additionally, commonalities between the larger 'annotated gene count' dataset (including all expression data not only significantly differentially expressed genes) and gene symbols from the selected KEGG and Reactome immune pathways were examined using R (R Core Team 2018). Heatmaps were constructed using the plotly package (Sievert 2018) in R (R Core Team 2018). Heatmaps were not scaled and were therefore a direct representation of the regularised and log2transformed gene transcript count.

Significantly differentially expressed genes and related biological processes, molecular function and immune pathways were analysed and visualised using the gene ontology (GO) resource (http://geneontology.org/), biomaRt package (Steffen Durinck 2009) in R (R Core Team 2018) and KEGG (https://www.genome.jp/kegg/pathway.html).

3.3 Results

3.3.1 Assessing Stability of AHSV-5 VP7 Quasi-Crystals

Vaccines often require storage over long periods of time at varying temperatures. The stability or thermolability of a vaccine is therefore an important consideration when determining its vaccine potential. We therefore sought to establish the stability of AHSV-5 VP7 quasi-crystals at 4°C, -20°C and -80°C over 28 weeks.

Figure 3.4 shows the western immunoblot and Coomassie staining analysis of AHSV-5 VP7 over a 28-week period at 4°C, -20°C and -80°C. Overall the AHSV-5 VP7 protein bands seemed qualitatively similar in density with no sign of degradation

indicating that the protein is stable over varying temperatures and over the assessment period of 28-weeks.

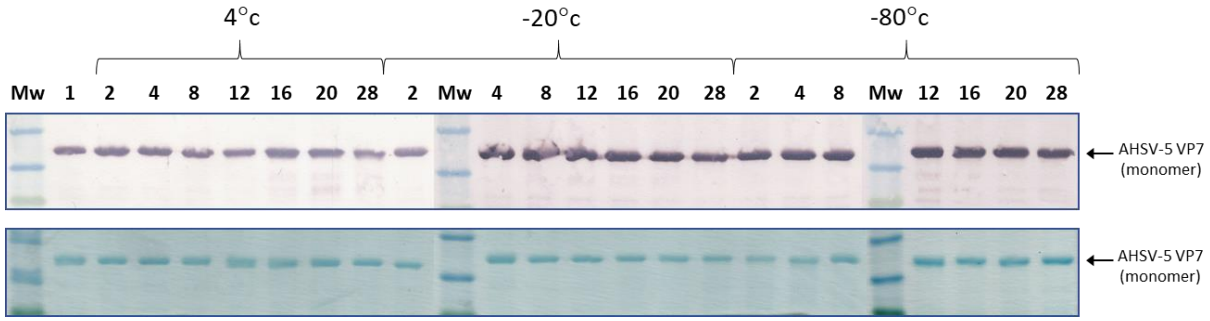

Figure 3.4: Stability assessment of AHSV-5 VP7. Western immunoblots (top) and Coomassie stained SDS-PAGE gels (bottom) of purified AHSV-5 VP7 samples stored at 4°C, -20°C and -80°C. 15 µl volumes of stored samples were added to each lane. Arrows indicate the positions of AHSV-5 VP7 monomer (37 kDa). Mw: NEB molecular weight marker (sizes displayed in kDa), 1: 1-day post purification (pp), 2, 4, 8, 12, 16, 20, 28: no. of weeks pp.

Table 3.2 shows TEM images of purified AHSV-5 VP7 samples over a 28-week period at 4°C, -20°C and -80°C. Only one image per sample, of the largest crystal observed, is displayed in **Table 3.2**. The rate of crystal observation was much higher when analysing the -20°C and -80°C stored samples compared to samples stored at 4°C. By the 4th week pp samples stored at 4°C displayed very few AHSV-5 VP7 quasi-crystals and only one very large crystal of ±900 nm was observed by the 8th week pp. No crystals were observed after 8 weeks when storing samples at 4°C. More crystals of a greater size were observed in samples stored at -80°C when compared to -20°C. However, the largest crystals observed over the 28-week assessment period were found in the -20°C sample on 28-weeks pp (±819 nm) and the 4°C sample on 8-weeks pp (±900 nm).

Table 3.2: Stability assessment of AHSV-5 VP7 quasi-crystals. Quasi-crystals observed via TEM analysis. Purified AHSV-5 VP7 samples stored at 4°C, -20°C and -80°C. Days or weeks pp indicated in the left column. Only one image per sample of largest crystal seen displayed. Scale bars: 100 nm or 200 nm (indicated in image).

Days or weeks post-purification (pp)	Storage Temperature		
	4°C	-20°C	-80°C
1 Day pp		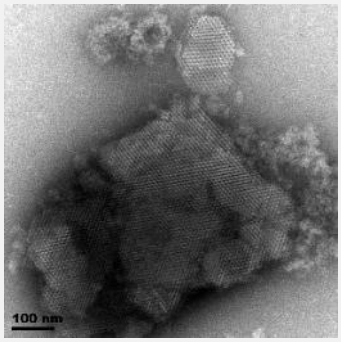	
2 Weeks pp	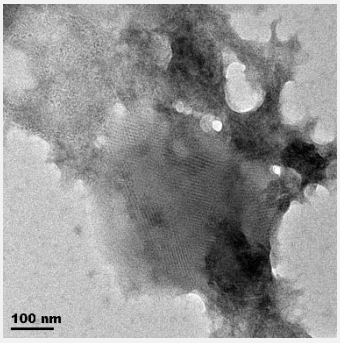	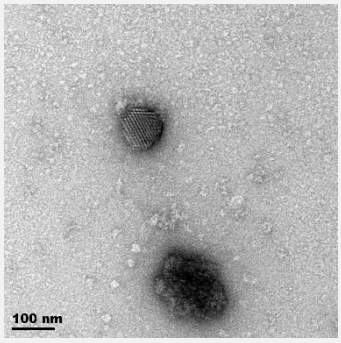	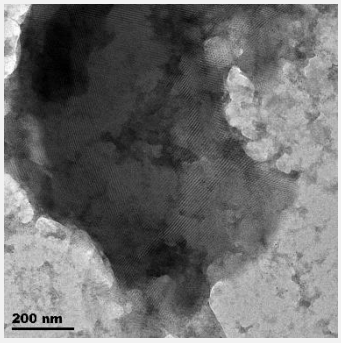
4 Weeks pp	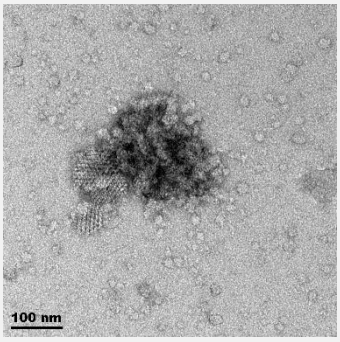	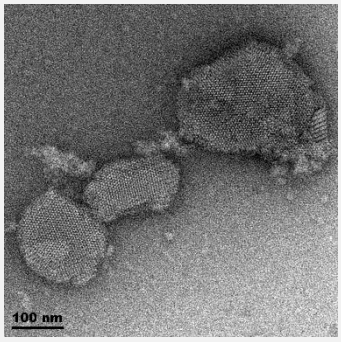	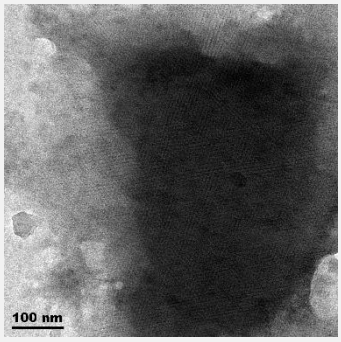

8 Weeks pp	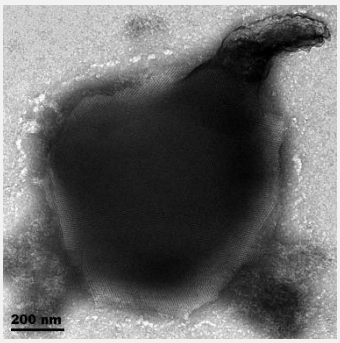	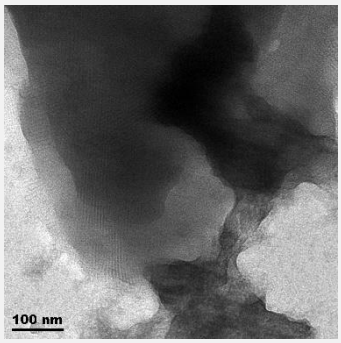	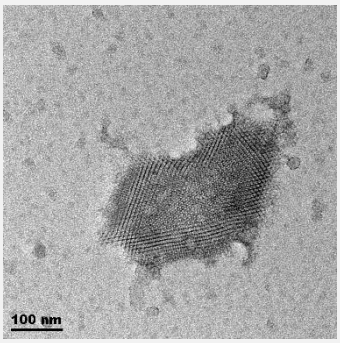
12 Weeks pp		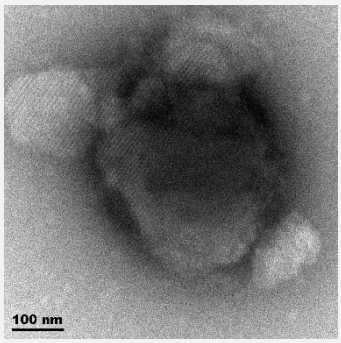	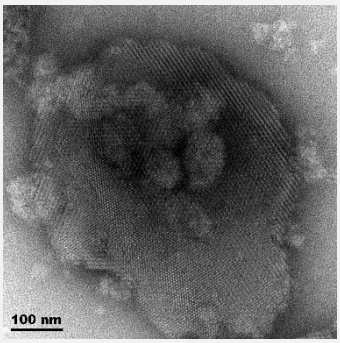
16 Weeks pp		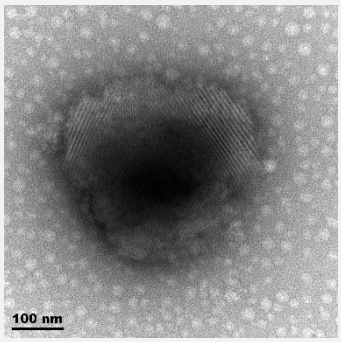	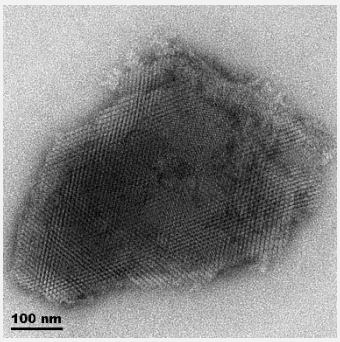
20 Weeks pp		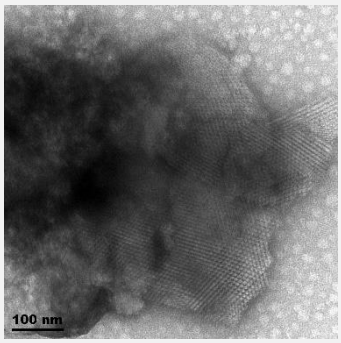	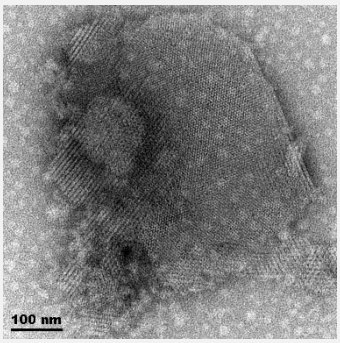
28 Weeks pp		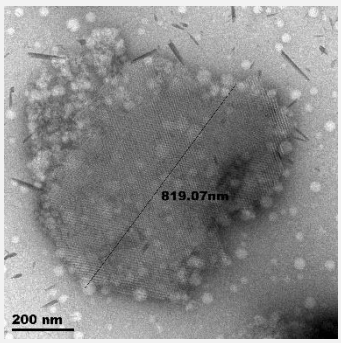	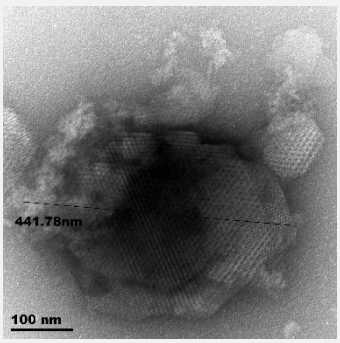

3.3.2 Guinea-Pig Immunogenicity Study

In order to assess the vaccine potential of plant-produced AHSV-5 VP7 quasi-crystals, immunogenicity studies were performed on five experimental (X1-5) and five control (C1-5) female Hartley strain guinea-pigs. AHSV-5 VP7 quasi-crystals were purified from *N. benthamiana* plants using density gradient ultracentrifugation (**2.2.4.6**) and the presence of quasi-crystals confirmed by TEM (**2.2.6**). Concentrations of AHSV-5 VP7 quasi-crystals in the primary inoculum was estimated to be 87.83 µg/ml and the booster 67.18 µg/ml (quantified by gel densitometry as per **2.2.5**). These concentrations were considered acceptable for inoculation as 10-50 µg in ≤400 µl was previously determined as sufficient to yield an adequate immune response in guinea-pigs. AHSV-5 VP7 inocula were assessed for contamination as per **3.2.2.** No growth was observed on LB agar plates subjected to the AHSV-5 VP7 quasi-crystal preparation and endotoxin tests demonstrated very low results of between 0.64 EU/ml and 0.84 EU/ml (EU= endotoxin unit).

Directly preceding guinea-pig inoculation, 5% Montanide™ PET Gel A adjuvant was added (**3.2.2**). PET Gel A is a polymeric adjuvant and an immunostimulant which stimulates the innate immune system by a pro-inflammatory response. Additionally, the polyacrylates in PET Gel A adsorb the antigen particles, enhancing phagocytosis and therefore the activity of antigen presenting cells (APC). In this study, PET Gel A was selected as an adjuvant to stimulate the innate immune response which would subsequently enhance adaptive immunity to build a specific immune response to AHSV-5 VP7 quasi-crystals (Deville et al. 2011; Parker et al. 2009; Vialle et al. 2010).

After subcutaneous primary inoculation on day 0 and a booster on day 13 (**Figure 3.3**) a slight raised bump appeared at the injection site in both control and experimental animals. However, no severe signs of inflammation were observed at any time during the study. Guinea-pigs seemed healthy and continued to gain weight well throughout the experiment. On day 41 guinea-pigs were anaesthetised, exsanguinated, euthanised and their spleens removed. The sera were extracted from whole blood (**3.2.3**) and used to examine the humoral immune response to AHSV-5 VP7 quasi-crystals (**3.3.3**). Additionally, spleens were extracted, incubated in RNA*later*™ and used to isolate mRNA for transcriptome sequencing to analyse the cell-mediated immune response (**3.3.4**).

3.3.3 Analysis of Humoral Immune Response to AHSV-5 VP7 Quasi-Crystal

Guinea-pig anti-AHSV-5 VP7 serum was analysed via SNTs (**3.2.4**) and western immunoblotting (**3.2.5**) to assess serum neutralisation capability and the humoral response to AHSV-5 VP7 quasi-crystals respectively. As expected, the SNT results revealed that guinea-pig anti-AHSV-5 VP7 serum had no neutralisation capability. Whilst western immunoblot analysis of anti-AHSV-5 VP7 guinea-pig sera showed very high levels of antigen binding capacity.

3.3.3.1 Western immunoblot analysis of pre-bleed and final-bleed guinea-pig sera (1:50 000 dilution)

Figure 3.5 displays western immunoblot analysis of anti-AHSV-5 VP7 guinea-pig sera derived from one of the experimental guinea-pigs denoted X2 and one of the control guinea-pigs denoted C2. X2 serum demonstrated high levels of AHSV-5 VP7 immunogenicity. At a 1:50 000 dilution anti-AHSV-5 VP7 final-bleed X2 detected 0.77 µg AHSV-5 VP7 (lane 4). Detection was at a similar level to that of the positive control, anti-AHSV-5 VLP serum, however the positive control had a 10-fold lower dilution of 1:5000. Interestingly, although the pre-bleeds C2 and X2 (1:50 000) (lanes 1 and 2 respectively) did not detect AHSV-5 VP7 as expected, the final-bleed taken from control animal C2 (1:50 000 dilution) (lane 3) demonstrated detection of AHSV-5 VP7, albeit at a much lower level (**Figure 3.5**). Furthermore, anti-AHSV-5 VP7 pre-bleed C2 (1:50 000) and final-bleed C2 (1:50 000) did not detect Shuni viral protein (lane 8 and 9 respectively) as expected. However, the anti-AHSV-5 VP7 final-bleed X2 (1:50 000) did detect 0.77 µg Shuni viral protein (lane 10) to a similar level as that of the control (lane 3), suggesting non-specificity. The secondary antibody (goat anti-guinea-pig) alone (lane 5) did not detect AHSV-5 VP7, ruling out the possibility of secondary antibody contamination **Figure 3.5**.

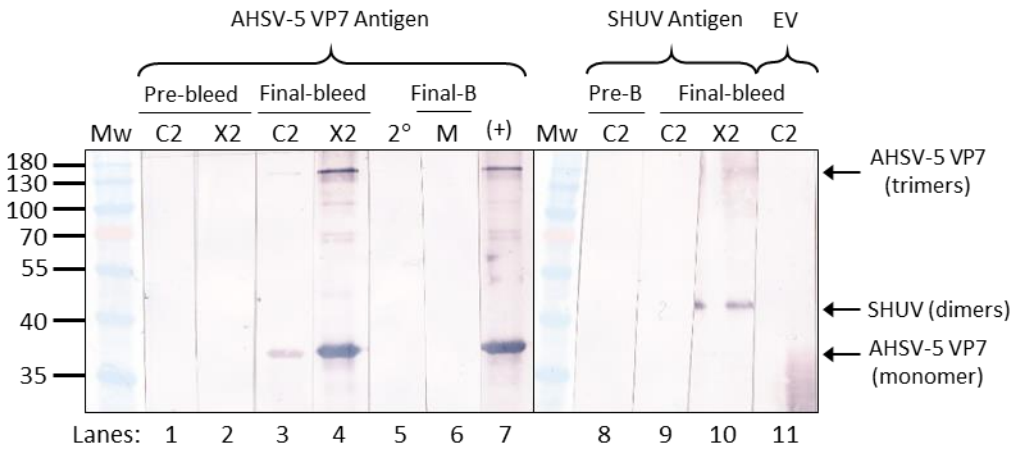

Figure 3.5: Western immunoblot analysis of anti-AHSV-5 VP7 guinea-pig pre-bleed and final-bleed sera (X2 and C2). Lanes 1-7: Purified AHSV-5 VP7 antigen (0.77 µg) probed with pre-bleed C2, pre-bleed X2, final-bleed C2, final-bleed X2, goat anti-guinea-pig secondary Ab only at 1:5000 dilution (2°), mouse final-bleed control serum at 1:20 000 dilution (M) and positive control anti-AHSV-5 VLP guinea-pig serum at 1:5000 dilution (+). Lanes 8-10: SHUV antigen (0.77 µg) probed with pre-bleed C2, final-bleed C2 and final-bleed X2. Lane 11: Empty vector (EV) control probed with final-bleed C2. Pre-bleed and final-bleed, C2 and X2 guinea-pig sera used at 1:50 000 dilution. Mw: NEB molecular weight marker (sizes displayed in kDa); Final-B: Final-Bleed: Pre-B: Pre-Bleed. Arrows indicate the positions of AHSV-5 VP7 monomer (37kDa), AHSV-5 VP7 trimer (135 kDa) and SHUV dimer (50 kDa). Lane numbers (1-11) displayed below the image.

3.3.3.2 Pre-absorption technique to increase binding specificity of guinea-pig sera (1:50 000 dilution)

In an attempt to increase antibody-antigen binding specificity of anti-AHSV-5 VP7 guinea-pig sera (C2 and X2), two methods were used. Namely, the pre-absorption technique (**3.2.5.2**) or the addition of 3% BSA in blocking buffer as an alternative to 5% non-fat dairy milk (**3.2.5.1**).

Western immunoblot analysis of the impact of these two methods on binding specificity of anti-AHSV-5 VP7 guinea-pig sera (C2 and X2) is represented in **Figure 3.6**. Pre-absorbed final-bleed X2 serum at 1:50 000 dilution (lane 2) detected purified AHSV-5 VP7 (0.63 µg) whilst the pre-absorbed final-bleed C2 (1:50 000) (lane 1) was unable to detect 0.63 µg AHSV-5 VP7. Additionally, when using 3% BSA blocking buffer, a very light band was observed when using the final-bleed C2 serum (1:50 000) to probe

for AHSV-5 VP7 (lane 5) and a strong band was observed when probed with final-bleed X2 (1:50 000) (lane 6). SHUV antigen (0.63 µg) was not detected using the pre-absorbed anti-AHSV-5 VP7 final-bleed X2 serum (1:50 000) (lane 3). Anti-FMDV guinea-pig serum (not pre-absorbed) detected AHSV-5 VP7 (lane 7), however this was at a serum dilution of 1:2000 and may therefore be as a result of non-specificity at such low dilutions. Alternatively, this may be due to plant-specific antibodies binding residual host plant proteins in the AHSV-5 VP7 sample as the anti-FMDV guinea-pig serum was not pre-absorbed. No plant protein was detected in lane 4 where the semi-crude empty vector control was used and probed with the pre-absorbed final-bleed C2 at a 1:50 000 dilution.

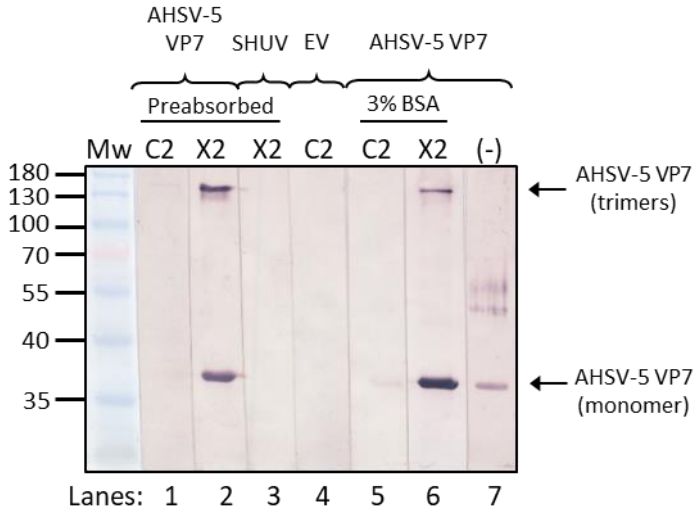

Figure 3.6: Western immunoblot analysis of pre-absorbed anti-AHSV-5 VP7 guinea-pig #2 final-bleed sera. Lanes 1 and 2: Purified AHSV-5 VP7 antigen (0.63 µg) probed with preabsorbed final-bleed C2, and preabsorbed final-bleed X2. Lane 3: SHUV antigen (0.63 µg) probed with preabsorbed final-bleed X2. Lane 4: Semi-crude empty vector control probed with preabsorbed final-bleed C2. Lanes 5, 6 and 7: Purified AHSV-5 VP7 antigen (0.63 µg) probed with final-bleed C2 diluted in 3% BSA, final-bleed X2 diluted in 3% BSA, and anti-FMDV guinea-pig serum at 1:2000 dilution. Final-bleed C2 and X2 guinea-pig sera used at 1:50 000 dilution. Mw: NEB molecular weight marker (sizes displayed in kDa). Arrows indicate the positions of AHSV-5 VP7 monomer (37 kDa), VP7 trimer (135 kDa) and SHUV dimer (50 kDa). Lane numbers (1-7) displayed below the image.

3.3.3.3 Western immunoblot analysis of pre-bleed and final-bleed guinea-pig sera (1:100 000 dilution)

Figure 3.7 shows a western immunoblot analysis of anti-AHSV-5 VP7 guinea-pig pre-bleed (**Figure 3.7**.**a**) and pre-absorbed final-bleed (**Figure 3.7**.**b**) sera (C1-5, X1-5) at a 1:100 000 dilution. As expected, pre-bleeds C1-5 and X1-5 (a) were unable to detect 0.53 µg AHSV-5 VP7 antigen. At a 1:100 000 dilution guinea-pig final-bleed sera X1, X2 and X4 were capable of detecting 0.53 µg AHSV-5 VP7, whilst X3 showed very faint bands similar to that of the final-bleed control sera C1, C3 and C4 suggesting non-specificity still present although at low levels. This suggests that the pre-absorption technique was not completely successful in increasing the specificity of all samples. No bands were present in lanes where 0.53 µg AHSV-5 VP7 was loaded and detected by C2, C5 and X5 final-bleed sera (**Figure 3.7**. **b).** No band was observed when using 0.53 µg Shuni viral protein and probing with final-bleed X1 guinea-pig serum at a 1:100 000 dilution (lane 12).

a)

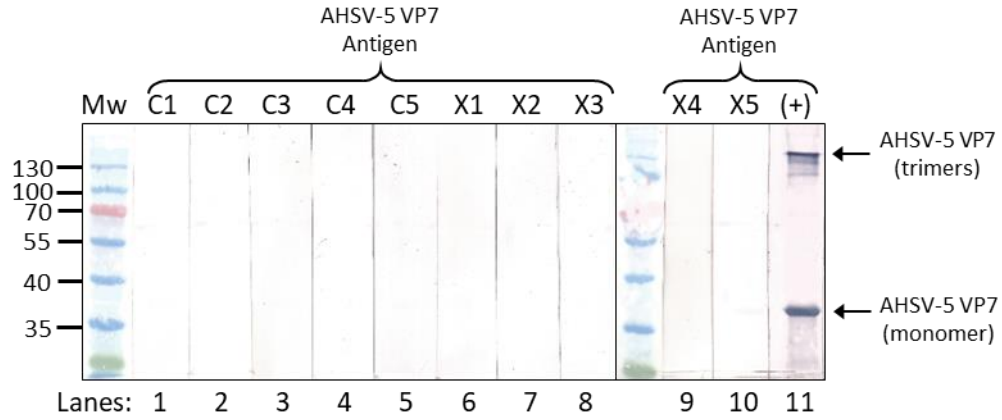

b)

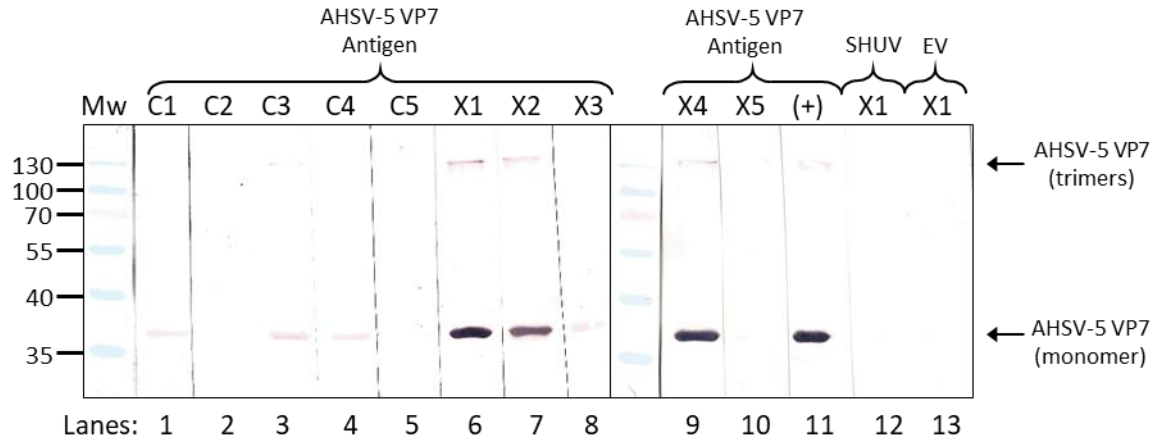

Figure 3.7: Western immunoblot analysis of anti-AHSV-5 VP7 guinea-pig pre-bleed and final-bleed sera (C1-5 and X1-5). Analysis of (a) pre-bleed and (b) pre-absorbed final-bleed sera. (a) and (b) Lanes 1-10: Purified AHSV-5 VP7 antigen (0.53 µg) probed with control sera (C1-5) and experimental guinea-pig sera (X1-5). (+): Purified AHSV-5 VP7 antigen (0.53 µg) probed with anti-AHSV-5 VLP guinea-pig serum at 1:5000 dilution. (b) Lane 12: SHUV protein (0.53 µg) probed with final-bleed X1 serum. Lane 13: Empty vector (EV) crude control probed with final-bleed X1 serum. All pre-bleed and final-bleed guinea-pig sera (C1-5 and X1-5) used at 1:100 000 dilution. Arrows indicate the positions of AHSV-5 VP7 monomer (37 kDa), AHSV-5 VP7 trimer (135 kDa) and SHUV dimer (50 kDa). Mw: NEB molecular weight marker (sizes displayed in kDa). Lane numbers displayed below the image.

3.3.4 RNA-seq Transcriptome Profiling

3.3.4.1 RNA extraction & integrity analysis

28 days after the booster inoculation, guinea-pigs were exsanguinated, and spleens removed. Whole RNA was isolated from stabilised spleen tissue as per (**3.2.6.1**). Resultant RNA concentrations as determined by NanoDrop (**3.2.6.1**) ranged from 348.1-672.2 ng/µl before transportation to Omega Bio-tek (Georgia, USA) (**Table 3.3**). 260/280 ratios ranged from 2.09 to 2.13 indicated high levels of RNA purity and very low levels of protein and phenol contamination. However, 260/230 ratios ranged from 1.24 to 2.08 (**Table 3.3**), these low values are likely to indicate the presence of guanidine salt which absorbs at 230 nm and is included in the RNeasy Mini Kit lysis buffer.

Table 3.3: RNA concentration and purity for spleen derived guinea-pig samples as determined by NanoDrop. Control (C1-5) and experimental (X1-5) samples indicated. RNA purity assessed by 260/280 and 260/230 ratios which indicate protein and guanidine contamination respectively if ≤ 2.0.

RNA Sample	Concentration (ng/µl)	260/280	260/230
C1	672.2	2.11	2.08
C2	616.1	2.13	2.07
C3	354.4	2.12	1.68
C4	348.1	2.11	1.74
C5	437.8	2.09	1.74
X1	369.3	2.10	1.48
X2	585.7	2.12	1.24
X3	437.4	2.09	1.92
X4	634.2	2.12	2.02
X5	466.8	2.08	2.01

Figure 3.8 shows the RNA quality of samples as assessed by 1% agarose gel electrophoresis, performed as per **3.2.6.1**. Levels of ribosomal RNA 28S and 18S were used as a proxy to determine the quality of total RNA extracted. 28S and 18S bands seemed strong however the levels of 28S were similar to that of the 18S band. 28S levels should be twice as high as 18S and therefore a high 28S/18S ratio indicates that purified RNA is intact. However, this observation may be as a result of using a

simple 1% agarose gel as opposed to the inclusion of formaldehyde. A denaturing agent such as formaldehyde ensures that RNA remains single-stranded and separates accurately during gel electrophoresis. Additionally, RNA does not incorporate EtBr as well as DNA and this may skew observations.

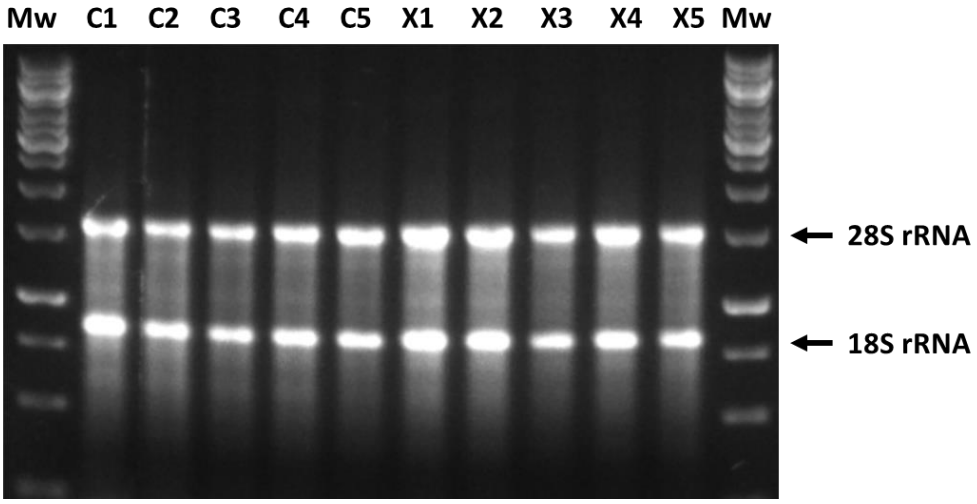

Figure 3.8: Agarose gel electrophoresis to assess RNA quality. 1% agarose gel including 3 µl EtBr electrophoresed at 60 volts for approximately 1.5 h. 2 µg of whole RNA loaded in lanes 1-10. C1-5: Spleen derived RNA from control guinea-pigs, X1-5: Spleen derived RNA from experimental guinea-pigs, Mw: O'GeneRuler™1 kb DNA ladder. Arrows indicate 28S (5 kb) and 18S (1.9 kb) ribosomal RNA (rRNA) bands.

Once received by Omega Bio-tek (Georgia, USA), a further assessment of RNA quality was performed using an Agilent 2200 TapeStation Bioanalyser. **Figure 3.9** displays RNA integrity as assessed by the Agilent Bioanalyser. The overall quality of RNA seemed high with RIN^e values greater than 7.2. The RIN algorithm takes into account various electrophoretic RNA measurements as recorded by a bioanalyzer to compute RIN scores. The most significant of these being the 28S/18S ratio and analysis of the 'fast region' (area between 18S and 5S rRNA) which signifies RNA degradation (Schroeder et al. 2006). Due to high RIN^e results, samples were considered ready for mRNA library preparation and RNA sequencing. Additionally, the Agilent 2200 TapeStation System (Agilent, California, USA) revealed between 5.91 µg to 21.68 µg of total RNA in our samples.

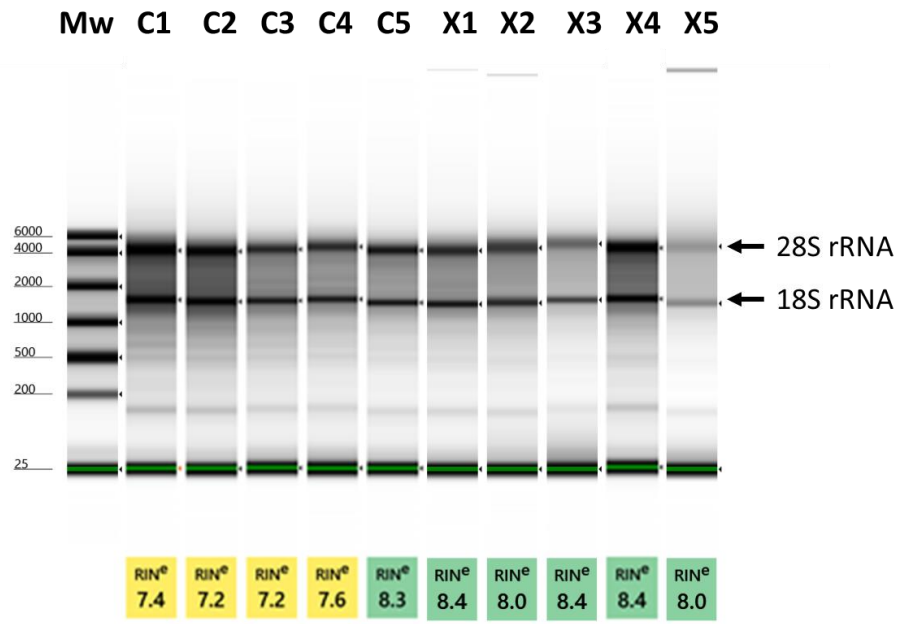

Figure 3.9: RNA quality as assessed by the Agilent 2200 TapeStation and RNA Screen Tape. C1-5: Spleen derived RNA from control guinea-pigs, X1-5: Spleen derived RNA from experimental guinea-pigs, Mw: RNA molecular weight marker. Arrows indicate 28S (5 kb) and 18S (1.9 kb) ribosomal RNA (rRNA) bands. RIN^e values indicate the integrity of RNA.

3.3.4.2 RNA sequencing & bioinformatics

The mRNA library was prepared from spleen-derived total RNA by Omega Bio-tek (Georgia, USA) as per (**3.2.6.2**). Ten RNA-seq transcriptome datasets, five experimental (X1-5) and five control (C1-5), were produced from the mRNA library. These datasets consisted of between 20.21 to 53.54 million 150 bp paired-end reads (**Table 3.4**) after low quality bases and reads had been removed.

Table 3.4: Total number of reads/transcripts and % of total reads which aligned to the reference genome. Control (C1-5) and experimental (X1-5) samples indicated.

Samples		Total number of reads (after trimming)	% reads aligned (total genome)
Control Guinea-Pigs	C1	35.74 x 10^6	78.50%
	C2	34.31 x 10^6	77.39%
	C3	40.00 x 10^6	83.68%
	C4	20.21 x 10^6	80.70%
	C5	49.36 x 10^6	73.52%
Experimental Guinea-Pigs	X1	40.89 x 10^6	82.15%
	X2	37.27 x 10^6	84.00%
	X3	52.15 x 10^6	82.45%
	X4	53.54 x 10^6	82.56%
	X5	43.84 x 10^6	80.02%

DESeq2 results revealed an annotated gene count of 26 855 prior to normalisation and transformation (**Table 3.5**). Gene annotation was performed by GENCODE. Sequencing depth normalisation and log2 transformation was performed on all datasets, resulting in an assessed gene count of 7213. The assessed gene count (7213) was tested for statistical significance and of these 350 genes were found to be significantly differentially expressed (DE) when compared to the control (FDR corrected p-value (q-value) ≤0.05) (**Table 3.5**). Explanation of q-value in **3.2.6.2**.

Table 3.5: Gene count assessment. Annotation gene count = no. of genes annotated, Assessed gene count = no. of genes tested for statistical significance, Differentially expressed (DE) gene count = no. of significantly DE genes (q≤0.05), DE immune response gene count = no. of significantly DE genes involved in immune pathways (q≤0.05).

Annotation Gene Count	Assessed Gene Count	DE Gene Count (q≤0.05)	DE Immune Response Gene Count
26 855	7 213	350	30

3.3.4.3 Analysis of global immune response to AHSV-5 quasi-crystals

Of the 350 significantly DE genes (q≤0.05) only 30 of these correlated with genes from 18 of the 22 KEGG and Reactome immune pathways as shown by **Table 3.6**. and the heatmap in **Figure 3.10**.

Table 3.6: Significantly (q≤0.05) DE immune response genes and related pathways and molecular function. Immune pathways accessed via KEGG and Reactome Pathway databases. And molecular function accessed via KEGG and String database. Gene names/symbols of DE genes indicated.

Pathways	**Significantly DE Genes**	**Molecular Function from KEGG (https://www.genome.jp/kegg/pathway.html) & String (https://string-db.org)**
Innate Immune Response Pathways		
Chemokine Signalling Pathway	Prkcz	Protein kinase C, zeta
	Stat2	Signal transducer and activator of transcription 2
	Grk2	G protein-coupled receptor kinase 2
	Cx3cr1	Chemokine (C-X3-C motif) receptor 1; Belongs to the G-protein coupled receptor 1 family
Natural Killer Cell – Mediated Cytotoxicity	Fcer1g	Fc fragment of IgE receptor Ig; High affinity immunoglobulin epsilon receptor subunit gamma; Associates with a variety of FcR alpha chains to form a functional signalling complex. Regulates several aspects of the immune response. The gamma subunit has a critical role in allowing the IgE Fc receptor to reach the cell surface.
C-Type Lectin Receptor Signalling Pathway	Stat2	Signal transducer and activator of transcription 2
	Bcl3	B-cell CLL/lymphoma 3, transcription coactivator
	Fcer1g	Fc fragment of IgE receptor 1g; High affinity immunoglobulin epsilon receptor subunit gamma; Associates with a variety of FcR alpha chains to form a functional signalling complex. Regulates several aspects of the immune response. The gamma subunit has a critical role in allowing the IgE Fc receptor to reach the cell surface.
Leukocyte Transendothelial Migration	Mmp2	Matrix metallopeptidase 2; Belongs to the peptidase M10A family
	Limk1	LIM domain kinase 1

FC Gamma R-Mediated Phagocytosis	Wasf2	WAS protein family, member 2
	Plpp3	Phospholipid phosphatase 3
NOD-Like Receptor Signalling Pathway	Hsp90aa1	Heat shock protein 90kDa alpha (cytosolic), class A member 1
	Nampt	Nicotinamide phosphoribosyltransferase
	Stat2	Signal transducer and activator of transcription 2
	Vdac1	Voltage dependent anion channel 1
Complement and Coagulation Cascade	C1s	Complement component 1, s subcomponent
	C1qa	Complement C1q subcomponent subunit A
Platelet Activation	Vamp8	Vesicle associated membrane protein 8
	Col3a1	Collagen type III alpha 1 chain
	Prkcz	Protein kinase C zeta
	Fcer1g	Fc fragment of IgE receptor Ig; High affinity immunoglobulin epsilon receptor subunit gamma; Associates with a variety of FcR alpha chains to form a functional signalling complex. Regulates several aspects of the immune response. The gamma subunit has a critical role in allowing the IgE Fc receptor to reach the cell surface. Also involved in collagen-mediated platelet activation and in neutrophil activation mediated by integrin
Adaptive (Cell-Mediated) Immune Response Pathways		
T-Cell Receptor Signalling Pathway	Nck2	NCK adaptor protein 2 gene
TH1 & 2 Cell Differentiation	Notch2	Neurogenic locus notch homolog protein 2
Class 1 MHC Antigen Processing and Presentation	Scarb1	Scavenger receptor class B, member 1; Belongs to the CD36 family
TH17 Cell Differentiation	Hsp90aa1	Heat shock protein 90kDa alpha (cytosolic), class A member 1
	Smad4	Mothers against decapentaplegic homolog; SMAD family member 4
	Rara	Retinoic acid receptor, alpha
IL-17 Signalling Pathway	Hsp90aa1	Heat shock protein 90kDa alpha (cytosolic), class A member 1
	Usp25	Ubiquitin specific peptidase 25; Belongs to the peptidase C19 family

	Il17ra	Interleukin 17 receptor A
Antigen Processing & Presentation	Hsp90aa1	Heat shock protein 90kDa alpha (cytosolic), class A member 1
Pathways involved in both Innate and Adaptive Immune Responses		
Cytokine-Cytokine Receptor Interaction	Il17ra	Interleukin 17 receptor A
	Cx3cr1	Chemokine (C-X3-C motif) receptor 1; Belongs to the G-protein coupled receptor 1 family
	Ifnlr1	Interferon, lambda receptor 1
	Tnfsf14	Tumour necrosis factor (ligand) superfamily, member 14
Ras Signalling Pathway	Rel	REL proto-oncogene, NF-kB subunit; V-rel avian reticuloendotheliosis viral oncogene homolog
Rap1 Signalling Pathway	Prkd3	Protein kinase D3; Belongs to the protein kinase superfamily. CAMK Ser/Thr protein kinase family
	Arap3	Arf-GAP with Rho-GAP domain, ankyrin repeat and PH domain-containing protein 3
	Prkcz	Protein kinase C zeta
Jak-Stat Pathway	Stat2	Signal transducer and activator of transcription 2
	Pim1	Pim-1 proto-oncogene, serine/threonine kinase
	Ifnlr1	Interferon, lambda receptor 1

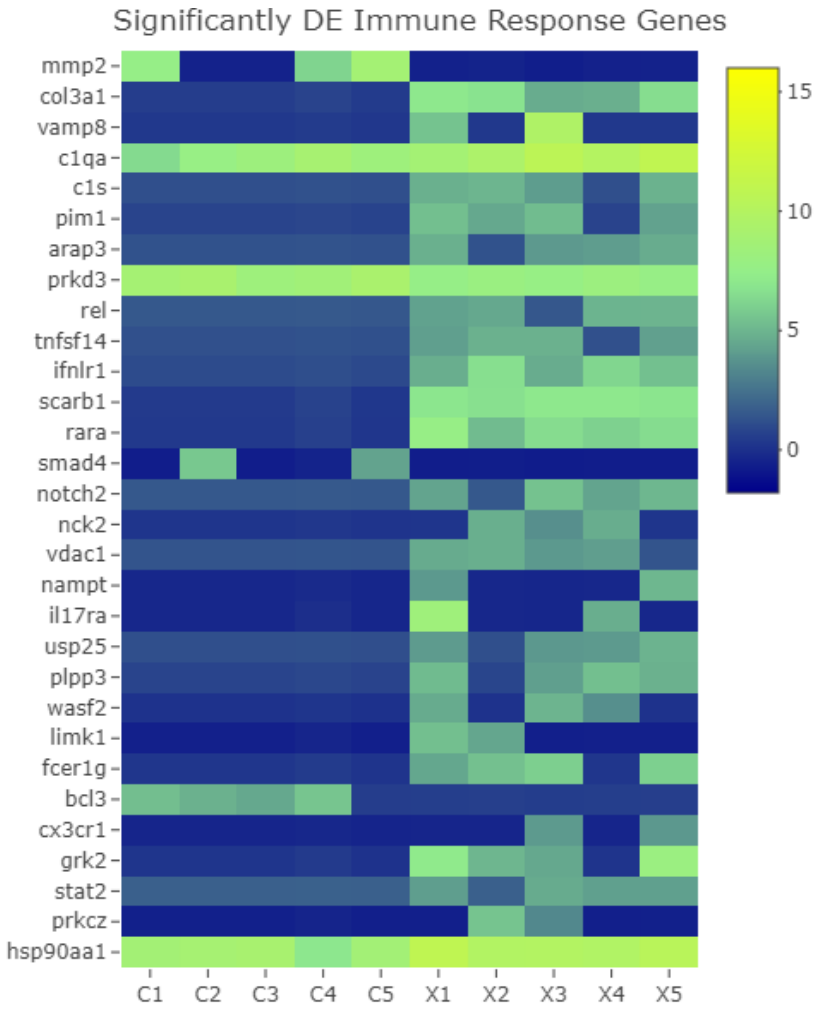

Figure 3.10: Heatmap displaying 30 significantly DE genes involved in immune pathways. Gene pathways accessed via KEGG and Reactome pathway databases. Gene names/ symbols displayed on the y axis. Colour bar signifies the regularised and log2transformed gene transcript count. Guinea pig control (C1-5) and experimental (X1-5) samples displayed below the x axis. Significant DE determined by q-value ≤ 0.05.

The 30 significantly DE genes (q≤0.05) were found to be involved in 18 global immune response pathways shown in **Table 3.6**. With respect to genes involved in innate immunity, 17 genes were found to be significantly differentially expressed in these pathways. 8 genes were found to be involved in adaptive, cell-mediated responses, and 10 of the 30 significantly DE genes were found to play a role in pathways relating to both innate and adaptive immunity (**Table 3.6**).

Interestingly, no significantly DE genes were highlighted in the B-cell receptor signalling pathway and in the innate pattern recognition receptor pathways: Toll-like receptor signalling, RIG-I-like receptor signalling and Cytosolic DNA-sensing pathway.

3.3.4.4 Analysis of innate immune pathways which trigger adaptive responses

Chemokines play a pivotal role in cell trafficking and aid in inflammatory immune responses. They are part of innate immunity and assist in triggering adaptive immune responses. The heatmap represented in **Figure 3.11** demonstrates the expression of genes involved in the chemokine signalling pathway across all control and experimental samples. A significant increase ($q \leq 0.05$) in expression of *Grk2* (G protein-coupled receptor (GPCR) kinase 2), *Cx3cr1* (C-X3-C motif chemokine receptor 1), *Stat2* (Signal transducer and activator of transcription 2) and *Prkcz* (Protein kinase C zeta) was observed. Additionally, an increase in expression of *Grk5* (GPCR kinase 5), *Cx3cl1* (C-X3-C motif chemokine), *Ccr9* (C-C motif chemokine receptor 9), *Pik3R5* (phosphoinositide-3-kinase regulatory subunit 5) and *Raf1* (B-Raf proto-oncogene serine/threonine-protein kinase) in at least four of the experimental samples was noted, however this was not found to be significant.

Chemokines regulate many biological processes such as cell growth, differentiation and apoptosis. After chemokine receptor (*Cx3cr1* and *Ccr9*) activation, the signal is transduced by GPCRs (*Grk2* and *Grk5*) expressed on immune cells, and the G protein subunits dissociate to activate various downstream pathways. The GPCR beta subunit then activates various protein kinases (*Pik3R5*, *Prkcz* and *Raf1*) which consequently activate *MapK*1/3 (mitogen-activated protein kinase 1/3) triggering cytokine production, cell growth, differentiation, migration and apoptosis (Kanehisa and Goto 2000).

Additionally, chemokine receptor (*Cx3cr1* and *Ccr9*) stimulation activates the Jak-STAT signalling pathway (*Stat2*) which results in the same cellular processes and cytokine production as mentioned above ((Kanehisa and Goto 2000).

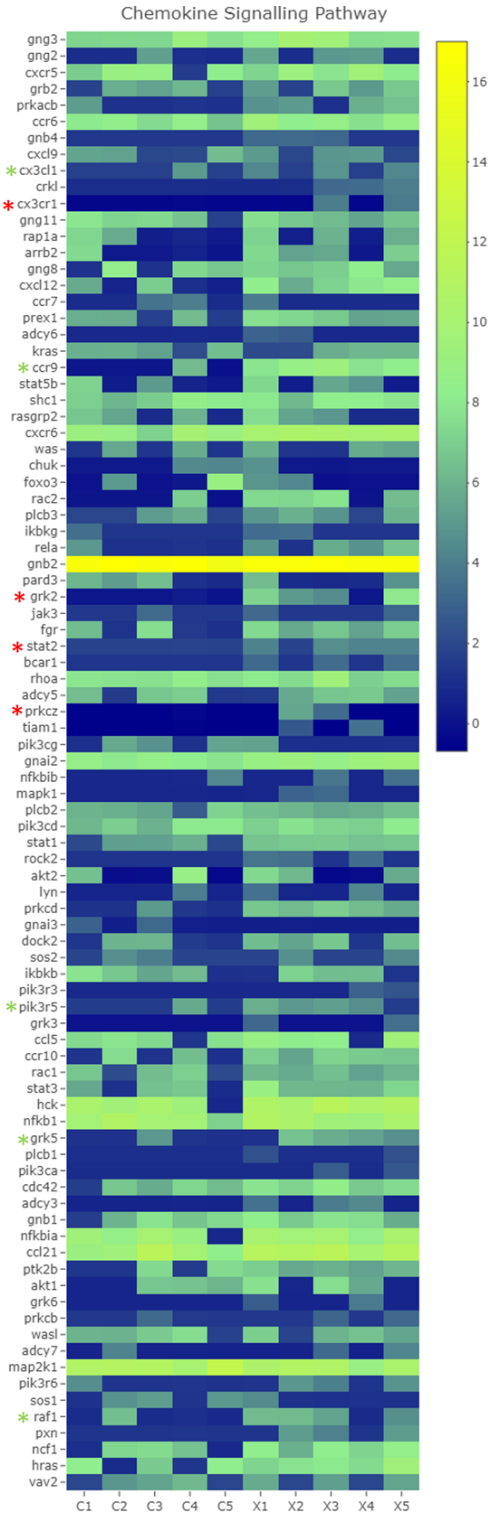

Figure 3.11: Heatmap displaying gene expression in the chemokine signalling pathway. Gene pathway accessed via KEGG pathway database. Red asterisks indicate significantly DE genes, q-value ≤ 0.05. Green asterisks indicate differential expression observed but not significant. Gene names/ symbols displayed on the y axis. Colour bar signifies the regularised and log2transformed gene transcript count. Guinea pig control (C1-5) and experimental (X1-5) sample ID displayed below the x axis.

Natural killer (NK) cells are involved in early innate defence responses to pathogens, however under many circumstances T helper cells further stimulate the production of NK cells. The heatmap in **Figure 3.12** shows expression levels of genes involved in NK cell-mediated cytotoxicity. A significant ($q \leq 0.05$) increase was found in the expression of *Fcer1g* (Fc fragment of IgE receptor Ig). Additionally, an increase in expression of *Lck* (lymphocyte cell-specific protein tyrosine kinase), *Raf1* (B-Raf proto-oncogene serine/threonine-protein kinase), *Itgal* (integrin subunit alpha L), *Rac2* (Ras-related C3 botulinum toxin substrate 2 - small GTP binding protein) and *Ifngr1* (interferon gamma receptor 1) was observed in at least four of the experimental samples when compared to the controls. However, this observation was not found to be significant ($q \geq 0.05$).

Various NK cell surface receptors exist and bind ligands on the target cell's surface triggering NK cell-mediated cytotoxicity. NKP46 is one of these receptors which after activation triggers the adapter protein FCER1g. This adapter protein then transduces the signal and results in signalling cascades which include the activation of protein kinases, *Raf1* and *Rac2*. This leads to the release of cytokines, in particular *Ifgn* (Interferon gamma), which then binds to its receptor (*Ifngr1*) on the target cell and activates *Fas* (Cell surface death receptor) initiating apoptosis (Kanehisa and Goto 2000).

Additionally, *Itgal* and *Itgb2* (integrin subunit beta 2) form the integrin, lymphocyte function-associated antigen-1, expressed on NK cells. After infection, this integrin interacts with the target cell surface ligand, *Icam1/2*, indirectly activating *Rac2.* And as mentioned in the previous pathway, this also leads to apoptosis of the target cell via the interferon gamma receptor 1 and *Fas* activation (Kanehisa and Goto 2000).

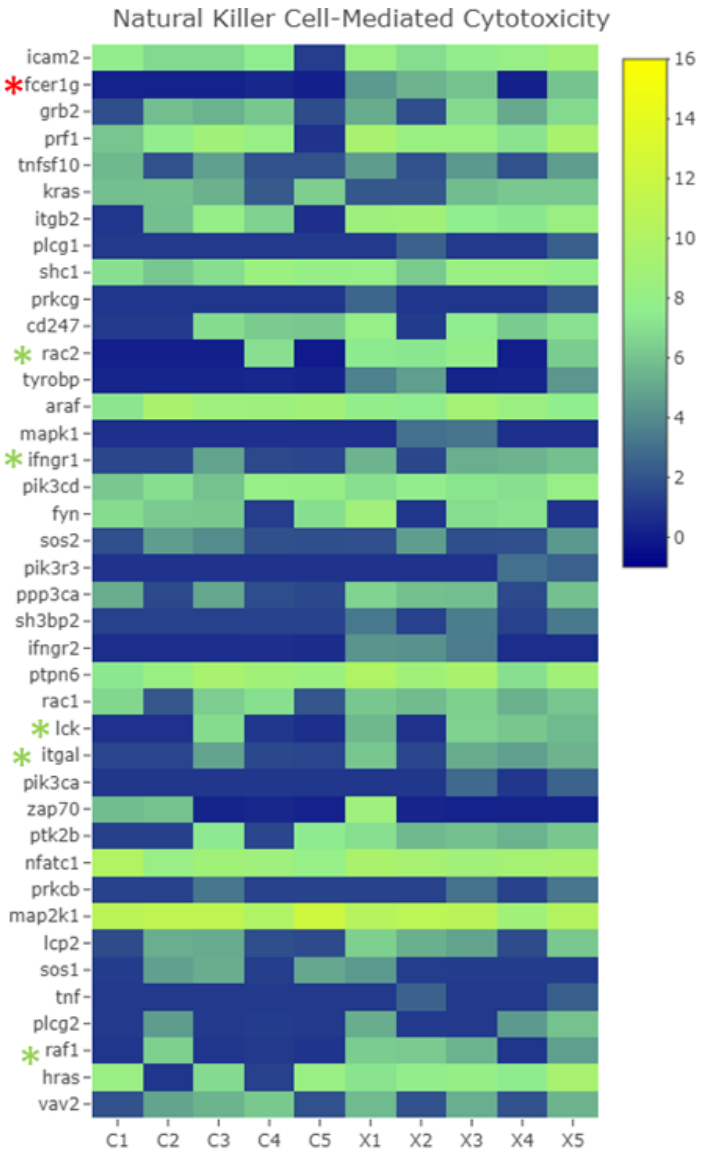

Figure 3.12: Heatmap displaying gene expression in the natural killer cell-mediated cytotoxicity pathway. Gene pathway accessed via KEGG pathway database. Red asterisk indicates significantly DE genes, q-value ≤ 0.05. Green asterisk indicates differential expression observed but not significant. Gene names/ symbols displayed on the y axis. Colour bar signifies the regularised and log2transformed gene transcript count. Guinea pig control (C1-5) and experimental (X1-5) sample ID displayed below the x axis.

C-type lectin receptors (CLRs) are a large superfamily of proteins. They are pattern-recognition receptors on macrophages, neutrophils and dendric cells which recognise ligands originating from pathogens. The binding of a ligand to CLR stimulates a signalling cascade which ultimately results in the production of inflammatory cytokines

and chemokines which trigger innate and adaptive immune responses (Kanehisa and Goto 2000). **Figure 3.13** shows a heatmap demonstrating expression of genes relating to the CLR signalling pathway. A significant (q≤0.05) decrease in *Bcl3* (B-cell CLL/lymphoma 3) and an increase in *Fcer1g* and *Stat2* (Signal transducer and activator of transcription 2) were observed. Furthermore, an increase in *Rela* (RELA proto-oncogene, NF-kB subunit), *Calm3* (calmodulin 3), *Prkcd* (protein kinase C delta), *Nfkb2* (nuclear factor kappa B subunit 2) and *Ikbke* (inhibitor of nuclear factor kappa B kinase subunit epsilon) expression was observed in at least four of the experimental samples.

By different signalling cascades, the Ig receptor FCER1G, the calcium-binding messenger protein CALM3, the protein kinase encoded by *Prkcd*, and the transcription factors *Nfkb2* and *Rela* are involved in activating transcription of various interleukins (IL-1b, IL-6, IL-10, IL-12b and IL-23a) which participate in Th1 (cell-mediated) and Th17 cell differentiation. Additionally, the protein kinase and transcription activator encoded by *Ikbke* and *Stat2* respectively are involved in T follicular helper (Tfh) cell differentiation. In the nucleus *Bcl3* is a transcription activator and is a co-regulator of cell proliferation (Massoumi et al. 2006). In the CLR signalling pathway, *Bcl3* is part of Th2 cell differentiation (humoral response) and therefore downregulation of *Bcl3* could indicate a decrease in Th2 cell differentiation (Kanehisa and Goto 2000).

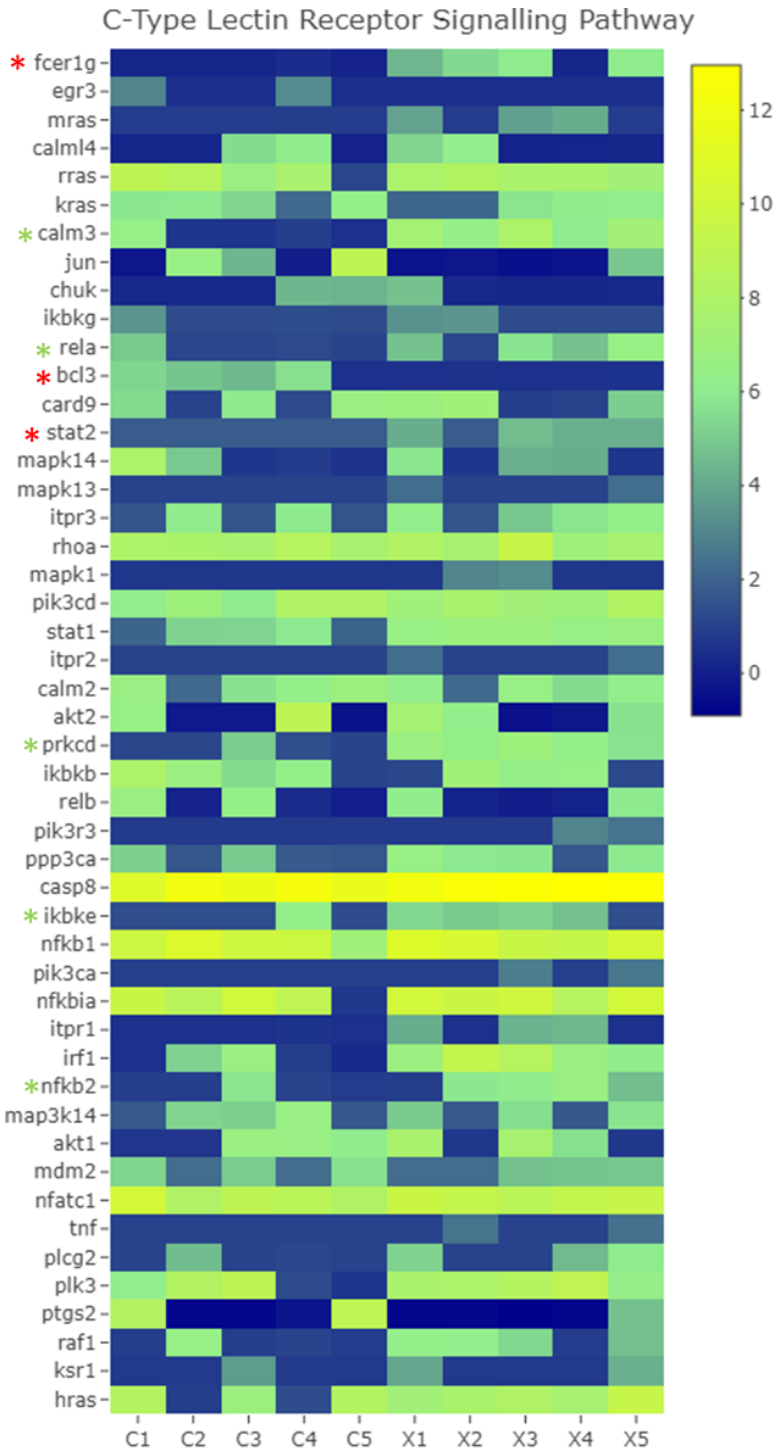

Figure 3.13: Heatmap displaying gene expression in C-type lectin receptor signalling pathway. Gene pathway accessed via KEGG pathway database. Red asterisk indicates significantly DE genes, q-value ≤ 0.05. Green asterisk indicates differential expression observed but not significant. Gene names/ symbols displayed on the y axis. Colour bar signifies the regularised and log2transformed gene transcript count. Guinea pig control (C1-5) and experimental (X1-5) sample ID displayed below the x axis.

3.3.4.5 Analysis of cell-mediated immune response to AHSV-5 VP7 quasi-crystals

When T-cell receptors encounter foreign antigens associated with major histocompatibility complexes (MHCs) and costimulatory molecules such as CD28, a series of signalling cascades occur leading to proliferation of T-cells, production of cytokines and cell-differentiation in effector T-helper (Th) or cytotoxic T-cells (CTLs). **Figure 3.14** displays a heatmap representing the expression of genes involved in the T-cell receptor signalling pathway. A significant increase ($q \leq 0.05$) in *Nck2* **(**NCK adaptor protein 2 gene) expression was observed and a notable difference in *Nck1* (NCK adaptor protein 1 gene) expression in four of the experimental samples. *Nck2* and *Nck1* are involved in the positive regulation of T-cell proliferation. And by associating with *Lcp2* (lymphocyte cytosolic protein 2) and activating the protein kinase, PAK (p21 (RAC1) activated kinase) these adaptor proteins play an important role in actin filament reorganisation (Kanehisa and Goto 2000).

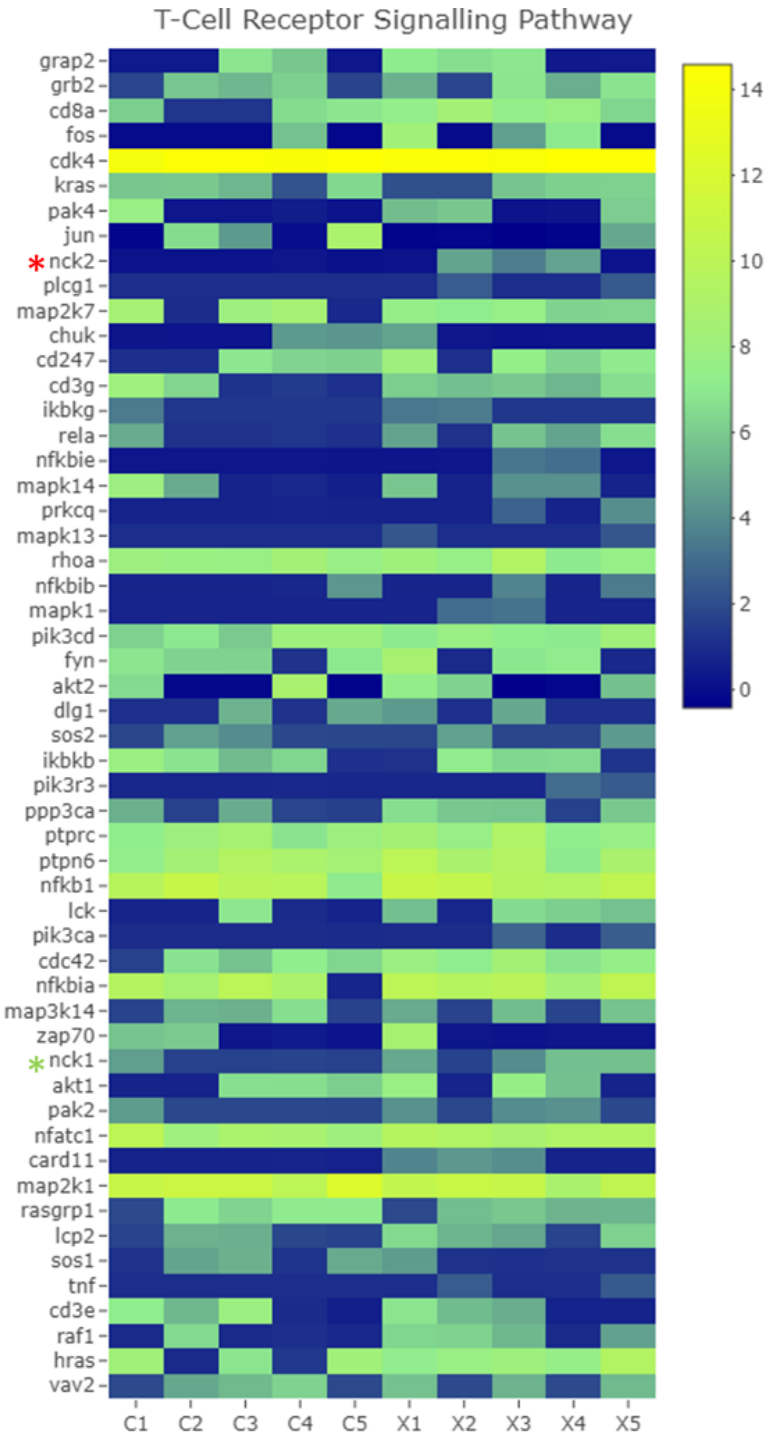

Figure 3.14: Heatmap displaying gene expression in the T-cell receptor signalling pathway. Gene pathway accessed via KEGG pathway database. Red asterisk indicates significantly DE genes, q-value ≤ 0.05. Green asterisk indicates differential expression observed but not significant. Gene names/ symbols displayed on the y axis. Colour bar signifies the regularised and log2transformed gene transcript count. Guinea pig control (C1-5) and experimental (X1-5) sample ID displayed below the x axis.

Effector T helper (Th) cells (Th1, Th2 and Th17) originate from naive CD4 T-cells in response to antigen presenting cell (APC) signals from MHCII. The heatmap represented in **Figure 3.15** shows the regularised and log transformed mRNA transcript counts/ expression levels of genes involved in Th1 and Th2 cell differentiation. A significant ($q \leq 0.05$) increase in the expression of *Notch2* (Neurogenic locus notch homolog protein 2) was observed, Additionally, an increase in expression of the interleukin and interferon receptors genes, *Il2rb* (interleukin 2 receptor subunit beta) and *Ifngr1* (interferon gamma receptor 1), was evident in four of the experimental guinea-pigs when compared to the controls. In response to foreign antigens, both the notch 2 protein and the interleukin 2 receptor lead to the production of interleukins such as IL-2, IL-4, IL-5 and IL-13 driving Th2 cell differentiation and therefore humoral immunity. Whilst, the interferon gamma receptor activates the Jak(1/2)-STAT1 pathway which drives the production of IFN-gamma and cell differentiation into Th1 cells, stimulating strong cell-mediated immune responses (Kanehisa and Goto 2000).

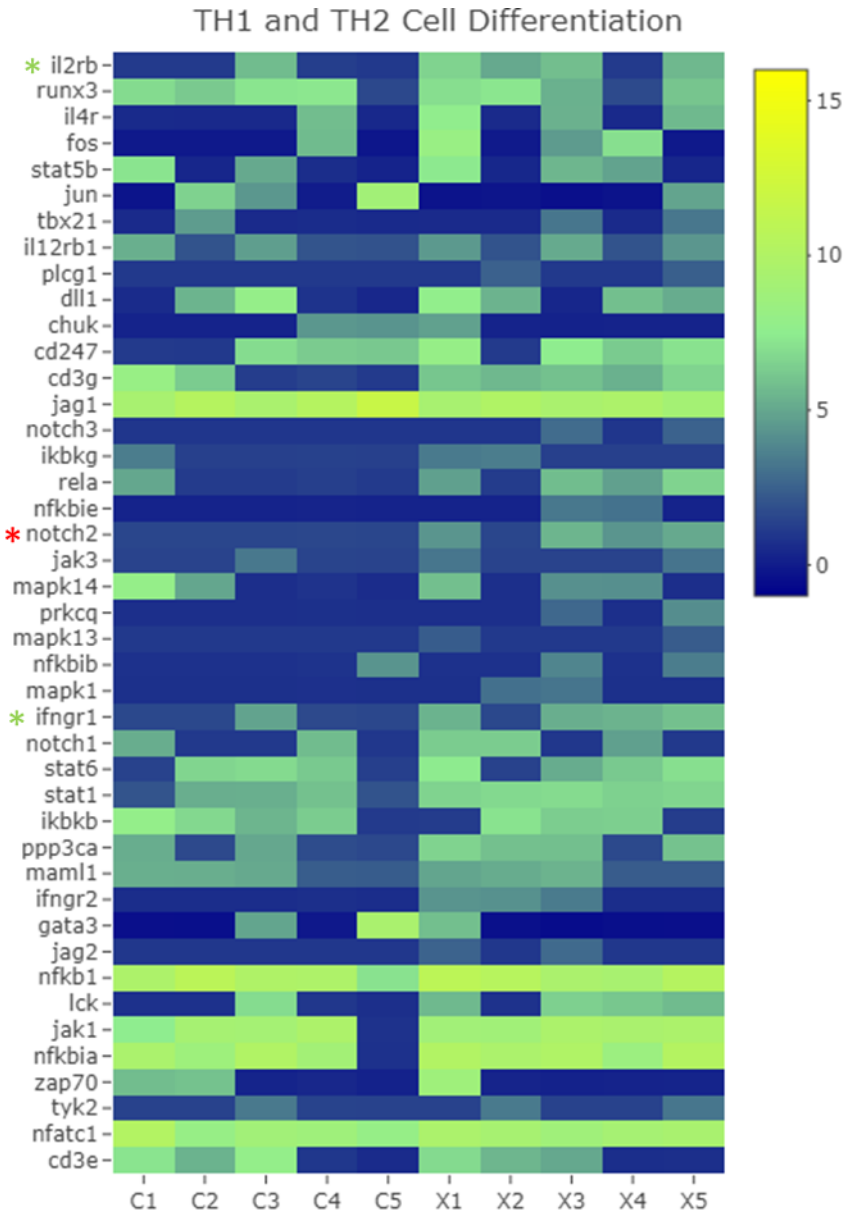

Figure 3.15: Heatmap displaying gene expression in the Th1 and Th2 cell differentiation pathway. Gene pathway accessed via KEGG pathway database. Red asterisk indicates significantly DE genes, q-value ≤ 0.05. Green asterisk indicates differential expression observed but not significant. Gene names/ symbols displayed on the y axis. Colour bar signifies the regularised and log2transformed gene transcript count. Guinea pig control (C1-5) and experimental (X1-5) sample ID displayed below the x axis.

Th17 cells originate from CD4 T cells and are involved in innate and cell-mediated immune responses. Previous studies have suggested a Th17 role in immunity to AHSV (Pretorius, 2016). The heatmap represented in **Figure 3.16** shows the

expression levels of genes involved in Th17 cell differentiation. A significant ($q \leq 0.05$) decrease in *Smad4* (SMAD family member 4) expression was found, and a significant increase in expression was evident for *Hsp90aa1* (Heat shock protein 90 alpha family class A member 1) and *Rara* (Retinoic acid receptor alpha).

Activation of the SMAD4 transcription factor is dependent on concentrations of TGF-β, high concentration of TGF-β have been shown to inhibit lL-17 production while low concentrations stimulate IL-17 production (Hahn et al. 2011; Kanehisa and Goto 2000). Therefore, low expression levels of SMAD4 are likely to stimulate cell differentiation into Th17 cells. Furthermore, the aryl hydrocarbon receptor (*Ahr*) associates with the molecular chaperone HSP90 (*Hsp90aa1*) and has been shown to induce the production of cytokines IL-17, IL-21 and IL-22 (Ehrlich et al. 2018; Tsuji et al. 2014). Therefore, upregulation of *Hsp90aa1* also suggests cell differentiation into Th17 cells.

In contrast, an increase in retinoid acid, as suggested by upregulation of *Rara*, in combination with the cytokines interleukin-2 and TGF-β upregulates *Foxp3* which inhibits Th17 cell differentiation (Kanehisa and Goto 2000).

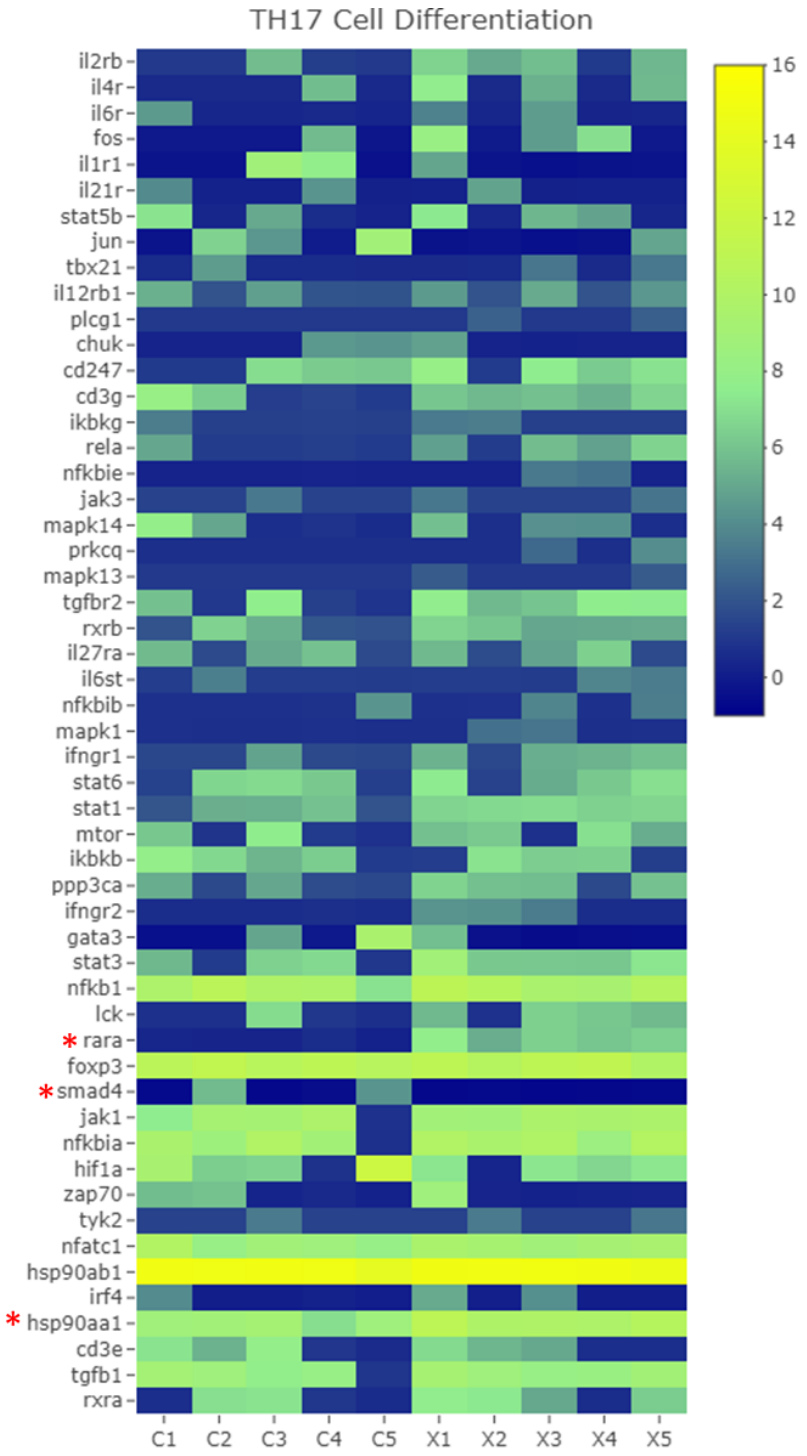

Figure 3.16: Heatmap displaying gene expression in Th17 cell differentiation. Gene pathway accessed via KEGG pathway database. Red asterisk indicates significantly DE genes, q-value ≤ 0.05. Green asterisk indicates differential expression observed but not significant. Gene names/ symbols displayed on the y axis. Colour bar signifies the regularised and log2transformed gene transcript count. Guinea pig control (C1-5) and experimental (X1-5) sample ID displayed below the x axis.

When considering the IL-17 signalling pathway in **Figure 3.17**, a significant increase in *Hsp90aa1*, *Il17ra* (Interleukin 17 receptor A) and *Usp25* (Ubiquitin specific peptidase 25) were observed. The IL-17A cytokine is produced by CD4-, CD8- and NK T cells and plays an important role in proinflammatory responses, recruitment of B cells and NK cells. After IL-17A receptor activation results in the association of the adaptor molecule Act1 and HSP90 and interaction is critical for IL-17-mediated activation of pro-inflammatory cytokines, chemokines and antimicrobial peptides. Therefore, upregulation of *Il17ra* and *Hsp90aa1* suggests IL-17 signal activation. However, the deubiquitinase USP25 has been shown to supress IL-17A signalling and downregulation of *Usp25* therefore suggests the converse to be true (Kanehisa and Goto 2000; Monin and Gaffen 2018; Song et al. 2016).

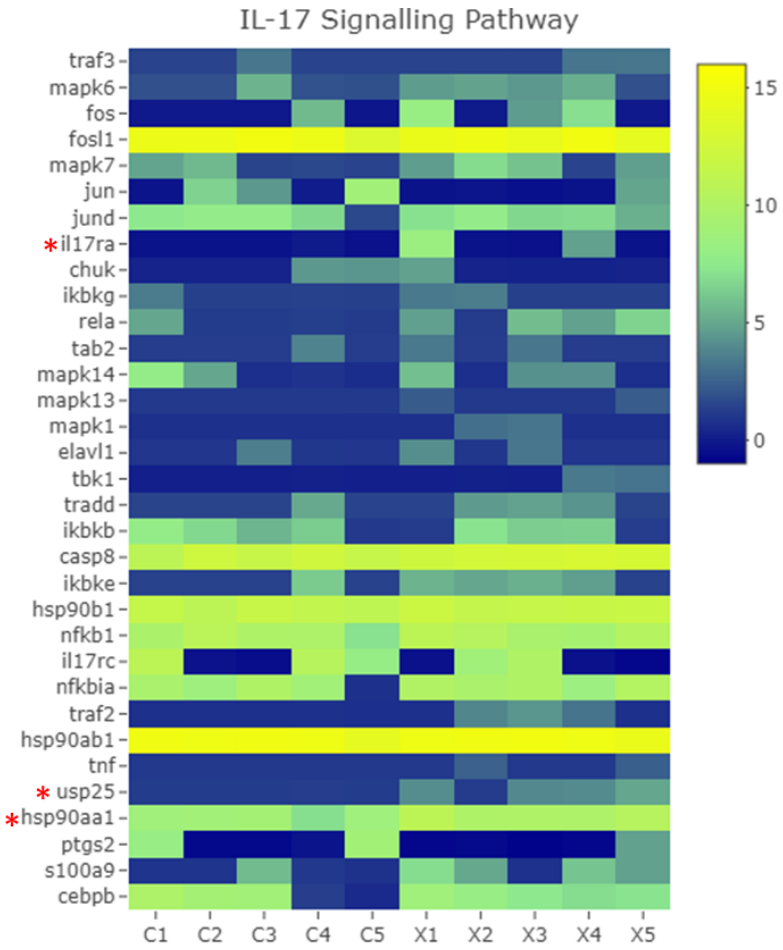

Figure 3.17: Heatmap displaying gene expression in IL-17 signalling pathway. Gene pathway accessed via KEGG pathway database. Red asterisk indicates significantly DE genes, q-value ≤ 0.05. Green asterisk indicates differential expression observed but not significant. Gene names/ symbols displayed on the y axis. Colour bar signifies the regularised and log2transformed gene transcript count. Guinea pig control (C1-5) and experimental (X1-5) sample ID displayed below the x axis.

Figure 3.18 and **Figure 3.19** show a significant increase (q≤0.05) in *Scarb1* (Scavenger receptor class B member 1) and *Hsp90aa1* gene expression respectively. The pattern recognition receptor SCARB1 and molecular chaperone HSP90 are both involved in MHC-1 antigen processing and presentation. SCARB1 mediates binding and uptake of peptides into macrophages, and HSP90 chaperones cytosolic peptides for MHC-I antigen presentation to CD8 T cells thereby playing an important role in cell-mediated immunity (Binder et al. 2001; Fabregat et al. 2018; Kanehisa and Goto 2000)**.**

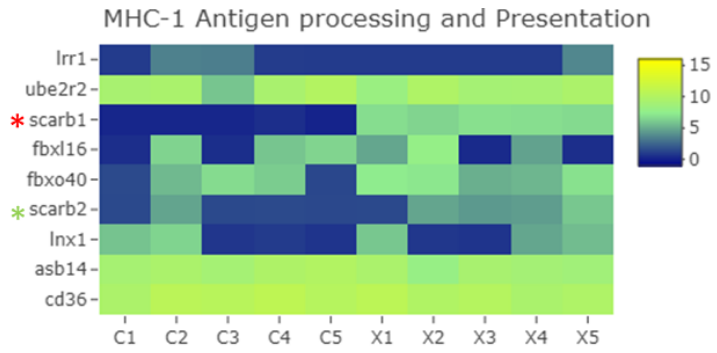

Figure 3.18: Heatmap displaying gene expression in the Class 1 MHC Antigen Processing and Presentation. Gene pathway accessed via Reactome pathway database. Red asterisk indicates significantly DE genes, q-value ≤ 0.05. Green asterisk indicates differential expression observed but not significant. Gene names/ symbols displayed on the y axis. Colour bar signifies the regularised and log2transformed gene transcript count. Guinea pig control (C1-5) and experimental (X1-5) sample ID displayed below the x axis.

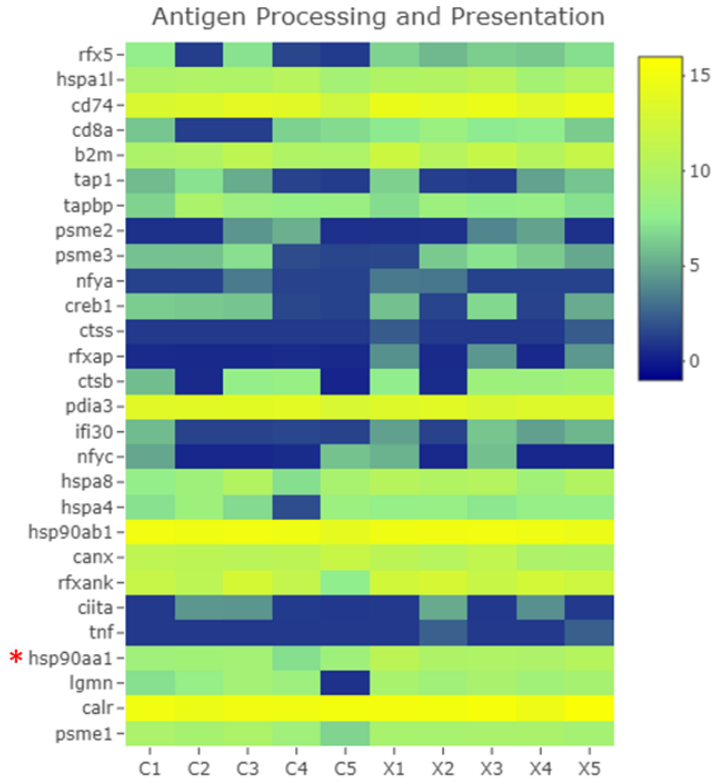

Figure 3.19: Heatmap displaying gene expression in antigen processing and presentation. Gene pathway accessed via KEGG pathway database. Red asterisk indicates significantly DE genes, q-value ≤ 0.05. Green asterisk indicates differential expression observed but not significant. Gene names/ symbols displayed on the y axis. Colour bar signifies the regularised and log2transformed gene transcript count. Guinea pig control (C1-5) and experimental (X1-5) sample ID displayed below the x axis.

Cytokines are signalling molecules which regulate cells involved in innate and adaptive immune responses. After activation, cytokines are released from various cells and induce responses by binding specific cell surface receptors. The heatmap presented in **Figure 3.20** demonstrates gene expression levels of cytokines and their specific receptors. Three cytokine receptor genes were found to be significantly ($q \leq 0.05$) upregulated, *Ifnlr1* (Interferon, lambda receptor 1), *Cx3cr1* and *Il17ra*, and the ligand *Tnfsf14* (Tumour necrosis factor (ligand) superfamily, member 14). As mentioned before, the transmembrane receptor protein encoded by *Il17ra*, is part of the IL-17 signalling pathway and is activated by the IL-17A cytokine produced by CD4-, CD8- and NK T cells. The chemoattractant encoded by *Cx3cr1* was highlighted in the chemokine signalling pathway and has been shown to have a role in activating CTLs and NK cells (Pretorius, 2016). The interferon lambda receptor encoded by *Ifnlr1* has been shown to play an important role in antiviral defences (Pott et al. 2011). The tumour necrosis factor ligand, TNFSF14, has been shown to stimulate T cell proliferation and interferon gamma (IFNG) production after binding to receptor TNFRSF14 (Tamada et al. 2000).

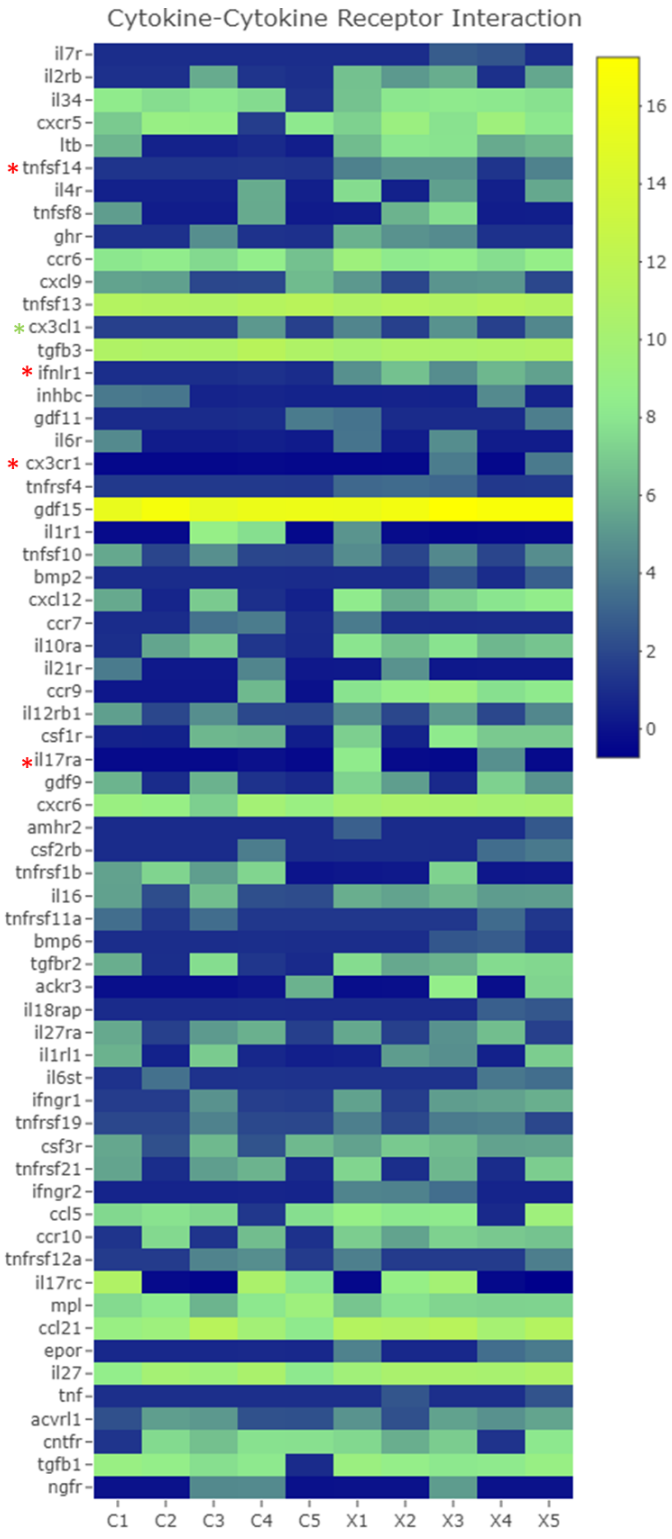

Figure 3.20: Heatmap displaying gene expression in cytokine-cytokine receptor interactions. Gene pathway accessed via KEGG pathway database. Red asterisk indicates significantly DE genes, q-value ≤ 0.05. Green asterisk indicates differential expression observed but not significant. Gene names/ symbols displayed on the y axis. Colour bar signifies the regularised and log2transformed gene transcript count. Guinea pig control (C1-5) and experimental (X1-5) sample ID displayed below the x axis.

3.4 Discussion

In order to test the viability of an AHSV-5 VP7 quasi-crystal vaccine we examined its stability over a 28-week period at 4°C, -20°C and -80°C. Western immunoblots and Coomassie staining revealed that AHSV-5 VP7 is a highly stable protein at 4°C, -20°C and -80°C (**Figure 3.4**). Quasi-crystals on the other hand were more stable at -20°C and -80°C over the 28-week period (**Table 3.2**). No crystals were observed in samples stored at 4°C after 8 weeks. Quasi-crystals seemed to increase in size over time at both -20°C and -80°C. This is an important consideration as vaccines are often stored over long periods of time and changes in particulate size may impact their efficacy. Particularly, since efficient APC processing and presentation depends on the size of the particulate (Bachmann and Jennings 2010; Manolova et al. 2008; Snapper 2018; Vidard et al. 1996). However, the largest plant-produced crystal sizes observed in this study were below 1 µm and therefore well below the maximum of 5 µm for efficient macrophage phagocytosis and display (Foged et al. 2005; Hirota and Ter 2012; Yue et al. 2010).

To thoroughly test the immunogenicity of an AHSV candidate vaccine the global immune response of the vaccine in relation to natural infection needs to be considered. Whilst the humoral response to AHSV has been well studied very little investigation has gone into cellular immunity. However, cell-mediated responses have been shown to play an important role in response to AHSV infection (Guthrie et al. 2009; Martinez-Torrecuadrada et al. 1996; Pretorius et al. 2016; Wade-Evans et al. 1997). In order to investigate the immunogenicity of plant-produced AHSV VP7 quasi-crystals we tested both the humoral and cell-mediated response by western immunoblotting and transcriptome analyses.

Guinea-pig immunogenicity studies of AHSV-5 VP7 were carried out over a 41-day period. Guinea-pigs were injected with experimental (X1-5) or control (C1-5) inocula on day 0 and the booster was received on day 13 (**3.2.3**). Experimental inocula concentrations were 35.13 µg and 26.87 µg for the primary and booster respectively. After performing SNTs using the extracted anti-AHSV-5 VP7 guinea-pig sera, sera demonstrated no neutralising capability (**3.3.3**). This was not surprising as various studies have shown that VP7 does not possess antigenic sites which induce

neutralising antibodies. AHSV VP2 is the major target for neutralising antibodies (Alberca et al. 2014; Bailey 2016; Kanai et al. 2014).

Western immunoblotting revealed that AHSV-5 VP7 quasi-crystals were highly immunogenic and stimulated a strong humoral response. At a dilution of 1:50 000, the anti-AHSV-5 VP7 final-bleed (X2) serum detected 0.77 µg AHSV VP7 protein. This detected VP7 at the same level as the positive control (anti-AHSV-5 VLPs) which was used at a 10-fold lower dilution of 1:5000 (**Figure 3.5**). Non-specific binding was still detected at 1:50 000 dilution. This premise was based on the fact that the control final-bleed (C2) serum still detected AHSV-5 VP7 and moreover, the anti-AHSV-5 VP7 final-bleed (X2) serum detected 0.77 µg SHUV protein (**Figure 3.5**). The pre-absorption technique (**Figure 3.6**) was then used in an attempt to extract *N. benthamiana* host-specific antibodies and increase specificity of the sera. However, even at 1:100 000 dilution the final-bleed control (C1, C3 and C4) sera still lightly detected AHSV-5 VP7 at a similar level to the final-bleed experimental sera X3 (**Figure 3.7**). This indicates that AHSV-5 VP7 quasi-crystals did not stimulate an AHSV-5 VP7 specific humoral response in guinea-pigs X3 and X5. However, a very strong humoral response is indicated in guinea-pigs X1, X2 and X4 shown by the strong bands observed when using the sera to probe for 0.53 µg AHSV-5 VP7 at a 1:100 000 dilution.

To assess the cell-mediated immune response, spleen-derived guinea-pig mRNA was isolated and deep RNA sequencing performed to assess the transcriptome of guinea-pigs vaccinated with AHSV-5 VP7 quasi-crystals. After whole RNA extraction, concentrations and integrity were considered satisfactory to continue with library construction and sequencing after NanoDrop assessment (**Table 3.3**), agarose gel electrophoresis (**Figure 3.8**) and analysis via the Agilent Bioanalyser with RIN^{e}scores of between 7.2 to 8.4 (**Figure 3.9**). After RNA sequencing, ten datasets were assembled (five per group) and analysed by Omega Bio-Tek using Illumina Basespace and the Deseq2 analysis tool (**3.2.6.2**). Between 37.27 and 53.54 million reads were obtained for the experimental sample datasets and between 20.21 and 49.36 million reads for the control group after trimming off low quality reads. Coverage of the reference genome was relatively high ranging from between 73.52 to 84.00%. DEseq2 results revealed 350 significantly differentially expressed genes ($q \leq 0.05$) and

unfortunately only 8.6% (30 genes) of these correlated with the global immune response involving eighteen immune related pathways (**Figure 3.10** and **Table 3.6**).

Significantly differentially expressed genes were identified in both innate and adaptive immune response pathways. Of these, seventeen were involved in innate immunity (**Table 3.6**). These pathways included those relating to the inflammatory immune response such as chemokine signalling and leukocyte transendothelial migration. And pathways connected to recognition and destruction of pathogens, such as the NOD-like receptor signalling pathway, FC gamma R-mediated phagocytosis, C-type lectin receptor signalling pathway, natural killer cell-mediated cytotoxicity and the complement and coagulation cascade. When focusing on the adaptive immune pathways, eight genes were found to be involved in cell-mediated responses (**Table 3.6**). Namely T-cell receptor signalling, Th1, Th2 and Th17 cell differentiation, IL-17 signalling and pathways relating to antigen processing and presentation. Additionally, ten of the 30 significantly DE genes were found to play a role in pathways related to both innate and adaptive immunity (**Table 3.6**). Namely cytokine-cytokine receptor interactions and signal transduction pathways: Ras, JAK-STAT and Rap1.

Several important cytokines and associated receptors were found to be upregulated in experimental samples. The chemokine CX3CL1 was upregulated in three of the experimental samples and its receptor CX3CR1 was significantly upregulated (**Figure 3.11**). CX3CL1 is a strong chemoattractant to effector lymphocytes and its receptor CX3CR1 is expressed on CTLs and NK cells (Pretorius et al. 2016; Umehara et al. 2004). Pretorius *et al.* showed a decrease in chemokines such as CX3CL1 48 h after inoculation with AHSV-4, in contrast even 28 days after the AHSV-5 VP7 booster inoculation, CX3CR1 was still significantly upregulated. Additionally upregulation of the chemokine receptor CCR9, G protein-coupled receptor kinases GRK2 and GRK5, protein kinases PIK3R5, PRKCZ and RAF1, and the transcription activator STAT2, suggest activation of the chemokine signalling pathway and consequently cytokine production, cell differentiation, migration and apoptosis (**Figure 3.11**) (Kanehisa and Goto 2000).

The interferon gamma receptor IFNGR1 was upregulated in four of the experimental samples (**Figure 3.12** and **Figure 3.15**). IFNGR1 activates the Jak (1/2)-STAT1 pathway and drives IFN-gamma production and cell differentiation into Th1 cells

inducing strong-cell mediated responses. IFNG is secreted by T-cells and NK cells and has been shown to have antiviral activity (Pretorius et al. 2016; Schroder et al. 2004; Kanehisa and Goto 2000). The cytokine TNFSF14 (Tumour necrosis factor (ligand)) was also found to be significantly upregulated. TNFSF14 plays a role in activating T-cell proliferation and the production of IFNG after binding to is receptor TNFRSF14 (**Figure 3.20**) (Tamada et al. 2000). Furthermore, the interferon lambda receptor IFNLR1 was significantly upregulated in experimental samples. IFNLR1 and its cytokine IFNL1 have been shown to play an important role in antiviral defences (**Figure 3.20**) (Pott et al. 2011).

Along with IFNGR1, various components regulating NK cell-mediated cytotoxicity were found to be upregulated including the adapter protein FCER1G, protein kinases LCK, RAF1 and RAC2 and the integrin ITGAL (**Figure 3.12**). Activation of NK cytotoxicity activates the cell surface death receptor FAS which binds to ligands on the target cell's surface and leads to target cell apoptosis. Additionally, NK cells regulate the differentiation of CD4 T-cells (Kanehisa and Goto 2000; Pallmer and Oxenius 2016).

Evidence of Th1 and Th17 immune responses was observed. Various genes involved in activating Th1 and Th17 cell differentiation via the C-type lectin receptor (CLRs) signalling pathway were found to be upregulated including FCER1G, the calcium-binding messenger protein CALM3, the protein kinase PRKCD and the transcription factors NFKB2 and RELA (**Figure 3.13**) (Kanehisa and Goto 2000). Furthermore a significant decrease in expression of the transcription factor BCL3, a co-regulator of T-cell proliferation and Th2 cell differentiation, suggests downregulation of Th2 cell differentiation and therefore humoral immunity (**Figure 3.13**) (Kanehisa and Goto 2000; Massoumi et al. 2006). In contrast, upregulation of NOTCH2 and the interleukin receptor IL-2RB suggest activation of Th2 cell differentiation. The interleukin IL-2 induces proliferation and differentiation of T-cells, B-cells, NK cells and CTL activation (Justiz Vaillant and Qurie 2019) (**Figure 3.15**). Furthermore, upregulation of the adaptor protein genes *Nck2* and *Nck1* in the T-cell receptor signalling pathway suggest the activation of T-cell proliferation (**Figure 3.14**) (Kanehisa and Goto 2000).

A significant increase in the interleukin receptor IL-17RA suggests previous upregulation of the interleukin IL-17 produced by Th17 cells (**Figure 3.17**). Previous

studies have suggested that Th17 plays an important role in immunity to AHSV and a subgroup of CD8 T-cells have also been shown to produce IL-17 (Hamada et al. 2013; Pretorius et al. 2016). In addition, further studies have shown IL-17 to be crucial for recruiting B-cells, NK cells, macrophages and neutrophils to the site of infection and for viral clearance after RNA virus infection (Ryzhakov et al. 2011; Hamada et al. 2013). A significant downregulation of the transcription factor SMAD4 further suggests that IL-17 production was stimulated (**Figure 3.16**). SMAD4 is dependent on concentrations of TGF-β, high concentration of TGF-β have been shown to inhibit IL-17 production while low concentrations TGF-β and therefore SMAD4 stimulate IL-17 production and cell differentiation into Th17 cells (Hahn et al. 2011; Kanehisa and Goto 2000). Significant upregulation of the molecular chaperone HSP90AA1 concurs with an increase in Th17 cell differentiation (**Figure 3.16**). HSP90AA1 associates with the aryl hydrocarbon receptor AHR and induces the production of cytokines IL-17 and IL-21 in the Th17 cell differentiation pathway (Ehrlich et al. 2018; Tsuji et al. 2014). Furthermore, in the IL-17 signalling pathway, activation of the IL-17A receptor results in the association of the adaptor molecule Act1 and HSP90 (**Figure 3.17**). This association is important for the IL-17-mediated activation of pro-inflammatory cytokines, chemokines and antimicrobial peptides. Therefore, upregulation of *Il17ra* and *Hsp90aa1* suggests IL-17 signal activation and reconfirms the Th17 response. However, in contrast, downregulation of the deubiquitinase USP25 inhibits IL-17A signalling and therefore suggests downregulation of the IL-17-mediated activation of pro-inflammatory cytokines, chemokines and antimicrobial peptides (**Figure 3.17**) (Kanehisa and Goto 2000; Monin and Gaffen 2018; Song et al. 2016).

Furthermore, upregulation of the pattern recognition receptor SCARB1 and HSP90 indicates an increase in MHC-1 antigen processing and presentation to CD8 T-cells (**Figure 3.18** and **Figure 3.19**). SCARB1 plays a critical role in mediating binding and uptake of peptides into macrophages, and HSP90 is responsible for chaperoning cytosolic peptides for MHC-I antigen presentation to CD8 T cells thereby playing an important role in cell-mediated immunity (Binder et al. 2001; Fabregat et al. 2018; Kanehisa and Goto 2000)**.**

Moreover, whilst the experimental guinea-pigs X3 and X5 showed no evidence of a humoral response they did show differential expression (similar to that of X1, X2 and

X4) with regard to genes involved in cell-mediated responses. In fact, the chemokine gene *Cx3cl1* and its receptor gene *Cx3cr1* were highly upregulated in X3 and X5. And as mentioned before, this receptor and its chemokine play an important role in CTL and NK cell activation.

Interestingly, no significantly differentially expressed genes were observed in the B-cell receptor signalling pathway, but this may be because the spleens were removed 28 days post the booster inoculation. This may not be the most favourable time for observing upregulation of the B-cell receptor signalling pathway. Future experiments should therefore include an AHSV VP7 booster at least one week prior to guinea-pig euthanasia this is likely to enhance the immune transcriptome including humoral and cellular responses.

In conclusion, western immunoblotting revealed a favourable humoral response to AHSV-5 VP7 quasi-crystals. Transcriptome analysis of the cell-mediated immune response demonstrated upregulation of some key cytokines and associated receptors involved in CTL responses such as CX3CL1 and CX3CR1 and Th1, Th2 and Th17 immune responses. This was a preliminary study and was therefore beyond its scope to perform qPCR experiments to validate the RNA-seq results. Future studies should include qPCR validation and the booster inoculation should be adjusted to at least one week prior to exsanguination and spleen removal to enhance the immune transcriptome. Additionally, at the time of this study the *Cavia porcellus* genome was not available as a standard reference genome. Because of this differentially expressed genes involved in the humoral and cellular immune response to AHSV-5 VP7 may have been missed. Another animal model whose standard reference genome is available should therefore be considered for future studies, unless the *Cavia porcellus* reference genome is available. It would also be interesting to investigate the immune response to AHSV-5 VP7 crystals over various timepoints by transcriptome profiling of PBMCs.

CHAPTER 4: CONCLUSIONS

Reoccurring international AHS outbreaks and the recent outbreaks in South Africa occurring in 2016 and 2019 emphasise the need for a safer, affordable and more reliable vaccine alternative for the prevention of AHS. The literature suggests that a particulate subunit vaccine (SUV) combined with a plant expression system provides an economically viable, safer, easily scalable and DIVA compliant alternative (Chen et al. 2013; Mir-Artigues et al. 2019; Rybicki 2019; Schillberg et al. 2019). AHSV-5 VP7 is highly immunogenic, serogroup-specific and its quasi-crystal configuration aids in the repetition of immunologically important epitopes making it a good monovalent vaccine alternative to the commercially available polyvalent live-attenuated vaccine (Maree and Paweska 2005; Martinez-Torrecuadrada et al. 1996; Bailey 2016; Zientara et al. 2015.

The main aim of this study was to develop plant-produced AHSV-5 VP7 quasi-crystals, and to test their immunogenicity. The objectives included: (1) Optimising the expression conditions for production of AHSV-5 VP7 in *N. benthamiana*; (2) Characterising and optimising the purification protocol for AHSV VP7 quasi-crystal production; and (3) Testing the specific humoral and cell-mediated immune response in guinea-pigs induced by immunisation of the VP7 quasi-crystals. Furthermore, the thermostability of AHSV VP7 quasi-crystals and *in-situ* crystal formation in *N. benthamiana* leaves was assessed.

In order to produce adequate AHSV VP7 yields in *N. benthamiana* of high enough purity for guinea-pig immunogenicity studies, optimal conditions for its expression and an optimised purification protocol was needed. AHSV-5 VP7 was successfully expressed in *N. benthamiana* and quasi-crystals purified using a discontinuous density gradient. Yields of approximately 213.16 µg/ml and 2.66 µg/g FW yield were achieved and the purity of these samples was found to be qualitatively good as very few contaminants were observed. While VP7 trimers (135 kDa) were observed in western immunoblots they were not observed in Coomassie stained gels. In an immunoassay such as western blotting, particularly when using a polyclonal primary antibody, more antibodies could potentially bind the trimer structure as opposed to the linear monomer resulting in a strong trimer band. This therefore is not quantitative as it does not equate to higher levels of trimers but rather higher levels of antibody-protein binding.

Coomassie stained gels and quantification using gel densitometry are therefore considered more quantitative. However, the lack of trimer observation in Coomassie stained gels could also be as a result of reduced staining of trimers by Coomassie® Brilliant Blue G-250 stain. If the latter is true, the reported yields may have been underestimated in this study.

Western blot and Coomassie staining analyses revealed pRIC3.0 as the optimal expression vector, as use of this vector resulted in higher yields of AHSV VP7 protein when compared to pEAQ-*HT.* Furthermore, the optimal harvest day of 6 dpi increased maturation time resulting in an increase in AHSV-5 VP7 quasi-crystal formation. The buffer 0.2 M Tris-0.15 M NaCl, pH 8, proved to be a favourable buffer for promoting trimer-trimer interactions. And after low-speed differential centrifugation large amounts of AHSV-5 VP7 quasi-crystals seemed to reside preferentially in the pellet. This pellet was adequate for use in low-speed density gradient ultracentrifugation as a means of purifying AHSV-VP7 quasi-crystals. Moreover, the results demonstrated that high-speed ultracentrifugation is likely to destroy AHSV VP7 quasi-crystals. The size distribution of AHSV-5 VP7 quasi-crystals produced in *N. benthamiana* seemed smaller (200-700 nm) than those reported in the literature (Burroughs et al. 1994; Chuma et al. 1992; Maree and Paweska 2005; Wall et al. 2017; Bailey 2016. And whilst they maintained the crystal lattice they formed uncharacteristic shapes in contrast to the commonly reported hexagonal crystals. This may be as a result of utilising plant expression systems. For the purposes of this study, this size range of crystals was satisfactory for APC presentation to the adaptive arm of the immune response as discussed in Chapter 3.

Future studies should investigate more scalable alternatives to density gradient centrifugation for large-scale purification of AHSV VP7 quasi-crystals such as depth filtration and tangential flow cytometry (Dennis 2019). Furthermore, the purity of these plant-produced quasi-crystals should be more quantitatively assessed by means of chromatography methods (i.e. affinity, gel permeation or reverse phase chromatography) or mass spectrometry (Rhodes and Laue 2009).

In situ TEM was performed in order to affirm that AHSV-5 VP7 quasi-crystal assembly occurs within *N. benthamiana* leaf cells as opposed to during the extraction process. Unfortunately, no AHSV-5 VP7 quasi-crystals were observed *in-situ.* This experiment

would need to be repeated to confirm whether this is due to pH changes in the plant cell (Chapter 2), a technical error or whether quasi-crystals are in fact forming during the purification process due to an ideal physiological environment being created during the extraction process. The latter seems unlikely since large VP7 crystals were observed in plant crude extract approximately two hours after harvesting and before density gradient purification.

To assess the validity of an AHSV VP7 candidate vaccine, the stability of VP7 quasi-crystals was assessed over a 28-week period across a range of temperatures (4°C, -20°C and -80°C). VP7 protein was found to be highly stable when assessed by western immunoblots and Coomassie staining. While quasi-crystals were more stable at -20°C and -80°C over the 28-week period. Crystals stored at 4°C were not preserved after 8 weeks. In contrast, crystals stored at -20°C and -80°C increased in size over the 28-week period. This is a crucial consideration when considering protein crystals as candidate vaccines. As APC presentation is dramatically affected by particle size and changes in particulate size can therefore alter the efficacy of a vaccine (Bachmann and Jennings 2010; Manolova et al. 2008; Snapper 2018; Vidard et al. 1996).

A vaccine stimulating both humoral and cell-mediated responses is likely to be preferential to one which solely induces neutralising antibodies (Guthrie et al. 2009; Martinez-Torrecuadrada et al. 1996; Wade-Evans et al. 1997; Pretorius et al. 2016). In order to test the immunogenicity of AHSV-5 VP7 quasi-crystals as a candidate vaccine, guinea-pig immunogenicity studies were successfully carried out over a 41-day period and the humoral and cell-mediated immune responses to AHSV-5 VP7 quasi-crystals were investigated. Western immunoblotting revealed that plant-produced AHSV-5 crystals are highly immunogenic and stimulate a strong humoral response as a 1:100 000 dilution of anti-AHSV-5 VP7 serum in three of the experimental guinea-pigs detected 0.53 µg AHSV-5 VP7. These are encouraging results for a candidate vaccine and suggest that plant-produced AHSV VP7 quasi-crystals may also be a good diagnostic reagent for ELISAs. Presently, VP7 based diagnostic tests are the OIE accepted method for AHSV diagnosis (Bekker et al. 2017; Zientara et al. 2015). A plant-production platform may therefore be a more economical

alternative compared to other eukaryotic cell culture production systems (Chen et al. 2013; Rybicki 2009; Lomonossoff and D'Aoust 2016).

With regard to the cell-mediated immune response to AHSV-5 VP7 quasi-crystals, transcriptome analysis of spleen-derived mRNA via RNA-seq revealed 350 significantly differentially expressed genes ($q \leq 0.05$). Unfortunately, only 8.6% of these genes were associated with the global immune system making it difficult to highlight the exact immune pathways at play. However, it was noted that these genes were part of eighteen different innate and adaptive immune related pathways. Differential expression of genes involved in the T-cell receptor signalling pathway, T-helper (Th)1, Th2 and Th17 cell differentiation and IL17 signalling pathway suggest a cell-mediated immune response to AHSV-5 VP7 quasi-crystals. The upregulation of several key cytokines and associated receptors were evident in response to AHSV VP7 crystals i.e. TNFSF14, CX3CR1, IL17RA and IFNLR1, some of which play an important role in cytotoxic T-cell responses e.g. CX3CL1 and CX3CR1 (Burroughs et al. 1994; Chuma et al. 1992; Maree and Paweska 2005; Wall et al. 2017; Bailey 2016. Additionally, TNFSF14 activates T-cell proliferation, and IFNLR1 and its cytokine IFNL1 have been shown as key interferons in antiviral defences (Pott et al. 2011). IL-17RA suggests previous upregulation of the interleukin IL-17 produced by Th17 cells and Th17 cells are hypothesised to play an important part in AHSV immunity (Hamada et al. 2013; Pretorius et al. 2016).

With regard to AHSV VP7 quasi-crystal production, future research should look to further assess buffer pH and the extent to which buffer pH affects crystal formation. Immunogold labelling for *in situ* TEM should be considered to aid in AHSV VP7 quasi-crystal visualisation. And with regard to transcriptome analyses, studies to follow should consider adjusting the booster inoculation to at least one week prior to termination of immunogenicity studies in order to enhance the humoral and cell-mediated immune response. Furthermore, the expression levels of a subset of immune response genes should be quantified by qPCR in order to validate the RNA-seq results. And since the *Cavia porcellus* reference genome was not available at the time of this study, further studies should seek to utilise another animal model whose reference genome is available for RNA-seq alignment. Most importantly, there are limitations in assessing the immune response in an animal model that is not the natural host. Pretorius *et al.* (2016) assessed the immune transcriptome using PBMCs from

horses vaccinated with attenuated AHSV-4. PBMCs may therefore be a suitable option for investigating the immune response to AHSV VP7 quasi-crystals.

To the best of our knowledge this is the first report of plant-produced AHSV VP7 quasi-crystals and, furthermore, the first time that the specific cell-mediated immune response to VP7 quasi-crystals has been assessed. Further investigation needs to be done to investigate the validity of AHSV VP7 quasi-crystals as an effective vaccine. A techno-economic analysis was beyond the scope of this study but needs to be addressed in order to thoroughly assess the vaccine production cost. Additionally, future immunogenicity studies need to be performed and if AHSV VP7 crystals demonstrate higher levels of immunogenicity when compared to commercially used LAVs this may highlight a safer, easy to produce, more cost-effective vaccine alternative. Furthermore, this plant-production platform could also be utilised to produce AHSV VP7 quasi-crystals for diagnostic reagents in ELISAs.

APPENDIX A: GenBank Accession Numbers

GenBank Accession Numbers for AHSV-5 VP7	KP009668	HM035391	HM035382	HM035370
	KM886350	HM035399	HM035375	HM035366
	KP009787	HM035387	HM035374	HM035362

REFERENCES

Alberca, B., K. Bachanek-Bankowska, M. Cabana, E. Calvo-Pinilla, E. Viaplana, L. Frost, S. Gubbins, A. Urniza, P. Mertens, and J. Castillo-Olivares. 2014. 'Vaccination of horses with a recombinant modified vaccinia Ankara virus (MVA) expressing African horse sickness (AHS) virus major capsid protein VP2 provides complete clinical protection against challenge', *Vaccine*, 32: 3670-4.

Alberts, B. , A. Johnson, and J. Lewis. 2002. *Molecular Biology of the Cell* (Garland Science: New York).

Anamika, Krishanpal, Srikant Verma, Abhay Jere, and Aarti Desai. 2016. 'Transcriptomic Profiling Using Next Generation Sequencing - Advances, Advantages, and Challenges.' in, *Next Generation Sequencing - Advances, Applications and Challenges*.

Andrew, Marion, Pam Whiteley, Vijaya Janardhana, Zelia Lobato, Allan Gould, and Barbara Coupar. 1995. *Antigen specificity of the ovine cytotoxic T lymphocyte response to bluetongue virus*.

Bachmann, M. F., and G. T. Jennings. 2010. 'Vaccine delivery: a matter of size, geometry, kinetics and molecular patterns', *Nat Rev Immunol*, 10: 787-96.

Bailey, L.V. 2016. *Immunogenicity of AHSV-4 VP7 Crystals and Their Potential Use as a Vaccine Delivery Platform* (University of Nottingham).

Basak, A. K., P. Gouet, J. Grimes, P. Roy, and D. Stuart. 1996. 'Crystal structure of the top domain of African horse sickness virus VP7: comparisons with bluetongue virus VP7', *Journal of Virology*, 70: 3797-806.

Bekker, S., P. Burger, and V. van Staden. 2017. 'Analysis of the three-dimensional structure of the African horse sickness virus VP7 trimer by homology modelling', *Virus Res*, 232: 80-95.

Bekker, S., H. Huismans, and V. van Staden. 2014. 'Factors that affect the intracellular localization and trafficking of African horse sickness virus core protein, VP7', *Virology*, 456-457: 279-91.

Benjamini, Yoav, and Yosef Hochberg. 1995. 'Controlling the False Discovery Rate: A Practical and Powerful Approach to Multiple Testing', *Journal of the Royal Statistical Society. Series B (Methodological)*, 57: 289-300.

Binder, R. J., N. E. Blachere, and P. K. Srivastava. 2001. 'Heat shock protein-chaperoned peptides but not free peptides introduced into the cytosol are presented efficiently by major histocompatibility complex I molecules', *J Biol Chem*, 276: 17163-71.

Burroughs, J. N., apos, R. S. Hara, C. J. Smale, C. Hamblin, A. Walton, R. Armstrong, and P. P. C. Mertens. 1994. 'Purification and properties of virus particles, infectious subviral particles, cores and VP7 crystals of African horsesickness virus serotype 9', 75: 1849-57.

Calvo-Pinilla, E., F. de la Poza, S. Gubbins, P. P. Mertens, J. Ortego, and J. Castillo-Olivares. 2014. 'Vaccination of mice with a modified Vaccinia Ankara (MVA) virus expressing the African horse sickness virus (AHSV) capsid protein VP2

induces virus neutralising antibodies that confer protection against AHSV upon passive immunisation', *Virus Res*, 180: 23-30.

Calvo-Pinilla, E., S. Gubbins, P. Mertens, J. Ortego, and J. Castillo-Olivares. 2018. 'The immunogenicity of recombinant vaccines based on modified Vaccinia Ankara (MVA) viruses expressing African horse sickness virus VP2 antigens depends on the levels of expressed VP2 protein delivered to the host', *Antiviral Res*, 154: 132-39.

Castillo-Olivares, J., E. Calvo-Pinilla, I. Casanova, K. Bachanek-Bankowska, R. Chiam, S. Maan, J. M. Nieto, J. Ortego, and P. P. Mertens. 2011. 'A modified vaccinia Ankara virus (MVA) vaccine expressing African horse sickness virus (AHSV) VP2 protects against AHSV challenge in an IFNAR -/- mouse model', *PLoS One*, 6: e16503.

Chen, Q., H. Lai, J. Hurtado, J. Stahnke, K. Leuzinger, and M. Dent. 2013. 'Agroinfiltration as an Effective and Scalable Strategy of Gene Delivery for Production of Pharmaceutical Proteins', *Adv Tech Biol Med*, 1.

Chiam, R., E. Sharp, S. Maan, S. Rao, P. Mertens, B. Blacklaws, N. Davis-Poynter, J. Wood, and J. Castillo-Olivares. 2009. 'Induction of antibody responses to African horse sickness virus (AHSV) in ponies after vaccination with recombinant modified vaccinia Ankara (MVA)', *PLoS One*, 4: e5997.

Chuma, T., H. Le Blois, J. M. Sánchez-Vizcaíno, M. Diaz-Laviada, and P. Roy. 1992. 'Expression of the major core antigen VP7 of African horsesickness virus by a recombinant baculovirus and its use as a group-specific diagnostic reagent', 73: 925-31.

Clift, S. J., and M. L. Penrith. 2010. 'Tissue and Cell Tropism of African Horse Sickness Virus Demonstrated by Immunoperoxidase Labeling in Natural and Experimental Infection in Horses in South Africa', *Veterinary Pathology*, 47: 690-97.

Cui, J., Y. Chen, H. Y. Wang, and R. F. Wang. 2014. 'Mechanisms and pathways of innate immune activation and regulation in health and cancer', *Hum Vaccin Immunother*, 10: 3270-85.

de Waal, P. J., and H. Huismans. 2005. 'Characterization of the nucleic acid binding activity of inner core protein VP6 of African horse sickness virus', *Arch Virol*, 150: 2037-50.

Dennis, S. J. 2019. 'The development of plant-produced African horse sickness virus-like particle (VLP) vaccines', University of Cape Town.

Dennis, S. J., A. E. Meyers, Hitzeroth, II, and E. P. Rybicki. 2019. 'African Horse Sickness: A Review of Current Understanding and Vaccine Development', *Viruses*, 11.

Dennis, S. J., M. M. O'Kennedy, D. Rutkowska, T. Tsekoa, C. W. Lourens, Hitzeroth, II, A. E. Meyers, and E. P. Rybicki. 2018. 'Safety and immunogenicity of plant-produced African horse sickness virus-like particles in horses', *Vet Res*, 49: 105.

Deville, S., E. Carneaux, F. Bertrand, S. Cauchard, J. Cauchard, and L. Dupuis. 2011. 'Adjuvant Formulation for Companion Animals Vaccines', *Procedia in Vaccinology*, 4: 104-12.

Dorner, T., and A. Radbruch. 2007. 'Antibodies and B cell memory in viral immunity', *Immunity*, 27: 384-92.

Ehrlich, A. K., J. M. Pennington, W. H. Bisson, S. K. Kolluri, and N. I. Kerkvliet. 2018. 'TCDD, FICZ, and Other High Affinity AhR Ligands Dose-Dependently Determine the Fate of CD4+ T Cell Differentiation', *Toxicol Sci*, 161: 310-20.

Faber, F. E., M. van Kleef, S. I. Tshilwane, and A. Pretorius. 2016. 'African horse sickness virus serotype 4 antigens, VP1-1, VP2-2, VP4, VP7 and NS3, induce cytotoxic T cell responses in vitro', *Virus Res*, 220: 12-20.

Fabregat, Antonio, Steven Jupe, Lisa Matthews, Konstantinos Sidiropoulos, Marc Gillespie, Phani Garapati, Robin Haw, Bijay Jassal, Florian Korninger, Bruce May, Marija Milacic, Corina Duenas Roca, Karen Rothfels, Cristoffer Sevilla, Veronica Shamovsky, Solomon Shorser, Thawfeek Varusai, Guilherme Viteri, Joel Weiser, Guanming Wu, Lincoln Stein, Henning Hermjakob, and Peter D'Eustachio. 2018. 'The Reactome Pathway Knowledgebase', *Nucleic acids research*, 46: D649-D55.

Fathallah, A. M., R. B. Bankert, and S. V. Balu-Iyer. 2013. 'Immunogenicity of subcutaneously administered therapeutic proteins--a mechanistic perspective', *AAPS J*, 15: 897-900.

Fehr, Thomas, Dace Skrastina, Paul Pumpens, and Rolf M. Zinkernagel. 1998. 'T cell-independent type I antibody response against B cell epitopes expressed repetitively on recombinant virus particles', 95: 9477-81.

Foged, Camilla, Birger Brodin, Sven Frokjaer, and Anne Sundblad. 2005. 'Particle size and surface charge affect particle uptake by human dendritic cells in an in vitro model', *International Journal of Pharmaceutics*, 298: 315-22.

Ford, T., J. Graham, and D. Rickwood. 1994. 'Iodixanol: A Nonionic Iso-osmotic Centrifugation Medium for the Formation of Self-Generated Gradients', *Analytical Biochemistry*, 220: 360-66.

French, T. J., and P. Roy. 1990. 'Synthesis of bluetongue virus (BTV) corelike particles by a recombinant baculovirus expressing the two major structural core proteins of BTV', *Journal of Virology*, 64: 1530-36.

Friede, M., and M. T. Aguado. 2005. 'Need for new vaccine formulations and potential of particulate antigen and DNA delivery systems', *Adv Drug Deliv Rev*, 57: 325-31.

Gasteiger, E., C. Hoogland, A. Gattiker, S. Duvaud, M.R. Wilkins, R.D. Appel, and A. Bairoch. 2005. 'Protein Identification and Analysis Tools on the ExPASy Server', *(In) John M. Walker (ed): The Proteomics Protocols Handbook, Humana Press*: 571-607.

Grewar, J. D., C. T. Weyer, G. J. Venter, L. S. van Helden, P. Burger, A. J. Guthrie, P. Coetzee, K. Labuschagne, G. Buhrmann, B. J. Parker, and P. N. Thompson.

2019. 'A field investigation of an African horse sickness outbreak in the controlled area of South Africa in 2016', *Transbound Emerg Dis*, 66: 743-51.
Grosse-Holz, F., S. Kelly, S. Blaskowski, F. Kaschani, M. Kaiser, and R. A. L. van der Hoorn. 2018. 'The transcriptome, extracellular proteome and active secretome of agroinfiltrated Nicotiana benthamiana uncover a large, diverse protease repertoire', *Plant Biotechnol J*, 16: 1068-84.
Gunter, C. J., G. L. Regnard, E. P. Rybicki, and Hitzeroth, II. 2019. 'Immunogenicity of plant-produced porcine circovirus-like particles in mice', *Plant Biotechnol J*.
Guthrie, Alan, Melvyn Quan, Carina Lourens, Jean-Christophe Audonnet, Jules Minke, Jiansheng Yao, Ling He, Robert Nordgren, Ian Gardner, and Nigel Maclachlan. 2009. *Protective immunization of horses with a recombinant canarypox virus vectored vaccine co-expressing genes encoding the outer capsid proteins of African horse sickness virus*.
Hahn, J. N., V. G. Falck, and F. R. Jirik. 2011. 'Smad4 deficiency in T cells leads to the Th17-associated development of premalignant gastroduodenal lesions in mice', *J Clin Invest*, 121: 4030-42.
Hamada, Hiromasa, Elizabeth Bassity, Amanda Flies, Tara M. Strutt, Maria de Luz Garcia-Hernandez, K. Kai McKinstry, Tie Zou, Susan L. Swain, and Richard W. Dutton. 2013. 'Multiple Redundant Effector Mechanisms of CD8⁺ T Cells Protect against Influenza Infection', *The Journal of Immunology*, 190: 296.
Hassan, S. H., C. Wirblich, M. Forzan, and P. Roy. 2001. 'Expression and Functional Characterization of Bluetongue Virus VP5 Protein: Role in Cellular Permeabilization', *Journal of Virology*, 75: 8356-67.
Hassan, S. S., and P. Roy. 1999a. 'Expression and functional characterization of bluetongue virus VP2 protein: role in cell entry', *J Virol*, 73: 9832-42.
Hassan, Sharifah S., and Polly Roy. 1999b. 'Expression and Functional Characterization of Bluetongue Virus VP2 Protein: Role in Cell Entry', *Journal of Virology*, 73: 9832-42.
Hirota, Keiji, and Hiroshi Ter. 2012. 'Endocytosis of Particle Formulations by Macrophages and Its Application to Clinical Treatment.' in, *Molecular Regulation of Endocytosis*.
House, J. A., M. Lombard, P. Dubourget, C. House, and C. A. Mebus. 1994. 'Further studies on the efficacy of an inactivated African horse sickness serotype 4 vaccine', *Vaccine*, 12: 142-4.
Janeway, C.A., P. Travers, and M. Walport. 2001. *Immunobiology: The Immune System in Health and Disease* (Garland Science: New York).
Jeggo, Martyn, R. C Wardley, and Joe Brownlie. 1984. *A study of the role of cell-mediated immunity in bluetongue virus infection in sheep, using cellular adoptive transfer techniques*.
Justiz Vaillant, A.A., and A. Qurie. 2019. *Interleukin* (StatPearls Publishing).

Kanai, Y., P. A. van Rijn, M. Maris-Veldhuis, Y. Kaname, T. N. Athmaram, and P. Roy. 2014. 'Immunogenicity of recombinant VP2 proteins of all nine serotypes of African horse sickness virus', *Vaccine*, 32: 4932-7.

Kanehisa, M. , and S. Goto. 2000. 'KEGG: Kyoto Encyclopedia of Genes and Genomes', *Nucleic Acids Res*, 28: 27-30.

Kapila, Jyoti, Riet De Rycke, Marc Van Montagu, and Geert Angenon. 1997. 'An Agrobacterium-mediated transient gene expression system for intact leaves', *Plant Science*, 122: 101-08.

Kar, A. K., B. Bhattacharya, and P. Roy. 2007. 'Bluetongue virus RNA binding protein NS2 is a modulator of viral replication and assembly', *BMC Mol Biol*, 8: 4.

Kar, A. K., M. Ghosh, and P. Roy. 2004. 'Mapping the assembly pathway of Bluetongue virus scaffolding protein VP3', *Virology*, 324: 387-99.

Kushnir, N., S. J. Streatfield, and V. Yusibov. 2012. 'Virus-like particles as a highly efficient vaccine platform: diversity of targets and production systems and advances in clinical development', *Vaccine*, 31: 58-83.

Kyte, J., and R. F. Doolittle. 1982. 'A simple method for displaying the hydropathic character of a protein', *J Mol Biol*, 157: 105-32.

Laughlin, R. C., R. Madera, Y. Peres, B. R. Berquist, L. Wang, S. Buist, Y. Burakova, S. Palle, C. J. Chung, M. V. Rasmussen, E. Martel, D. A. Brake, J. G. Neilan, S. D. Lawhon, L. G. Adams, J. Shi, and S. Marcel. 2019. 'Plant-made E2 glycoprotein single-dose vaccine protects pigs against classical swine fever', *Plant Biotechnol J*, 17: 410-20.

Lelli, R., U. Molini, G. F. Ronchi, E. Rossi, P. Franchi, S. Ulisse, G. Armillotta, S. Capista, S. Khaiseb, M. Di Ventura, and A. Pini. 2013a. 'Inactivated and adjuvanted vaccine for the control of the African horse sickness virus serotype 9 infection: evaluation of efficacy in horses and guinea-pig model', *Vet Ital*, 49: 89-98.

Lelli, Rossella, Umberto Molini, Gaetano Federico Ronchi, Emanuela Rossi, Paola Franchi, Simonetta Ulisse, Gisella Armillotta, Sara Capista, Siegfried Khaiseb, Mauro Di Ventura, and Attilio Pini. 2013b. *Inactivated and adjuvanted vaccine for the control of the African horse sickness virus serotype 9 infection: Evaluation of efficacy in horses and guinea-pig model*.

Lomonossoff, George P., and Marc-André D'Aoust. 2016. 'Plant-produced biopharmaceuticals: A case of technical developments driving clinical deployment', 353: 1237-40.

Loudon, P. T., and P. Roy. 1991. 'Assembly of five bluetongue virus proteins expressed by recombinant baculoviruses: inclusion of the largest protein VP1 in the core and virus-like proteins', *Virology*, 180: 798-802.

Love, Michael I., Wolfgang Huber, and Simon Anders. 2014. 'Moderated estimation of fold change and dispersion for RNA-seq data with DESeq2', *Genome Biology*, 15: 550.

Lulla, V., A. Losada, S. Lecollinet, A. Kerviel, T. Lilin, C. Sailleau, C. Beck, S. Zientara, and P. Roy. 2017. 'Protective efficacy of multivalent replication-abortive

vaccine strains in horses against African horse sickness virus challenge', *Vaccine*, 35: 4262-69.

Lulla, V., A. Lulla, K. Wernike, A. Aebischer, M. Beer, and P. Roy. 2016. 'Assembly of Replication-Incompetent African Horse Sickness Virus Particles: Rational Design of Vaccines for All Serotypes', *J Virol*, 90: 7405-14.

Ma, J. K., J. Drossard, D. Lewis, F. Altmann, J. Boyle, P. Christou, T. Cole, P. Dale, C. J. van Dolleweerd, V. Isitt, D. Katinger, M. Lobedan, H. Mertens, M. J. Paul, T. Rademacher, M. Sack, P. A. Hundleby, G. Stiegler, E. Stoger, R. M. Twyman, B. Vcelar, and R. Fischer. 2015. 'Regulatory approval and a first-in-human phase I clinical trial of a monoclonal antibody produced in transgenic tobacco plants', *Plant Biotechnol J*, 13: 1106-20.

Maclean, J., M. Koekemoer, A. J. Olivier, D. Stewart, Hitzeroth, II, T. Rademacher, R. Fischer, A. L. Williamson, and E. P. Rybicki. 2007. 'Optimization of human papillomavirus type 16 (HPV-16) L1 expression in plants: comparison of the suitability of different HPV-16 L1 gene variants and different cell-compartment localization', *J Gen Virol*, 88: 1460-9.

Manning, N. M., K. Bachanek-Bankowska, P. P. C. Mertens, and J. Castillo-Olivares. 2017. 'Vaccination with recombinant Modified Vaccinia Ankara (MVA) viruses expressing single African horse sickness virus VP2 antigens induced cross-reactive virus neutralising antibodies (VNAb) in horses when administered in combination', *Vaccine*, 35: 6024-29.

Manole, V., P. Laurinmaki, W. Van Wyngaardt, C. A. Potgieter, I. M. Wright, G. J. Venter, A. A. van Dijk, B. T. Sewell, and S. J. Butcher. 2012. 'Structural insight into African horsesickness virus infection', *J Virol*, 86: 7858-66.

Manolova, V., A. Flace, M. Bauer, K. Schwarz, P. Saudan, and M. F. Bachmann. 2008. 'Nanoparticles target distinct dendritic cell populations according to their size', *Eur J Immunol*, 38: 1404-13.

Maree, S, S Durbach, and H Huismans. 1998. 'Intracellular production of African horsesickness virus core-like particles by expression of the two major core proteins, VP3 and VP7, in insect cells', 79: 333-37.

Maree, S., F. F. Maree, J. F. Putterill, T. A. P. de Beer, H. Huismans, and J. Theron. 2016. 'Synthesis of empty african horse sickness virus particles', *Virus Res*, 213: 184-94.

Maree, S., and J. T. Paweska. 2005. 'Preparation of recombinant African horse sickness virus VP7 antigen via a simple method and validation of a VP7-based indirect ELISA for the detection of group-specific IgG antibodies in horse sera', *J Virol Methods*, 125: 55-65.

Martinez-Costas, Jose, Geoff Sutton, N. Ramadevi, and Polly Roy. 1998. *Guanylyltransferase and RNA 5'-triphopatase activities of the purified expressed VP4 protein of bluetongue virus*.

Martinez-Torrecuadrada, Jorge, María Díaz-Laviada, Polly Roy, Carmen Sánchez, Carmen Vela, Jose Sánchez-Vizcaíno, and J. Ignacio Casal. 1996. *Full protection*

against African horsesickness (AHS) in horses induced by baculovirus-derived AHS virus serotype 4 VP2, VP5 and VP7.
Martínez-Torrecuadrada, Jorge L., and J. Ignacio Casal. 1995. 'Identification of a Linear Neutralization Domain in the Protein VP2 of African Horse Sickness Virus', *Virology*, 210: 391-99.
Martiniere, A., E. Bassil, E. Jublanc, C. Alcon, M. Reguera, H. Sentenac, E. Blumwald, and N. Paris. 2013. 'In vivo intracellular pH measurements in tobacco and Arabidopsis reveal an unexpected pH gradient in the endomembrane system', *Plant Cell*, 25: 4028-43.
Massoumi, R., K. Chmielarska, K. Hennecke, A. Pfeifer, and R. Fassler. 2006. 'Cyld inhibits tumor cell proliferation by blocking Bcl-3-dependent NF-kappaB signaling', *Cell*, 125: 665-77.
Matsuo, Eiko, and Polly Roy. 2013. 'Minimum requirements for bluetongue virus primary replication in vivo', *Journal of Virology*, 87: 882-89.
Mellor, P. S., J. Boned, C. Hamblin, and S. Graham. 1990. 'Isolations of African horse sickness virus from vector insects made during the 1988 epizootic in Spain', *Epidemiol. Infect.*, 105: 447-54.
Mellor, P. S., and C. Hamblin. 2004. 'African horse sickness', *Vet Res*, 35: 445-66.
Mertens, P. P., J. Diprose, S. Maan, K. P. Singh, H. Attoui, and A. R. Samuel. 2004. 'Bluetongue virus replication, molecular and structural biology', *Vet Ital*, 40: 426-37.
Mertens, Peter. 2004. 'The dsRNA viruses', *Virus Research*, 101: 3-13.
Mir-Artigues, Pere, Richard M. Twyman, Derry Alvarez, Pedro Cerda Bennasser, Merce Balcells, Paul Christou, and Teresa Capell. 2019. 'A simplified techno-economic model for the molecular pharming of antibodies', 116: 2526-39.
Mirchamsy, H., and H. Taslimi. 1968. 'Inactivated African horse sickness virus cell culture vaccine', *Immunology*, 14: 81-8.
Monastyrskaya, Katherine, Norbert Staeuber, Geoff Sutton, and Polly Roy. 1997. 'Effects of Domain-Switching and Site-Directed Mutagenesis on the Properties and Functions of the VP7 Proteins of Two Orbiviruses', *Virology*, 237: 217-27.
Monin, L., and S. L. Gaffen. 2018. 'Interleukin 17 Family Cytokines: Signaling Mechanisms, Biological Activities, and Therapeutic Implications', *Cold Spring Harb Perspect Biol*, 10.
Morris, A. G. 1988. 'Interferons', *Immunology*, 64: 43-45.
Ngalonkulu, Melitta. 2018. 'The South African Horse Industry: A Potential Billion Rand Market', Accessed 2019/11/28. https://www.forbesafrica.com/economy/2018/04/10/south-african-horse-industry-potential-billion-rand-market/
Pallmer, Katharina, and Annette Oxenius. 2016. 'Recognition and Regulation of T Cells by NK Cells', *Frontiers in immunology*, 7: 251-51.
Parker, R., S. Deville, L. Dupuis, F. Bertrand, and J. Aucouturier. 2009. 'Adjuvant formulation for veterinary vaccines: Montanide™ Gel safety profile', *Procedia in Vaccinology*, 1: 140-47.

Paul, M., and J. K. Ma. 2011. 'Plant-made pharmaceuticals: leading products and production platforms', *Biotechnol Appl Biochem*, 58: 58-67.

Pillet, S., J. Couillard, S. Trepanier, J. F. Poulin, B. Yassine-Diab, B. Guy, B. J. Ward, and N. Landry. 2019. 'Immunogenicity and safety of a quadrivalent plant-derived virus like particle influenza vaccine candidate-Two randomized Phase II clinical trials in 18 to 49 and >/=50 years old adults', *PLoS One*, 14: e0216533.

Pott, Johanna, Tanel Mahlakõiv, Markus Mordstein, Claudia U. Duerr, Thomas Michiels, Silvia Stockinger, Peter Staeheli, and Mathias W. Hornef. 2011. 'IFN-lambda determines the intestinal epithelial antiviral host defense', *Proceedings of the National Academy of Sciences of the United States of America*, 108: 7944-49.

Pretorius, A., F. E. Faber, and M. van Kleef. 2016. 'Immune gene expression profiling of PBMC isolated from horses vaccinated with attenuated African horsesickness virus serotype 4', *Immunobiology*, 221: 236-44.

Qiu, X., G. Wong, J. Audet, A. Bello, L. Fernando, J. B. Alimonti, H. Fausther-Bovendo, H. Wei, J. Aviles, E. Hiatt, A. Johnson, J. Morton, K. Swope, O. Bohorov, N. Bohorova, C. Goodman, D. Kim, M. H. Pauly, J. Velasco, J. Pettitt, G. G. Olinger, K. Whaley, B. Xu, J. E. Strong, L. Zeitlin, and G. P. Kobinger. 2014. 'Reversion of advanced Ebola virus disease in nonhuman primates with ZMapp', *Nature*, 514: 47-53.

R Core Team. 2018. "R: A Language and Environment for Statistical Computing." In. Vienna, Austria: R Foundation for Statistical Computing.

Regnard, G. L., R. P. Halley-Stott, F. L. Tanzer, Hitzeroth, II, and E. P. Rybicki. 2010. 'High level protein expression in plants through the use of a novel autonomously replicating geminivirus shuttle vector', *Plant Biotechnol J*, 8: 38-46.

Rhodes, D. G., and T. M. Laue. 2009. 'Determination of protein purity', *Methods Enzymol*, 463: 677-89.

Romito, M., D. H. Du Plessis, and G. J. Viljoen. 1999. 'Immune responses in a horse inoculated with the VP2 gene of African horsesickness virus', *Onderstepoort J Vet Res*, 66: 139-44.

Roy, P. 2008. 'Functional mapping of bluetongue virus proteins and their interactions with host proteins during virus replication', *Cell Biochem Biophys*, 50: 143-57.

Roy, P., T. Hirasawa, M. Fernandez, V. M. Blinov, and Sanchez-Vixcain J. M. Rodrique. 1991. 'The complete sequence of the group-specific antigen, VP7, of African horsesickness disease virus serotype 4 reveals a close relationship to bluetongue virus', 72: 1237-41.

Roy, P., and G. Sutton. 1998. 'New generation of African horse sickness virus vaccines based on structural and molecular studies of the virus particles', *Arch Virol Suppl*, 14: 177-202.

Roy, Polly, Peter P.C. Mertens, and Ignacio Casal. 1994. 'African horse sickness virus structure', *Comparative Immunology, Microbiology and Infectious Diseases*, 17: 243-73.

Rutkowska, D. A., Q. C. Meyer, F. Maree, W. Vosloo, W. Fick, and H. Huismans. 2011. 'The use of soluble African horse sickness viral protein 7 as an antigen delivery and presentation system', *Virus Res*, 156: 35-48.

Rybicki, E. P. 2009. 'Plant-produced vaccines: promise and reality', *Drug Discov Today*, 14: 16-24.

Rybicki, Ed. 2019. 'Plant molecular farming of virus-like nanoparticles as vaccines and reagents', *Wiley Interdisciplinary Reviews: Nanomedicine and Nanobiotechnology*.

Ryzhakov, G., C. C. Lai, K. Blazek, K. W. To, T. Hussell, and I. Udalova. 2011. 'IL-17 boosts proinflammatory outcome of antiviral response in human cells', *J Immunol*, 187: 5357-62.

Sabara, Marta, Kerry F.M. Ready, Patrick J. Frenchick, and Lorne A. Babiuk. 1987. 'Biochemical Evidence for the Oligomeric Arrangement of Bovine Rotavirus Nucleocapsid Protein and Its Possible Significance in the Immunogenicity of This Protein', 68: 123-33.

Sainsbury, F., and G. P. Lomonossoff. 2014. 'Transient expressions of synthetic biology in plants', *Curr Opin Plant Biol*, 19: 1-7.

Sainsbury, F., E. C. Thuenemann, and G. P. Lomonossoff. 2009. 'pEAQ: versatile expression vectors for easy and quick transient expression of heterologous proteins in plants', *Plant Biotechnol J*, 7: 682-93.

Samuel, Charles E. 2001. 'Antiviral Actions of Interferons', *Clinical Microbiology Reviews*, 14: 778.

Savignac, M., B. Mellstrom, A. G. Bebin, J. C. Oliveros, L. Delpy, E. Pinaud, and J. R. Naranjo. 2010. 'Increased B cell proliferation and reduced Ig production in DREAM transgenic mice', *J Immunol*, 185: 7527-36.

Scanlen, M., J. T. Paweska, J. A. Verschoor, and A. A. van Dijk. 2002. 'The protective efficacy of a recombinant VP2-based African horsesickness subunit vaccine candidate is determined by adjuvant', *Vaccine*, 20: 1079-88.

Schillberg, Stefan, Nicole Raven, Holger Spiegel, Stefan Rasche, and Matthias Buntru. 2019. 'Critical Analysis of the Commercial Potential of Plants for the Production of Recombinant Proteins', 10.

Schroder, K., P. J. Hertzog, T. Ravasi, and D. A. Hume. 2004. 'Interferon-gamma: an overview of signals, mechanisms and functions', *J Leukoc Biol*, 75: 163-89.

Schroeder, Andreas, Odilo Mueller, Susanne Stocker, Ruediger Salowsky, Michael Leiber, Marcus Gassmann, Samar Lightfoot, Wolfram Menzel, Martin Granzow, and Thomas Ragg. 2006. 'The RIN: an RNA integrity number for assigning integrity values to RNA measurements', *BMC molecular biology*, 7: 3-3.

Sharp, F. A., D. Ruane, B. Claass, E. Creagh, J. Harris, P. Malyala, M. Singh, D. T. O'Hagan, V. Petrilli, J. Tschopp, L. A. O'Neill, and E. C. Lavelle. 2009. 'Uptake of particulate vaccine adjuvants by dendritic cells activates the NALP3 inflammasome', *Proc Natl Acad Sci U S A*, 106: 870-5.

Shen, J. S., A. Busch, T. S. Day, X. L. Meng, C. I. Yu, P. Dabrowska-Schlepp, B. Fode, H. Niederkruger, S. Forni, S. Chen, R. Schiffmann, T. Frischmuth, and A. Schaaf. 2016. 'Mannose receptor-mediated delivery of moss-made alpha-galactosidase A efficiently corrects enzyme deficiency in Fabry mice', *J Inherit Metab Dis*, 39: 293-303.

Sievert, Carson. 2018. 'Plotly for R'.

Snapper, C. M. 2018. 'Distinct Immunologic Properties of Soluble Versus Particulate Antigens', *Front Immunol*, 9: 598.

Song, X., X. He, X. Li, and Y. Qian. 2016. 'The roles and functional mechanisms of interleukin-17 family cytokines in mucosal immunity', *Cell Mol Immunol*, 13: 418-31.

St Clair, N., B. Shenoy, L. D. Jacob, and A. L. Margolin. 1999. 'Cross-linked protein crystals for vaccine delivery', *Proceedings of the National Academy of Sciences of the United States of America*, 96: 9469-74.

Steffen Durinck, Paul T. Spellman, Ewan Birney and Wolfgang Huber. 2009. 'Mapping identifiers for the integration of genomic datasets with the R/Bioconductor package biomaRt', *Nature Protocols 4*: 1184-119.

Storni, T., T. M. Kundig, G. Senti, and P. Johansen. 2005. 'Immunity in response to particulate antigen-delivery systems', *Adv Drug Deliv Rev*, 57: 333-55.

Takeuchi, O., and S. Akira. 2009. 'Innate immunity to virus infection', *Immunol Rev*, 227: 75-86.

———. 2010. 'Pattern recognition receptors and inflammation', *Cell*, 140: 805-20.

Tamada, Koji, Koji Shimozaki, Andrei I. Chapoval, Yifan Zhai, Jeffery Su, Su-Fang Chen, Shie-Liang Hsieh, Shigekazu Nagata, Jian Ni, and Lieping Chen. 2000. 'LIGHT, a TNF-Like Molecule, Costimulates T Cell Proliferation and Is Required for Dendritic Cell-Mediated Allogeneic T Cell Response', *The Journal of Immunology*, 164: 4105.

Thompson, Geoffrey M., Stephen Jess, and Archie K. %J Irish Veterinary Journal Murchie. 2012. 'A review of African horse sickness and its implications for Ireland', 65: 9.

Thuenemann, Eva, Paolo Lenzi, Andrew Love, Michael Taliansky, Martina Becares, Sonia Zuniga, Luis Enjuanes, Gergana Zahmanova, Ivan Minkov, Slavica Matic, Emanuela Noris, Ann Meyers, Alta Hattingh, Edward Rybicki, Oleg Kiselev, Nikolai Ravin, Michael Eldarov, Konstantin Skryabin, and George Lomonossoff. 2013. 'The Use of Transient Expression Systems for the Rapid Production of Virus-like Particles in Plants', *Current Pharmaceutical Design*, 19: 5564-73.

Tsuji, N., K. Fukuda, Y. Nagata, H. Okada, A. Haga, S. Hatakeyama, S. Yoshida, T. Okamoto, M. Hosaka, K. Sekine, K. Ohtaka, S. Yamamoto, M. Otaka, E. Grave, and H. Itoh. 2014. 'The activation mechanism of the aryl hydrocarbon receptor (AhR) by molecular chaperone HSP90', *FEBS Open Bio*, 4: 796-803.

Turnbull, Pamela J., Sharon B. Cormack, and H. Huismans. 1996. 'Characterization of the gene encoding core protein VP6 of two African horsesickness virus serotypes', 77: 1421-23.

Tuse, D., N. Ku, M. Bendandi, C. Becerra, R. Collins, Jr., N. Langford, S. I. Sancho, A. Lopez-Diaz de Cerio, F. Pastor, R. Kandzia, F. Thieme, F. Jarczowski, D. Krause, J. K. Ma, S. Pandya, V. Klimyuk, Y. Gleba, and J. E. Butler-Ransohoff. 2015. 'Clinical Safety and Immunogenicity of Tumor-Targeted, Plant-Made Id-KLH Conjugate Vaccines for Follicular Lymphoma', *Biomed Res Int*, 2015: 648143.

Umehara, H., E. T. Bloom, T. Okazaki, Y. Nagano, O. Yoshie, and T. Imai. 2004. 'Fractalkine in vascular biology: from basic research to clinical disease', *Arterioscler Thromb Vasc Biol*, 24: 34-40.

Urbanowski, M. E. 2012. 'Development of a Cytosolic pH Reporter for Tobacco By 2 Cells', University of Massachusetts Amherst.

van de Water, S. G., R. G. van Gennip, C. A. Potgieter, I. M. Wright, and P. A. van Rijn. 2015. 'VP2 Exchange and NS3/NS3a Deletion in African Horse Sickness Virus (AHSV) in Development of Disabled Infectious Single Animal Vaccine Candidates for AHSV', *J Virol*, 89: 8764-72.

van Niekerk, M., M. Freeman, J. T. Paweska, P. G. Howell, A. J. Guthrie, A. C. Potgieter, V. van Staden, and H. Huismans. 2003. 'Variation in the NS3 gene and protein in South African isolates of bluetongue and equine encephalosis viruses', *J Gen Virol*, 84: 581-90.

van Rijn, P. A., M. A. Maris-Veldhuis, C. A. Potgieter, and R. G. P. van Gennip. 2018. 'African horse sickness virus (AHSV) with a deletion of 77 amino acids in NS3/NS3a protein is not virulent and a safe promising AHS Disabled Infectious Single Animal (DISA) vaccine platform', *Vaccine*, 36: 1925-33.

van Staden, V., M. A. Stoltz, and H. Huismans. 1995. 'Expression of nonstructural protein NS3 of African horsesickness virus (AHSV): evidence for a cytotoxic effect of NS3 in insect cells, and characterization of the gene products in AHSV infected Vero cells', *Archives of Virology*, 140: 289-306.

Venter, G. J., I. M. Wright, T. C. Van der Linde, and J. T. Paweska. 2009. 'The oral susceptibility of South African field populations of Culicoides to African horse sickness virus', *Medical and Veterinary Entomology*, 23: 367-78.

Vialle, R., L. Dupuis, S. Deville, F. Bertrand, J. Gaucheron, and J. Aucouturier. 2010. 'Microgel particulate adjuvant: characterisation and mechanisms of action', *Procedia in Vaccinology*, 2: 12-16.

Vidard, L., M. Kovacsovics-Bankowski, S. K. Kraeft, L. B. Chen, B. Benacerraf, and K. L. Rock. 1996. 'Analysis of MHC class II presentation of particulate antigens of B lymphocytes', *J Immunol*, 156: 2809-18.

Vreede, F. T., and H. Huismans. 1998. 'Sequence analysis of the RNA polymerase gene of African horse sickness virus', *Archives of Virology*, 143: 413-19.

Wade-Evans, A. M., L. Pullen, C. Hamblin, R. O'Hara, J. N. Burroughs, and P. P. C. Mertens. 1997. 'African horse sickness virus VP7 sub-unit vaccine protects mice against a lethal, heterologous serotype challenge', *Journal of General Virology*, 78: 1611-16.

Wall, G. V., D. A. Rutkowska, E. Mizrachi, H. Huismans, and V. van Staden. 2017. 'A Dual Laser Scanning Confocal and Transmission Electron Microscopy Analysis

of the Intracellular Localization, Aggregation and Particle Formation of African Horse Sickness Virus Major Core Protein VP7', *Microsc Microanal*, 23: 56-68.
Williams, Catherine F., Toru Inoue, Anne-Marie Lucus, Paolo M. de A. Zanotto, and Polly Roy. 1998. 'The complete sequence of four major structural proteins of African horse sickness virus serotype 6: evolutionary relationships within and between the orbiviruses', *Virus Research*, 53: 53-73.
Wojdasiewicz, Piotr, Lukasz A. Poniatowski, Andrzej Kotela, Jarosław Deszczyński, Ireneusz Kotela, and Dariusz Szukiewicz. 2014. 'The chemokine CX3CL1 (fractalkine) and its receptor CX3CR1: occurrence and potential role in osteoarthritis', *Archivum immunologiae et therapiae experimentalis*, 62: 395-403.
World Organisation for Animal Health, OIE 2018. 'Map of AHS official status', Accessed 11/07/2019. http://www.oie.int/en/animal-health-in-the-world/official-disease-status/african-horse-sickness/en-ahs-carte/.
Yue, H., W. Wei, Z. Yue, P. Lv, L. Wang, G. Ma, and Z. Su. 2010. 'Particle size affects the cellular response in macrophages', *Eur J Pharm Sci*, 41: 650-7.
Zientara, S., C. T. Weyer, and S. Lecollinet. 2015. 'African horse sickness', *Rev. Sci. Tech Off. Int. Epiz*, 34: 315-27.
Zupan, John, Theodore R. Muth, Olga Draper, and Patricia Zambryski. 2000. 'The transfer of DNA from Agrobacterium tumefaciens into plants: a feast of fundamental insights', 23: 11-28.
Zwart, L., C. A. Potgieter, S. J. Clift, and V. van Staden. 2015. 'Characterising Non-Structural Protein NS4 of African Horse Sickness Virus', *PLoS One*, 10: e0124281.